Field Observations of Atmospheric Aerosol Properties and the Impacts of New Particle Formation on the Radiative Properties of Clouds

Mamali, Dimitra

DOI
10.4233/uuid:0aef0047-2020-443a-b27a-86aa2bc9b35e

Publication date
2020

Document Version
Final published version

Citation (APA)
Mamali, D. (2020). *Field Observations of Atmospheric Aerosol Properties and the Impacts of New Particle Formation on the Radiative Properties of Clouds*. [Dissertation (TU Delft), Delft University of Technology]. https://doi.org/10.4233/uuid:0aef0047-2020-443a-b27a-86aa2bc9b35e

FIELD OBSERVATIONS OF ATMOSPHERIC AEROSOL PROPERTIES AND THE IMPACTS OF NEW PARTICLE FORMATION ON THE RADIATIVE PROPERTIES OF CLOUDS

FIELD OBSERVATIONS OF ATMOSPHERIC AEROSOL PROPERTIES AND THE IMPACTS OF NEW PARTICLE FORMATION ON THE RADIATIVE PROPERTIES OF CLOUDS

Proefschrift

ter verkrijging van de graad van doctor
aan de Technische Universiteit Delft,
op gezag van de Rector Magnificus Prof.dr.ir. T.H.J.J. van der Hagen,
voorzitter van het College voor Promoties,
in het openbaar te verdedigen op Vrijdag 7 Februari 2020 om 12:30

door

DIMITRA MAMALI

Master of Science in Atmospheric and Climate Science,
Eidgenössische Technische Hochschule (ETH), Zürich, Zwitserland,
geboren te Athene, Griekenland.

Dit proefschrift is goedgekeurd door de

promotor: Prof. Dr. ir. H.W.J. Russchenberg

Samenstelling promotiecommissie:

Rector Magnificus	voorzitter
Prof. dr. ir. H.W.J. Russchenberg	Technische Universiteit Delft
Dr. G. Biskos	Technische Universiteit Delft
	The Cyprus Institute
Onafhankelijke leden:	
Prof. dr. A. Schmidt-Ott	Technische Universiteit Delft
Prof.dr. N. Michalopoulos	University of Crete, Greece
Prof. dr. M.C. Krol	Wageningen University & Research
Dr. S.R. De Roode	Technische Universiteit Delft
Dr. U. Dusek	University of Groningen
Reserve lid:	
Prof. dr. ir. S. Steele-Dunne	Technische Universiteit Delft

This work was founded by Climate KIC.

Keywords: aerosol climatology, hygroscopicity, dust mass concentration, lidar, unmanned aerial vehicles, aerosol-cloud interaction, activated aerosols, radiative forcing, new particle formation events nucleation

Printed by: IPSKAMP Printing https://www.ipskampprinting.nl/

Front: The front page depicts artistic representations of the different aerosol measurement techniques used in this thesis. From left to right:
1. In-situ aerosol observations from the Cabauw tower (CESAR observatory)
2. Remote sensing aerosol measurements using Lidar
3. Airborne in-situ aerosol measurements (on Unmanned Aerial Vehicles (UAVs)).
Figures 2.2 and 4.1 (inset) include pictures of the actual UAVs used in the thesis and the Cabauw mast at the CESAR observatory.

Wisdom begins in wonder.
Socrates

CONTENTS

SUMMARY

Atmospheric aerosol particles are solid or liquid particles suspended in the atmosphere. They are directly emitted into the atmosphere or they are formed via the oxidation of gaseous precursors. Understanding the behavior of particles in the atmosphere is particularly important because they can affect the Earth's climate, visibility, air quality, human health, and the ecosystem. As a result, they are a topic of high interest for the scientific community.

Considering the climatic dimension, aerosol particles are associated with significant uncertainties to predictions of the future climate due to lack of complete understanding of the atmospheric processes they are involved in and the limitations in predicting the emission rates of the different sources. This thesis intends to shed light into the field of aerosol research by means of ground, air-borne, in-situ and remote sensing measurements and simulations. Using long term observation, this work also examines the role of new particle formation events in the atmosphere and their role in cloud formation and consequently on radiative warming.

Aerosol particles affect the incoming solar radiation directly through scattering and absorption of sunlight, and indirectly through the formation of clouds. Determining the magnitude of these effects is highly challenging partly because of the significant spatial (both vertically and horizontally) and temporal variability of the concentration, size, and chemical composition of atmospheric particles. The vertical variability of the atmospheric aerosol can be independently determined by modern in-situ measurements using airborne platforms and remote-sensing observations. Comparison of the measurements obtained by these two types of techniques, however, is fundamental for improving the accuracy of the resulting observational data for use in climate models. **Chapter 2** compares vertical profiles of the aerosol mass concentration, derived from ground-based remote sensing instrumentation, and in-situ instruments on-board Unmanned Aerial Vehicles (UAV). The findings show an agreement between the two measurement methods, within experimental uncertainty. This signifies that the two techniques can be used interchangeably for determining the vertical profiles of the aerosol concentrations, bringing them a step closer towards their systematic exploitation in climate models.

To better understand the role of aerosols on climate, and thus to improve the predictability of atmospheric-climate models, we need long-term measurements of the aerosol properties. Apart from the concentration of airborne particles, information on the temporal variability of their size and chemical composition is highly required for understanding the processes they are involved in. **Chapter 3** reports measurements of aerosol size distribution conducted at Cabauw from 2008 to 2015, and analyzes their trends and seasonal variability. In addition, it provides aerosol hygroscopicity measurements and link them with the patterns observed in the recorded size distributions.

As mentioned above, atmospheric particles are either emitted directly in the atmosphere or they are formed from precursor gases when the atmospheric conditions are fa-

vorable; this process is called atmospheric nucleation. The new aerosol particles formed by nucleation grow in size and can eventually become cloud droplets when they get at higher altitudes. Clouds forming after atmospheric nucleation would have different microphysical properties than clouds forming in the absence of new particle formation events. This will impact on the radiative properties of clouds as well as their ability to precipitate. **Chapter 4** uses a combination of observations and models to assess the impacts of atmospheric nucleation on cloud formation and consequently on the atmospheric radiation budget, in a region that is highly influenced by anthropogenic activities. More specifically we use a year-long dataset of aerosol measurements, conducted at the Cabauw monitoring station in the Netherlands, is used to predict the cloud droplet number concentration using simulation of cloud formation. We then evaluate the climatological impact by determining how changes in the cloud number concentrations, induced by nucleation events, affect the radiative properties of the clouds and determine the associated climate forcing.

SAMENVATTING

Atmosferische aerosols zijn vaste of vloeibare deeltjes in de atmosfeer. Ze worden direct uitgestoten in de atmosfeer of komen er terecht via de oxidatie van voorlopergassen. aerosols hebben een effect op het klimaat, de zichtbaarheid, de luchtkwaliteit en het ecosysteem van de Aarde. Ook hebben ze een invloed op de menselijke gezondheid. Om al deze redenen zijn ze een zeer interessant onderwerp voor de wetenschapsgemeenschap. Betreffende het effect op het klimaat; aerosols zorgen voor significante onzekerheden in klimaatvoorspellingen, omdat er een gebrek aan begrip is over hun origine en de atmosferische processen waarin aerosols betrokken zijn. Deze scriptie richt zich op het onderzoek over aerosols door metingen en simulaties op grondniveau, in de lucht, in-situ en met remote-sensing.

Aerosols hebben een direct effect op inkomende zonnestraling door verstrooiing en absorptie, en een indirect effect via wolkvorming. Het bepalen van de grootte van deze effecten is onzeker door zowel de enorme grootte van de atmosfeer (verticaal en horizontaal), als de variatie in concentratie, grootte en chemische samenstelling van de aerosols over de tijd. De verticale variatie in de eigenschappen van atmosferische aerosol kan onafhankelijk bepaald worden door moderne in-situ metingen die gebruik maken van platformen in de lucht en remote-sensing observaties. De vergelijking van de observaties afkomstig van de twee meetmethoden is fundamenteel voor het verbeteren van de nauwkeurigheid van resultaten in klimaatmodellen. In **hoofdstuk 2** vergelijken we verticale profielen van massaconcentratie van aerosols, afgeleid van remote-sensing instrumentatie of grondniveau en in-situ instrumenten aan boord van onbemande luchtvoertuigen (UAV).

Hoofdstuk 2 gaat over de ruimtelijke (verticale) verdeling van atmosferische deeltjes, terwijl **hoofdstuk 3** focust om de tijdsvariabiliteit. Om de rol van aerosols in het klimaat beter te begrijpen, en daarmee de voorspelkracht van atmosfeer-klimaatmodellen te verbeteren, hebben we lange termijn metingen van aerosoleigenschappen nodig. Naast de concentratie van luchtdeeltjes is informatie over de variabiliteit in de grootte en chemische samenstellingen over de tijd vereist om de processen waarin ze betrokken zijn te begrijpen. In **hoofdstuk 3** rapporteren we meetresultaten van de grootteverdeling van aerosols uitgevoerd in Cabauw tussen 2008 en 2015, analyseren we hun trend en seizoensvariabiliteit. Bovendien leveren we hygroscopiciteitsmetingen van aerosols en koppelen we deze aan de patronen die geobserveerd zijn in de grootteverdelingen.

Zoals hierboven genoemd worden atmosferische deeltjes uitgestoten in de atmosfeer of worden ze er gevormd door voorlopergassen als de atmosferische omstandigheden gunstig zijn. Dit laatste proces heet atmosferische nucleatie. De door nucleatie gevormde aerosols groeien in grootte en kunnen meegenomen worden in wolkvorming. Wolken die gevormd zijn na atmosferische nucleatie zouden andere microfysische eigenschappen hebben dan wolken die gevormd zijn voor de productie van nieuwe deeltjes. Dit zal de stralingseigenschappen van wolken en hun neerslagvermogen beïnvloe-

den. In **hoofdstuk 4** gebruiken we een combinatie van observaties en modellen om de impact van atmosferische nucleatie op wolkvorming en vervolgens op de atmosferische stralingsbalans te bepalen, en dat in een omgeving die zeer beïnvloed wordt door antropogene activiteiten. Meer in het bijzonder gebruiken we een jaarlange dataset van aerosol metingen die uitgevoerd zijn bij het Cabauw meetstation in Nederland om de wolkdruppelconcentratie te voorspelen aan de hand van simulaties van wolkvorming. Daarna evalueren we de klimaatimpact door het bepalen van het effect van veranderingen in wolkaantalconcentraties via atmosferische nucleatie op de stralingseigenschappen van wolken en bepalen we de bijbehorende klimaatforcering.

1

INTRODUCTION

"The moment one gives
close attention to anything,
even a blade of grass,
it becomes a mysterious,
awesome, indescribably
magnificent world in itself."

Henry Miller

1.1. BACKGROUND AND MOTIVATION

Production of the atmospheric aerosol

The atmospheric aerosol consists of solid or liquid particles, suspended in air, with diameters from about 0.002 μm to about 100 μm. These particles are emitted in the atmosphere directly from their source (primary aerosols) or they are formed from precursor gases (secondary aerosols) under favorable conditions. Primary aerosol sources can be both natural and anthropogenic as illustrated in Fig. 1.1. Natural aerosol sources include deserts (wind gusts suspend dust particles in the atmosphere), sea spray, pollens, wild fires, plant fragments, volcanic eruptions, etc. Human activities also introduce particles in the atmosphere through industrial emissions, power generation, road transport, maritime transport, cooking, wood-burning, etc. [1].

1

Figure 1.1: Natural and anthropogenic aerosol sources, including: (top panel) deserts, oceans, forest fires, (bottom panel) industry and transportation.

The life of aerosols

Once emitted or formed, the residence time of aerosol particles in the troposphere ranges from a few minutes to several days or even weeks, depending on the particle size and the meteorology. Following the wind currents, larger aerosol particles can travel distances of tens of km, while smaller particles can reach areas up to thousands of km away from their origin.

During their lifetime in the atmospheric environment, aerosol particles may have an impact on visibility, human health, and also on climate at a local, regional and global scale. Figure 1.2 shows pictures taken in the Mediterranean on a clear day and during a saharan dust episode. It is obvious that dust particles affect the visibility and block the incoming solar radiation. In addition, when present in the lower part of the atmosphere, aerosol particles can cause adverse health effects. Ultra-fine aerosol particles (i.e., particles having diameters <100 nm), in particular, are small enough to penetrate through the respiratory track and enter the blood circulation. Numerous epidemiological studies have shown that fine particulate matter and traffic-related air pollution are linked to cardiovascular and respiratory problems, allergic reactions and premature mortality[2–5].

With regard to the climatic impact, atmospheric aerosol particles interact with the

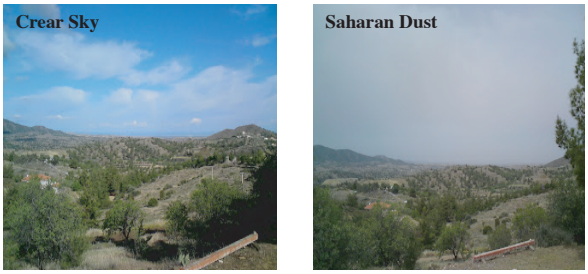

Figure 1.2: The impact of atmospheric aerosols on visibility. The pictures were taken during the BACCHUS campaign (cf. Chapter 2) before and during a saharan dust outbreak.

incoming solar radiation directly (through scattering and absorption of incoming solar radiation), altering the amount of energy that reaches the Earth's surface (aerosol direct effect; Fig. 1.3). Atmospheric aerosol particles also affect the radiation budget of the planet indirectly through the formation of clouds since they can serve as seeds onto which water vapor condenses to form cloud droplets. The clouds that can form in a polluted atmosphere (i.e., high aerosol loading) would have more and smaller cloud droplets compared to the clouds that would form under clean conditions (low aerosol burden). The resulting variability in the microphysical structure of clouds alters the cloud radiative properties (cloud albedo) resulting in the increase of the backscattered solar radiation back to space. This effect is referred to as first indirect effect or the Twomey effect (after the scientist who first studied the phenomenon; [6], Fig. 1.3). Apart from altering the cloud optical properties, smaller cloud droplets suppress the production of precipitation and prolong the cloud lifetime. As a result they reflect more sunlight back to space, thereby altering the Earth's radiative balance.

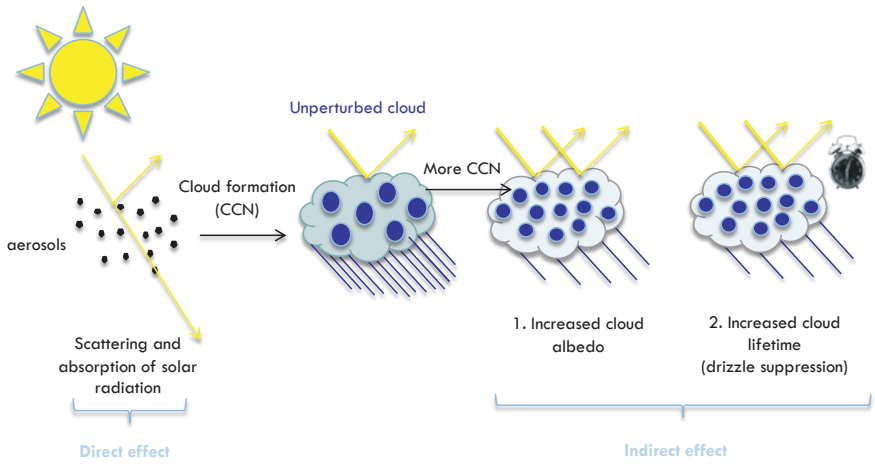

Figure 1.3: Illustration showing all the aerosol-radiation and aerosol-cloud-radiation interactions. Figure adapted by https://www.metoffice.gov.uk/research/climate/earth-system-science/aerosols.

Deposition of atmospheric aerosol particles

Airborne particles are removed from the atmosphere through dry and wet deposition. Dry deposition is the process of the transport of the species from the atmosphere to the surface in the absence of precipitation. The factors that determine the efficiency of dry deposition are the intensity of the atmospheric turbulence at the lowest part of the atmosphere, the type of aerosol species and the surface itself.

A more effective process of aerosol removal from the atmosphere is wet deposition. As mentioned above, atmospheric particles can serve as seeds for the productions of cloud droplets, and thus are removed from the atmosphere by precipitation. This process is called precipitation scavenging. In addition to that, during precipitation, aerosol particles below the cloud will also be scavenged. Wet deposition (which includes both scavenging methods mentioned above) also includes fog and snow deposition.

The importance of aerosols

Aerosol particles have multiple effects on the climate and even small perturbations in their properties can contribute to climate change. It is generally believed that part of the warming caused by the greenhouse gases has been counteracted by aerosols as a result of their increased burden from anthropogenic emissions since pre-industrial times. At the same time, aerosols affect human health, and because most of their emissions are within cities, there is a great effort in reducing them. As much as we would need to increase the aerosol load to cool the planet we need to reduce their amount in order to protect our health, which makes the whole discussion and research on atmospheric aerosols of particular importance.

Challenges in aerosol measurements

The size of atmospheric aerosol particle ranges over five orders of magnitude: from a few nm up to a few hundreds of μm. In a world that we cannot perceive with naked eyes this difference might sound insignificant, however, if we translate this size difference into sizes that we can see that would mean that aerosols could be as small as a pinhead or as big as a 20-story building! Because of that, one of the challenges in atmospheric aerosol research is the development and use of appropriate instruments capable of measuring the particles that are relevant to our research questions.

Apart from the size, aerosol particles have different chemical compositions and shapes. They consist of inorganic compounds (e.g., nitrates, sulfates, ammonium, sea salt), organic compounds, mineral species (mineral dust) and biological components [7]. Primary and secondary particles from different sources undergo chemical processes and mix with each other during their residence in the atmosphere. This alters their chemical composition, optical properties and their ability to serve as cloud condensation nuclei (CCN).

Another complexity of aerosols is their temporal and spatial variability within the atmospheric environment (both horizontally and vertically). As a result, aerosol particles exhibit significant differences from region to region and throughout the atmospheric

column. Fig. 1.4 a shows an example of the spatial distribution of atmospheric particles where it is very obvious that the highest concentrations are measured over heavily industrialized areas (e.g. China) and over the deserts. Regarding the vertical distribution, Fig. 1.4 b shows that aerosols can be concentrated in the lowest parts of the atmosphere, however, at times, high aerosol loadings can reach up to 10 km altitude. All in all, the atmospheric aerosol constitutes a complex system the properties of which have to be fully understood in order to assess and quantify its impacts on climate. Aerosol chemical composition and number concentration exhibit also diurnal and seasonal variabilities depending on the different sources and sinks of particles.

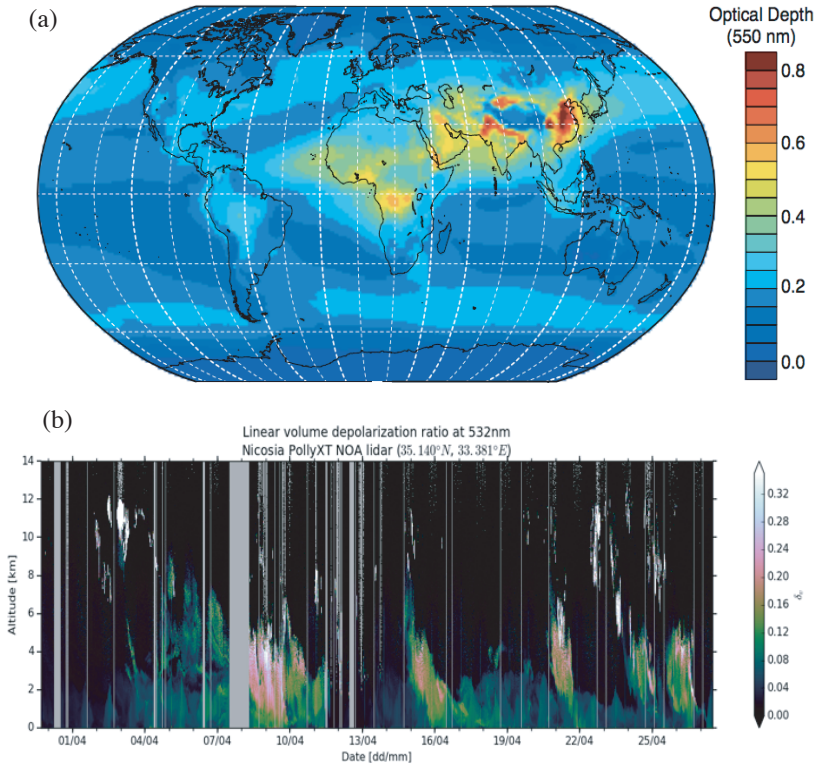

Figure 1.4: Examples of the spatial distribution of atmospheric aerosol particles in the horizontal (a) and vertical (b) dimension. (a) Global spatial distribution of the aerosol optical depth (at a wavelength of 550 nm) determined by the European Centre for Medium Range Weather Forecasts (ECMWF) Integrated Forecast System model with assimilation of Moderate Resolution Imaging Spectrometer (MODIS) [8, 9] over the period 2003–2010. (b) Vertical distribution of aerosol particles over Nicosia, Cyprus during the BACCHUS[1] campaign.

[1] Impact of Biogenic and Anthropogenic emissions on Clouds and Climate: towards a Holistic UnderStanding

1

1.2. OBJECTIVES OF THIS STUDY

The work presented in this thesis falls under the broader field of Atmospheric Sciences. It includes an evaluation of innovative aerosol measurement techniques, a climatological study of the aerosol particles in the Netherlands (the measurements were conducted at the main national atmospheric observatory at Cabauw) with a quantification of the regional indirect radiative forcing of atmospheric particles during new particle formation (NPF) events in the region. The thesis is organized in 5 chapters, including the current chapter that serves as an introduction to the thesis. Details for the rest of the chapters are provided in the following paragraphs.

Chapter 2

Atmospheric aerosol measurements can be performed by in-situ and remote sensing techniques. In-situ instruments sample the atmospheric aerosol from a single point that, under controlled conditions, can measure several aerosol parameters such as particle number, size, hygroscopicity etc. [10]. Remote sensing instruments measure bulk aerosol properties at ambient conditions. Passive remote sensing instrumentation (utilizing the sunlight for the measurements; e.g. sunphotometer) can measure parameters of the atmospheric aerosol within the entire atmospheric column while active remote sensing instruments (those that emit radiation; e.g. lidar and radar) provide range resolved measurements within the atmospheric column.

The need for vertically-resolved measurements, especially within the boundary layer where the largest part of the aerosol population resides, has given rise to innovative techniques that utilize UAVs. Along with this new way of measuring aerosols the necessity of validating the technique was brought about.

On the other end of the spectrum, newly developed retrieval algorithms that use as input light detection and ranging (lidar) measurements in combination with other remote sensing techniques, can retrieve vertically resolved aersol properties such as aerosol absorption and mass concentration. The quality of these algorithms needs to be validated with independent measurements. The key questions addressed in Chapter 2 are as follows.

Key Question I ***Can in-situ airborne instruments on-board UAVs provide reliable measurements of aerosol mass concentration?***

Key Question II ***How trustworthy are the newly developed retrieval algorithms that utilize the synergy of active and passive remote sensing instruments to retrieve vertically resolved aerosol properties?***

Chapter 3

Aerosol properties vary greatly over space and time. In order to better understand the role of aerosols in climate and minimize the uncertainty of the aerosol radiative forcing in climate models, we need long-term observations of aerosol particles around the Earth. Satellite instrumentation provide global coverage of certain atmospheric parameters, however in-situ measurements, although point measurements, can give detailed

information of aerosol properties. The key questions addressed in Capter 3 are as follows.

Key Question III ***What is the climatological trend of the fine particulate matter mass in the Netherlands?***

Key Question IV ***What is the climatological trend of the aerosol number concentration at Cabauw and its seasonal and diurnal variation?***

Key Question V ***What is the diurnal and seasonal variability of aerosol hygroscopicity at Cabauw?***

Chapter 4

Aerosols interact with the incoming solar radiation directly and indirectly. As climate change has already become from scenario a reality, the scientific community focuses its efforts to accurate predictions of the future climatic conditions in order to take action and mitigate, to the extend possible, possible disastrous effects. These model-based climate predictions have uncertainties [11] that mostly arise from our limited understanding of processes governing the source of natural aerosols and the complex interplay of aerosols with the hydrological cycle. A part of this uncertainty is linked to the effect of secondary aerosols on cloud properties and consequently on the radiation budget. Secondary aerosols are formed in the atmosphere from precursor gases through a process called nucleation. When this process occurs in the atmosphere, the newly formed particles start to grow in size. The presence of the newly formed particles affects the number of CCN. Thus, clouds formed during new particle formation events will contain different amounts of cloud droplets compared to the non-NPF days. This change in cloud droplet number will in turn affect the radiative properties of the cloud, its lifetime in the atmosphere and its ability to precipitate.

Key Question VI ***What is the impact of the NPF events on cloud droplet number concentrations in the Netherlands?***

Key Question VII ***How NPF events alter the cloud radiative properties in the Netherlands and other similar regions influenced strongly by anthropogenic activities, and what is the effect on the incoming solar radiation?***

1

REFERENCES

[1] J. H. Seinfeld and S. N. Pandis, *Atmospheric chemistry and physics: from air pollution to climate change* (John Wiley & Sons, 2012).

[2] K. Katsouyanni, G. Touloumi, E. Samoli, A. Gryparis, A. Le Tertre, Y. Monopolis, G. Rossi, D. Zmirou, F. Ballester, A. Boumghar, *et al.*, *Confounding and effect modification in the short-term effects of ambient particles on total mortality: results from 29 european cities within the aphea2 project,* Epidemiology , 521 (2001).

[3] J. A. Bernstein, N. Alexis, C. Barnes, I. L. Bernstein, A. Nel, D. Peden, D. Diaz-Sanchez, S. M. Tarlo, P. B. Williams, and J. A. Bernstein, *Health effects of air pollution,* Journal of Allergy and Clinical Immunology **114**, 1116 (2004).

[4] W. J. Gauderman, E. Avol, F. Gilliland, H. Vora, D. Thomas, K. Berhane, R. McConnell, N. Kuenzli, F. Lurmann, E. Rappaport, *et al.*, *The effect of air pollution on lung development from 10 to 18 years of age,* New England Journal of Medicine **351**, 1057 (2004).

[5] J. Lelieveld, J. S. Evans, M. Fnais, D. Giannadaki, and A. Pozzer, *The contribution of outdoor air pollution sources to premature mortality on a global scale,* Nature **525**, 367 (2015).

[6] S. Twomey, *Pollution and the planetary albedo,* Atmospheric Environment (1967) **8**, 1251 (1974).

[7] I. C. IPCC, *The physical science basis. contribution of working group i to the fifth assessment report of the intergovernmental panel on climate change,* (2013).

[8] A. Benedetti, J.-J. Morcrette, O. Boucher, A. Dethof, R. Engelen, M. Fisher, H. Flentje, N. Huneeus, L. Jones, J. Kaiser, *et al.*, *Aerosol analysis and forecast in the european centre for medium-range weather forecasts integrated forecast system: 2. data assimilation,* Journal of Geophysical Research: Atmospheres **114** (2009).

[9] J.-J. Morcrette, O. Boucher, L. Jones, D. Salmond, P. Bechtold, A. Beljaars, A. Benedetti, A. Bonet, J. Kaiser, M. Razinger, *et al.*, *Aerosol analysis and forecast in the european centre for medium-range weather forecasts integrated forecast system: Forward modeling,* Journal of Geophysical Research: Atmospheres **114** (2009).

[10] P. H. McMurry, *A review of atmospheric aerosol measurements,* Atmospheric Environment **34**, 1959 (2000).

[11] T. Stocker, *Climate change 2013: the physical science basis: Working Group I contribution to the Fifth assessment report of the Intergovernmental Panel on Climate Change* (Cambridge University Press, 2014).

2

VERTICAL PROFILES OF AEROSOL MASS CONCENTRATION DERIVED BY AIRBORNE IN-SITU AND REMOTE SENSING INSTRUMENTS

"If someone separated the art of counting
and measuring and weighing from all the other arts,
what was left of each would be,
so to speak, insignificant."

Plato

In-situ measurements using Unmanned Aerial Vehicles (UAVs) and remote sensing observations can independently provide dense vertically-resolved measurements of atmospheric aerosols; information which is highly required in climate models. In both cases, inverting the recorded signals to useful information requires assumptions and constraints, and this can make the comparison of the results difficult. Here we compare, for the first time, vertical profiles of the aerosol mass concentration derived from Light Detection And Ranging (LIDAR) observations and in-situ measurements using an Optical Particle Counter (OPC) on-board a UAV during moderate and weak Saharan dust episodes. Agreement between the two measurement methods was within experimental uncertainty for the coarse mode (i.e., particles having radii > 0.5 μm) where the properties of dust particles can be assumed with good accuracy. This result proves that the two techniques can be used interchangeably for determining the vertical profiles of the aerosol concentrations, bringing them a step closer towards their systematic exploitation in climate models.

This chapter has been published in Atmospheric Measurement Techniques: Mamali et al., 11, 2897-2910, https://doi.org/10.5194/amt-11-2897-2018.

2.1. INTRODUCTION

Aerosol particles affect the atmospheric energy balance directly by interacting with solar radiation, and indirectly through the formation of clouds [1]. Determining the radiative forcing of the atmospheric aerosol particles is highly uncertain partly because of the significant spatial (both vertically and horizontally) and temporal variability of their concentration, size, and chemical composition [2]. The vertical variability in the properties of the atmospheric aerosol can be independently determined by modern in-situ measurements using airborne platforms and remote-sensing observations. Comparison of the measurements obtained by these two types of techniques, however, is fundamental for improving the accuracy of the resulting observational data for use in climate models.

Light Detection And Ranging (LIDAR) instruments are among the most powerful tools for probing vertically-resolved properties of the atmospheric aerosol. A number of retrieval algorithms that have been developed over the years can be used to obtain aerosol optical parameters from the LIDAR raw signals, including the aerosol backscatter coefficient β_{aer} [3, 4], the aerosol extinction coefficient α_{aer} [5, 6], and the particle depolarization ratio δ^p [7]. Under certain assumptions, recently developed algorithms can now be used to retrieve other vertically resolved aerosol properties such as particle absorption and mass concentration using the synergy of LIDAR and sunphotometer [8–10]. To check the validity of these assumptions and to assure the quality of the final data, certain aerosol properties retrieved from LIDAR observations have been compared with vertical in-situ observations using research aircraft [11–17].

Airborne in-situ measurements using research aircraft are complex and costly, and therefore their availability is scarce and time-restricted, limiting comparability with remote sensing observations. What is more, manned aircraft cannot cover the lowermost part of the atmosphere due to safety restrictions, posing another major limitation. Recent efforts in aerosol instrumentation have provided lightweight and miniaturized instruments that can measure the size and concentration of aerosol particles on-board UAVs [18–24] in a much simpler and cost-effective manner. As a result, vertical profiling of key aerosol parameters can now be performed over long periods of time on a routine basis, and at much lower altitudes compared to measurements with manned research aircraft. Considering, however, that these advantages come in many cases at the expense of the quality of the recorded data, measurements of aerosol properties using miniaturized instruments on-board UAVs need to be validated before using them to bridge the long-lasting gap between in-situ measurements and remote sensing observations.

Here we compare, for the first time to our knowledge, vertical profiles of the aerosol mass concentration, derived from LIDAR measurements using the POlarization LIDAR PHOtometer Networking technique (POLIPHON), and in-situ measurements with an OPC onboard a UAV (hereafter referred to as OPC$_a$). It should be noted that the two techniques do not measure the mass concentration directly, but this is estimated from the recorded signals of the two instruments. The measurements were recorded during the BACCHUS-INUIT-ACTRIS (Impact of Biogenic Versus Anthropogenic emissions on Clouds and Climate: towards a Holistic UnderStanding; Ice Nuclei Research Unit; European Research Infrastructure for the observation of Aerosol, Clouds and Trace gases Research InfraSctructure network) campaign that took place in Cyprus during April 2016.

2.2. INSTRUMENTATION AND METHODS

2.2.1. SITE DESCRIPTION

Cyprus is located in the Eastern Mediterranean (cf. Fig. 2.1 inset), receiving air masses from Europe, the Middle East and North Africa [25]. Therefore, it represents an ideal location for characterizing different aerosol types and investigating the role of particles in various atmospheric processes.

The measurements reported here were conducted at three different locations. Aerial measurements, using a UAV, were carried out at Orounda (35°09′ N; 33°07′ E; 310 m above sea level; a.s.l.), providing highly-resolved spatially and temporally distributed data up to ca. 2 km above ground level (a.g.l.). Ground-based in-situ aerosol measurements, were performed at the Cyprus Atmospheric Observatory (CAO) at Agia Marina-Xyliatou (35°04′ N; 33°06′ E; 535 m a.s.l.), located 6.5 km south of Orounda. A Polly^{XT} Raman LIDAR was located at the suburbs of Nicosia (35°14′ N; 33°38′ E; 190 m a.s.l.), ca. 35 km east of Orounda, providing round-the-clock measurements of the atmospheric conditions up to 12 km a.g.l.. The exact locations of the measuring points are shown in Fig. 2.1 and detailed descriptions of the instruments are given below.

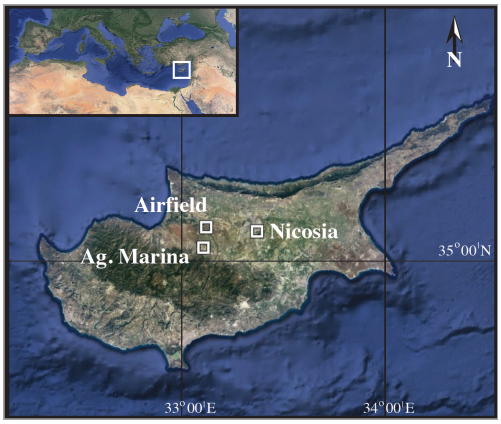

Figure 2.1: Map of Cyprus showing the locations of the observation sites used for the measurements reported in this paper. The inset in the upper-left corner shows the greater area of South Europe, North Africa, and the Middle East, with the white square indicating the location of Cyprus. The maps were generated by Google Earth Pro (https://www.google.com/earth/download/gep/agree.html).

2.2.2. UNMANNED AERIAL VEHICLE (UAV)

The UAV employed during the campaign (cf. Fig. 2.2) has a fixed wingspan of 3.8 m, and is powered by a two-stroke internal combustion engine. It has a take-off weight of 35 kg that results in a payload capacity of approximately 12 kg. The payload bay is 1.3 m × 0.23 m × 0.34 m (length-width-height), and can fit multiple instruments. When loaded, the UAV can fly for up to 4 hours with an air speed velocity of 25 ± 10 m s^{-1} and can reach altitudes up to 4 km a.g.l. (due to airspace limitations, however, only flights up to 2 km were permitted). An autopilot system allowed predetermined flight plans that involved spiral rectangular-shaped ascending and descending patterns preventing

contamination of the sampling system from the engine's exhaust. For consistency, the results shown in the rest of the paper correspond to measurements during ascends.

Figure 2.2: Photograph of the UAV of the Cyprus Institute used for the measurements reported in this work.

2.2.3. UAV-BASED OPTICAL PARTICLE COUNTER MEASUREMENTS

Vertical profiles of the particle size distributions of the atmospheric aerosol were measured using an OPC (i.e., the OPC$_a$; MetOne, Model 212-2) on-board the UAV, which reported particle size distributions, ranging from 0.15 to 5 μm in radius, in 8 size bins. The sampled aerosol was dried to below 50% relative humidity (RH) by gently heating the sampling tube of OPC$_a$. Assuming spherical shape and constant mass density for the particles, the size distributions were converted into aerosol mass concentrations (see Section 2.2.4). In addition to OPC$_a$, a single wavelength aethalometer (AethLabs - Model AE51) with a sampling time resolution of 1 second and a flow rate of 0.2 lpm, was on-board the UAV to verify that no contamination of the sampled air by the engine exhaust took place. Each instrument was equipped with an individual sampling inlet that extended 5 cm from the UAV nose to ensure representative sampling.

2.2.4. PARTICLE MASS CONCENTRATION CALCULATION FROM THE OPC$_a$ MEASUREMENTS

The mass concentration profiles of the coarse particles were calculated from the size distribution measurements recorded by OPC$_a$. Before converting the aerosol number concentrations to mass concentrations, the OPC measurements were averaged over 30 s (original time resolution 1 s). This was found to be optimal for suppressing a high frequency noise of the OPC raw data and at the same time maintaining a relatively high spatial resolution of ~ 80 m in the vertical direction. The number concentration (dN) of each size bin was converted to volume concentration according to $dV(r) = dN(r)\frac{4}{3}\pi r^3$, where r is the mean radius of each size bin in the recorded measurements. The volume concentration of particles with radii larger that 0.5 μm were summed and multiplied by ρ_d, yielding the coarse mode mass concentration. The variability in the number size

distributions averaged every 30 s propagated an uncertainty of the order of 10% in the estimated volume size distributions and the mass concentrations of the particles [26].

2.2.5. LIDAR MEASUREMENTS

A depolarization Raman LIDAR Polly^{XT} [27, 28] was used in the measurements reported here. This LIDAR emits laser pulses simultaneously at three wavelengths: 1064, 532 and 355 nm. The laser beam interacts with the atmospheric molecules and particles, and a part of it (backscattered light) is collected by the receiver unit that consists of two telescopes (near-field and far-field). The elastically backscattered signals are used as input to the Fernald-Klett algorithm [3, 4, 29] to retrieve the vertical profile of the particle backscatter coefficient β_{aer}. This method assumes a linear relationship between the aerosol extinction-to-backscatter ratio constant (i.e., the LIDAR ratio S) throughout the entire atmospheric column; a critical assumption that can induce uncertainties up to 20-30% of the retrieved property from statistical and systematic errors [30–32].

In addition to the elastically backscattered signal, Polly^{XT} receives the nitrogen Raman-shifted signal at wavelengths 387 and 607 nm, and the water vapor Raman signal at 407 nm wavelength. The Raman technique [6, 33] utilizes the elastic and inelastic signals to retrieve the particle extinction α_{aer} and scattering β_{aer} profiles independently, without any critical assumptions. The range-resolved aerosol LIDAR ratio can then be directly estimated as the ratio α_{aer}/β_{aer}. In our analysis, we used the Raman technique to retrieve the α_{aer} and β_{aer} profiles during night-time, and the Fernald-Klett method during day-time when the Raman signal is highly affected from the background noise induced by the scattered sunlight. The Polly^{XT} system also provides information on volume depolarization ratio δ^v from which the particle depolarization ratio δ^p can be estimated [7, 34–37]. This allows discrimination between spherical particles (e.g., water droplets) and non-spherical particles such as dust.

2.2.6. SUN/SKY PHOTOMETER MEASUREMENTS

A lunar/sun sky photometer of the Aerosol Robotic Network (AERONET; [38]) was collocated with the LIDAR at Nicosia, whereas an additional sunphotometer was situated at CAO. Both instruments provided measurements of the Aerosol Optical Thickness (AOT) at seven wavelengths (i.e., 340, 380, 440, 500, 675, 871 and 1020 nm). The AERONET products include, among others, parameters corresponding to the total atmospheric column such as the Ångström exponent Å (at several wavelength pairs), the particle volume size distributions in the size range 0.05 to 15 μm (particle radius), the fine and coarse mode AOT (τ_f and τ_c, respectively) at 440, 675, 871, 1020 nm [39] and the fine and coarse mode volume concentrations (v_f and v_c, respectively; 40, 41). According to Dubovik et al. [42] [43] the retrieval of the particle volume size distribution was demonstrated to be adequate in practically all situations with AOT > 0.05, which was also the case for the observations reported here. Cloud screened and quality assured level 2.0 data products were used in this work. The uncertainties of the AOT were < 0.02 for UV wavelengths and < 0.01 for wavelengths above 440 nm [44].

2.2.7. PARTICLE MASS CONCENTRATION PROFILES DERIVED BY THE LIDAR MEASUREMENTS AND THE POLIPHON METHOD

The mass concentration profiles from the LIDAR measurements were calculated using the POLIPHON method [8] as stated above. In the first step of the method, the contribution of the fine-mode and coarse mode particles to the total backscatter coefficient (β_t) is calculated based on depolarization measurements [45]. Here we assumed an externally-mixed aerosol consisting of a fine component with low depolarization (5 ± 1%; 8), and a coarse component that induces light depolarization of 31 ± 4% [7], corresponding to dust particles. The dust-related backscatter coefficient was determined as:

$$\beta_d = \beta_t \frac{(\delta_t - \delta_{nd})(1+\delta_d)}{(\delta_d - \delta_{nd})(1+\delta_t)} \ , \tag{2.1}$$

where δ_t, δ_{nd} and δ_d are respectively the observed total depolarization ratio, the assumed non-dust depolarization ratio and the measured depolarization ratio of dust particles. Once β_d was determined, the non-dust backscatter coefficient was calculated by $\beta_{nd} = \beta_t - \beta_d$. In the calculations presented here we used β and δ^p values corresponding to 532 nm wavelength.

In the second step of the method, the mass concentrations of the fine (non-dust; m_{nd}) and coarse (dust; m_d) aerosol fractions are calculated according to [8]:

$$m_d = \rho_d \, (\overline{v_c/\tau_c}) \, \beta_d S_d \tag{2.2}$$

$$m_{nd} = \rho_{nd} \, (\overline{v_f/\tau_f}) \, \beta_{nd} S_{nd} \ , \tag{2.3}$$

where ρ is the mass density, whereas the product of the backscattering coefficient and the LIDAR ratio $\beta \cdot S$ is the extinction coefficient of the particles, with subscripts d and nd denoting dust (coarse) and non-dust (fine) particles. It should be noted that the factors $\overline{v_c/\tau_c}$ and $\overline{v_f/\tau_f}$ are used to convert the extinction measurements to particle volume concentration for the coarse and the fine faction, respectively. In this work these factors were determined from the daily mean data of the sunphotometer that was collocated with the LIDAR. The volume concentrations v_f and v_c were obtained from the AERONET data, whereas the fine and coarse mode AOTs, τ_f and τ_c, at 532 nm wavelength, were calculated using Å (determined in the 440-675 wavelength range) according to:

$$\tau_{f,c(532)} = \tau_{f,c(440)} \times \left(\frac{440}{532}\right)^{\mathring{A}_{f,c(440-675)}} \tag{2.4}$$

Another assumption we made was that the LIDAR-derived dust and non-dust fractions are identical to the photometer-derived coarse and fine particle fractions. The inflection point of the AERONET data was adopted as the limit between the fine and the coarse mode particles. As a result, the fine mode ranged between 0.05 and 0.5 μm (particle radius) and the coarse mode between 0.5 and 15 μm as shown in Fig. 2.3. The calculated values of $\overline{v_f/\tau_f}$ and $\overline{v_c/\tau_c}$ (cf. Table 2.1) are in line with the conversion factors mentioned by Mamouri and Ansmann [46, 47] who performed an extensive analysis of the conversion factors of dust over Cyprus.

Apart from v/τ, the other parameters required for determining the aerosol mass concentration from the LIDAR measurements are ρ, β and S. Regarding ρ, we used a density

of 2.6 ± 0.6 g cm^{-3} for the coarse mode particles (corresponding to dust [48]). Chemical analysis of filter samples collected during the measurements showed that the dust density assumed here is valid (data not shown). Values for S_{nd} (60 ± 10 sr) were taken from the literature [49], and actual measurements were used for S_d. S_d measurements were only possible during night-time when the Raman channels were operating. We measured the same S_d values (47 ± 10 sr) for both events analyzed here. All the values of the parameters that are required as input for the calculations are summarized in Table 2.1 .

2.2.8. POLIPHON METHOD - ERROR ESTIMATION

The uncertainties of β_d and β_{nd} in Equation (2.1) were calculated using the Monte-Carlo method [50]. For each input parameter, we generated 100 normally distributed random numbers. The values provided in Table 1 were used as the mean parameter and the standard deviation of the normal distributions. Then, 100 β_d and β_{nd} values were calculated for each point in the atmospheric column and from these the mean values and the standard deviations (errors) of β_d and β_{nd} were estimated to be 22% and 28%, respectively. For equations (2.2) and (2.3) the uncertainties were calculated analytically using the error propagation law.

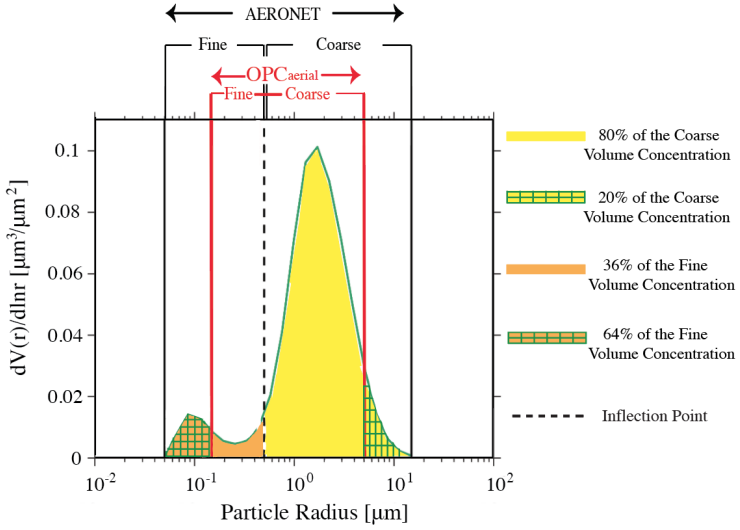

Figure 2.3: Column-integrated volume size distribution measured with the sunphotometer over Nicosia at 06:57 UTC on 15 April 2016. The ranges of particle sizes measured by AERONET sunphotometers, and by the OPC$_a$ are also indicated in the figure.

Table 2.1: Values of the input parameters used in the POLIPHON algorithm.

Parameter	**Symbol**	**Values**	**Source/Reference**
Dust depolarization ratio	δ_d	$31 \pm 4\%$	[7]
Non-dust depolarization ratio	δ_{nd}	$5 \pm 1\%$	[8]
Dust LIDAR ratio	S_d	47 ± 10 sr	Raman measurements
Non-dust LIDAR ratio	S_{nd}	60 ± 10 sr	[49]
Dust particle density	ρ_d	$2.6 \pm 0.6\ g\ cm^{-3}$	[51]
Dust conversion factor (15.04.2016)	$\frac{v_c}{\tau_c}$	$0.67 \pm 0.05 \times 10^{-6}$	Sunphotometer
Non-dust conversion factor (15.04.2016)	$\frac{v_f}{\tau_f}$	$0.24 \pm 0.018 \times 10^{-6}$	Sunphotometer
Dust conversion factor (22.04.2016)	$\frac{v_c}{\tau_c}$	$0.81 \pm 0.04 \times 10^{-6}$	Sunphotometer
Non-dust conversion factor (22.04.2016)	$\frac{v_f}{\tau_f}$	$0.14 \pm 0.019 \times 10^{-6}$	Sunphotometer

2.3. RESULTS AND DISCUSSION

2.3.1. HOMOGENEITY OF AEROSOL PROPERTIES OVER THE MEASUREMENT SITES

Given the proximity (6.5 km) of the ground (at CAO) and the airborne in-situ observations (at Orounda), as well as the absence of any strong pollution sources in the region, the measurements were considered to correspond to the same air parcel in terms of atmospheric composition. The third measurement location (Nicosia) was situated 35 km away from the airfield. As suggested by the comparison of sunphotometer measurements at Nicosia and CAO, however, all locations were affected by the same air masses with minor influence from local emissions that were mostly trapped within the Planetary Boundary Layer (PBL).

Figure 2.4 shows the AOT_{500} and the $Å_{440-870}$ measured by the sunphotometers in Nicosia and at CAO from 13 to 24 April 2016 when concurrent measurements were performed at the two locations. Overall, the temporal variability of these two parameters observed at Nicosia was very similar with the respective measurements at CAO, exhibiting correlations coefficients of 0.89 and 0.87 for AOT_{500} and $Å_{440-870}$, respectively. This good correlation was further enhanced during the dust event cases (e.g., on 15 April 2016) when the relative contribution of the aerosol fine mode was minimized, supporting that a comparison of aerosol measurements at these locations is meaningful. In terms of absolute values, AOT_{500} was 15-50% higher at Nicosia compared to CAO, even during the cases with the dust events, when coarse particles dominated. These higher values at Nicosia are mainly due to the altitudinal difference between the sites (Nicosia is at an altitude of 190 m whereas CAO at 535 m above sea level) and the contribution of the local aerosol sources to the total aerosol burden. This was further justified by the higher $Å_{440-870}$ measurements at Nicosia which signify the presence of small aerosol particles from anthropogenic sources.

2.3.2. COMPARISON OF THE MASS CONCENTRATION MEASUREMENTS

A total of 6 UAV flights with OPC_a on-board were performed during the entire campaign. However, only 2 fulfilled all the necessary requirements for comparison with the LIDAR observations. Those requirements are that 1) there are simultaneous measurements of LIDAR and OPC_a, 2) there are cloud-free conditions or clouds are above 7-8 km altitude so that the LIDAR retrievals can be made, 3) there is enough dust loading, 4) there is availability of AERONET data, and 5) the airborne in-situ measurements were performed before the full development of the PBL. All these requirements were fulfilled during the measurements on 15 and 22 April 2016, which are analyzed below.

CASE STUDY I: 15 APRIL 2016

The atmospheric situation over South-Eastern Europe on 15 April 2016 was dominated by a high-pressure system resulting in mostly cloud-free conditions over Cyprus. A dust event of moderate intensity was observed, resulting in an average AOT_{500} value of 0.4 over Nisosia and CAO (cf. discussion in Section 2.3.1 and Fig. 2.4). Figure 2.5 shows the LIDAR time-height display during that day, with the upper panel showing the range-corrected signal of the 1064-nm channel, which provides information about the aerosol loading and the presence of clouds, and the lower panel the linear volume depolarization

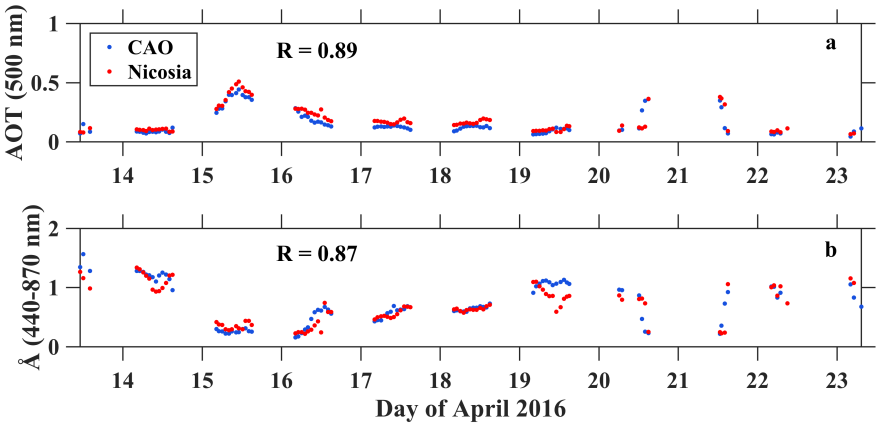

Figure 2.4: (a) AOT_{500} and (b) $Å_{440-870}$ as measured with the sun-photometers at CAO (blue circles) and Nicosia (red circles) from 13 to 24 April 2016.

ratio δ^v at 532 nm, which is used to discriminate particles of different shapes that can be indicative of different sources. Throughout the day, high concentrations of aerosol particles were observed even up to ca. 7 km altitude (Fig. 2.5a), with a persistent aerosol layer extending from 2.5 to ca. 7 km. Backtrajectory analysis (cf. Fig. 2.6) corroborated that this layer resulted from a Saharan dust event that originated in Algeria and traveled over Italy, Greece and Turkey before reaching Cyprus. Despite passing over polluted areas, the core of the dust layer remained pure (see analysis below) due to its high elevation (>2 km) throughout the path. The δ^v plot (Fig. 2.5b) also shows the temporal evolution of this dust layer. From 00:00-03:00 UTC the dust extends from 2 to 7 km altitude, but later (until 14:00 UTC) it becomes shallower. From the early morning hours (07:00 UTC) to early afternoon (14:00 UTC) when the boundary layer develops, the dust layer is confined above it, reaching up to 5 km altitude. After the collapse of the boundary layer, the dust layer starts to descend and finally reaches the ground at 18:00 UTC.

The cloud-free and time homogeneous atmospheric scene between 07:00 and 07:50 UTC, which overlapped with the time window of the UAV flight, was selected for calculating the parameters of the atmospheric aerosol using the POLIPHON method. As mentioned earlier, the S_d values used as input in POLIPHON were not measured at the same time window (07:00 and 07:50 UTC), but they were derived from night-time measurements. However, back-trajectory analysis verified that the LIDAR was measuring the same air mass type during these time spans (Fig. 2.6). The LIDAR profiles of β (retrieved with the Fernald-Klett method; Section 2.2.5) and δ^p, that were used as input in POLIPHON (532 nm only), are shown in Fig. 2.7a-b. The backscatter signal increased gradually from 1 $Mm^{-1}sr^{-1}$ at 1 km (532 nm), reaching a maximum of ca. 2.3 $Mm^{-1}sr^{-1}$ at 3 km where the dust layer core was. The pure dust layer spanned from ca. 2.5 to 3.8 km ($\delta^p \sim 30\pm2\%$) while below 2 km, the dust was mixed with almost spherical particles, probably from the residual layer, as indicated by the relatively low δ^p values ranging between 12% and 30%. Figure 2.7c shows the POLIPHON-derived dust and non-dust related backscatter coefficients β_d and β_{nd} from Equation (2.1), and respective uncer-

tainties determined by Monte-Carlo calculations (cf. Section 2.2.8). The backscatter coefficient of the fine-mode particles β_{nd} decreased with altitude, while the dust particles were present even down to 0.7 km. As discussed in Section 2.2.5, the LIDAR ratio value used in the Fernald-Klett retrieval and the LIDAR ratio corresponding to the dust particles S_d that is required as input in the POLIPHON algorithm, were estimated from Raman LIDAR measurements performed between 00:00-01:40 UTC (UTC+3 local time), just before sunrise. It should be noted here that Raman measurements are only possible at night as during the day scattered sunlight induces high background noise signal. The fact that the dust layer observed during the Raman measurements had the same origin and followed the same atmospheric path before reaching the measurement site between 07:00-07:50 UTC was confirmed by back-trajectory analysis (Fig. 2.6).

Vertical profiles of the RH measured with the UAV and predicted by the WRF−ARW atmospheric model [52] showed that the atmosphere was dry enough (RH $\lesssim$ 50%) at the ground level and up to 4 km altitude (Fig. 2.7d). As a result we could safely assume that the aerosol particles were dry and thus changes in the mass density and backscatter coefficient due to water uptake were negligible.

CASE STUDY II: 22 APRIL 2016

Contrary to Case Study I, a low intensity dust event (AOT_{500} = 0.1) was recorded over Cyprus on 22 April 2016. The evolution of the boundary layer dominating the atmospheric situation that day is depicted in the LIDAR time-height plots shown in Fig. 2.8. From 00:00 to 10:00 UTC a sparse dust layer extended between 1 and 2 km a.g.l. while after the PBL decay a shallower dust plume was observed between 1 and 1.5 km altitude. According to the back-trajectory analysis (Fig. 2.9) the dust air mass at 1.5 km originated from Egypt at the ground level, then it was elevated and passed over Libya, the Mediterranean and Turkey before reaching Cyprus.

The UAV flight on that day was performed between 04:22 and 05:16 UTC. The atmospheric scene between 04:20-05:00 UTC (Fig. 2.8) was selected for the comparison due to its stable conditions above 0.8 km. Also in this case, the same procedure as in case I was followed to retrieve the LIDAR profiles that were used as input in the POLIPHON algorithm. The backscatter coefficient, the particle depolarization ratio, the POLIPHON-derived dust and non-dust related backscatter coefficients as well as the RH profiles of this atmospheric scene are shown in Fig. 2.10. In contrast to the estimated δ^p values determined from the measurements on 15 April, here δ^p_{532} decreases gradually with height from 0.8 to 2 km having values between 10-17%. These relatively low δ^p_{532} values indicate a mixture of Saharan dust with spherical continental/pollution particles. This is supported by the paths that the air mass follow between 1-2 km which originated from north-eastern Africa close to Cairo and Alexandria. The LIDAR ratio of 40 ± 7 Sr, measured during the previous night (at a height where the signal is mostly free of noise; i.e. 1.2-1.4 km), agrees with the findings of [55] and [56] who reported respectively that S_{532} = 40 ± 5 Sr and S_{532} = 47 Sr for dust originating from eastern Sahara.

PARTICLE MASS CONCENTRATION PROFILES

Figures 2.11 a and 2.11 c show the mass concentration profiles for the coarse particles (particles larger than 0.5 μm in radius) as derived by the LIDAR observations using POLIPHON method for inversion, and the OPC_a measurements. The LIDAR profiles,

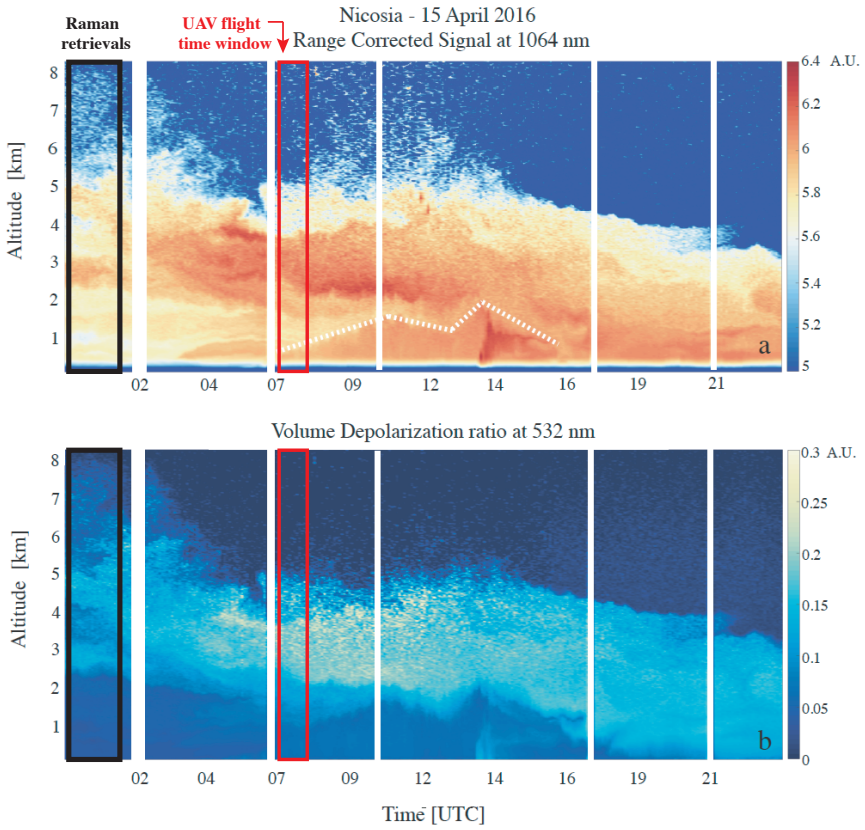

Figure 2.5: Range-corrected LIDAR signal at 1064 nm (a) and Volume Linear Depolarization ratio (b) reflecting the atmospheric conditions over Nicosia on 15 April 2016. Blue color indicates weak backscattering, yellow-red colors in the range corrected LIDAR signal (a) indicate backscattering mainly from fine aerosols and dust, whereas the dotted line shows the PBL top. The LIDAR observations used for the comparison with the UAV measurements were those recorded between 07:00-07:50 UTC.

were calculated by Equations (2.2) and (2.3) using the measured β_d and β_{nd}, profiles and the dust density values from the literature (cf. Table 2.1). The respective OPC_a profiles were determined by the recorded particle number size distributions assuming the same dust particle density (cf. Section 2.2.4 for details). To ensure that the LIDAR observations are representative of the atmospheric aerosol over Orounda and over CAO we compare the data for altitudes higher than 0.8 km a.s.l. during morning hours when the PBL was shallow.

The mass concentration profiles from the LIDAR and the OPC_a observed on 15 April 2016 (Fig. 2.11 a), show a good correlation, with R = 0.9. In terms of absolute values, the mass concentrations measured by the OPC_a (red curve) lie within the uncertainty limits (38%) of the LIDAR observations, with the former being equal or lower for the entire range of altitudes, exhibiting a bias ranging from -23.0 to -2.4 $\mu g\ m^{-3}$ with a mean

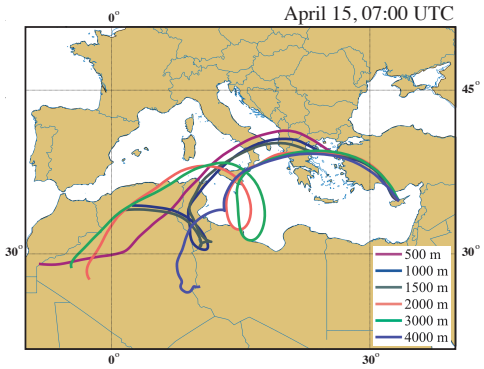

Figure 2.6: Back-trajectories of the air masses arriving at several altitudes over Cyprus on April 15, 07:00 (UTC). The back-trajectories were calculated for a duration of 5 days using the HYSPLIT transport and dispersion model [53, 54] with GDAS ° meteorological data through the Real-time Environmental Applications and Display sYstem (READY; http://ready.arl.noaa.gov/index.php).

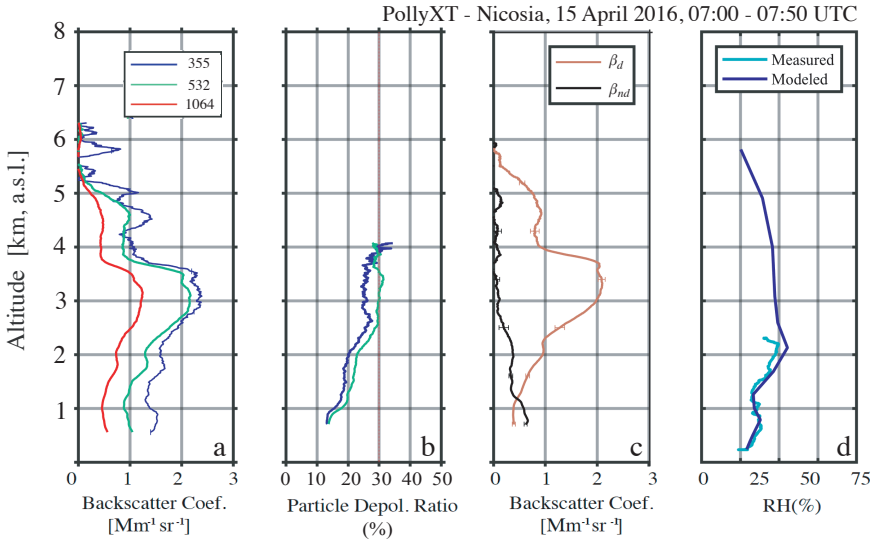

Figure 2.7: Day-time profiles of β (355-, 532-, and 1064-nm wavelength) (a) δ^p (355- and 532-nm wavelength) (b) β_d and β_{nd} (c) determined by POLIPHON, as well as RH profiles from in-situ measurements on-board the UAV and from WRF–ARW model simulations over Nicosia at 08:00 UTC (d).

of -12.0 μg m^{-3} (Fig. 2.11 b). The discrepancies between the two methods can be partly attributed to the assumptions used in POLIPHON: 1) constant S throughout the atmospheric column, 2) contribution in the coarse mode only from depolarizing particles, and 3) the assumption of an externally-mixed aerosol. Assumptions used for the manipulation of the OPC measurements that can explain differences between the two methods are mainly related to the refractive index and the shape of the particles. The refractive

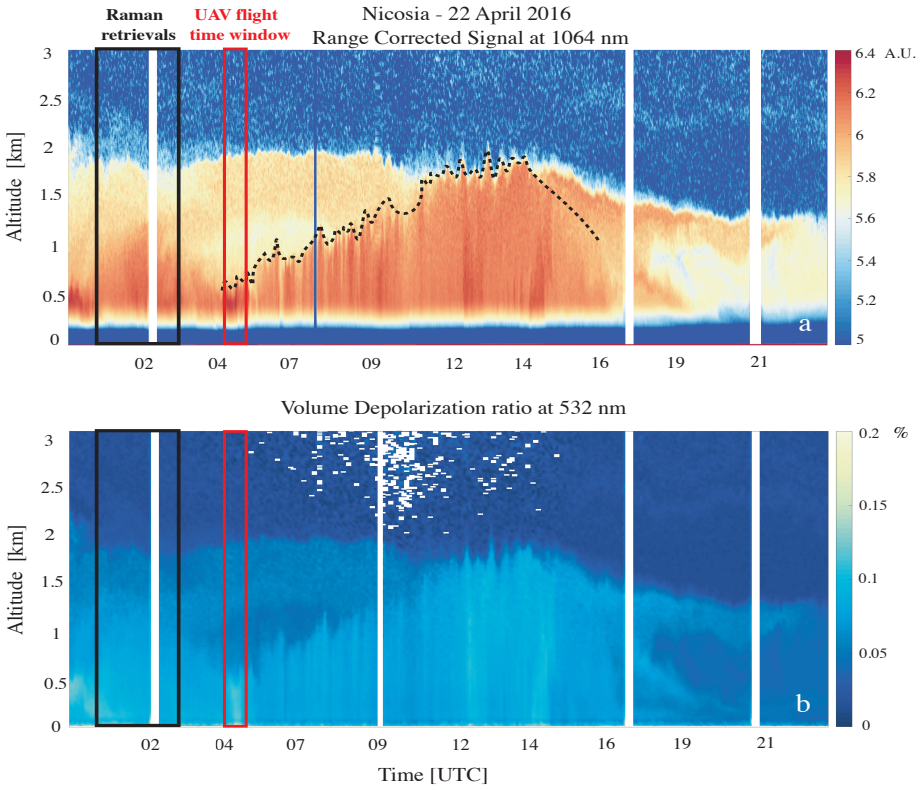

Figure 2.8: Range-corrected LIDAR signal at 1064 nm (a) and Volume Linear Depolarization ratio (b) reflecting the atmospheric conditions over Nicosia on 22 April 2016. Blue color indicates weak backscattering, yellow-red colors in the range corrected LIDAR signal (a) indicate backscattering mainly from fine aerosols and dust, whereas the dotted line shows the PBL top. The LIDAR observations used for the comparison with the UAV measurements were those recorded between 04:22-05:00 UTC.

index can notably influence the size distribution measured by the OPC, inducing sizing uncertainties of up to 30% [14, 57]. The refractive index used for calibrating OPC$_a$, however, has a value of for n = 1.59, which is very close to literature values for Saharan dust (n = 1.56; 58). The difference between the refractive index values used for the calibration of OPC$_a$ and that used for the retrieval of the LIDAR measurements is estimated to introduce a bias of 2% to the calculated mass concentration values. Regarding particle shape, the effect of non-sphericity the particle sizing by light-scattering instruments having similar scattering angle range that of OPC$_a$ (90°±60°) is within less than 20%, with a tendency towards undersizing [59].

Another source of discrepancy between the mass concentrations determined by OPC$_a$ and the LIDAR is the limitation of the former to measure particles larger than a few tens of microns due to aerodynamic inlet loses (sedimentation and inertial deposition), resulting in an underestimation of 20% of the coarse mode volume concentration (cf. yellow-green hatched area in Fig. 2.3). To account for that, we corrected the OPC$_a$ mea-

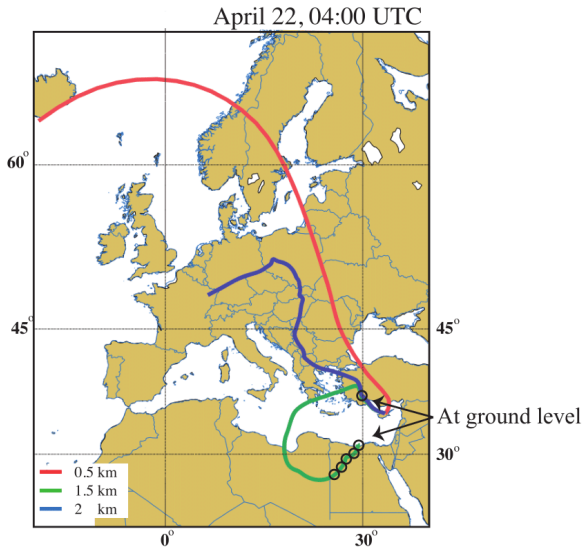

Figure 2.9: Back-trajectories of the air masses arriving at 500 m, 1000 m and 1500 m over Cyprus at 04:00 UTC on April 22. The back-trajectories were calculated for a duration of 6 days; the black circles indicate the locations where the air-mass was below 100 m altitude.

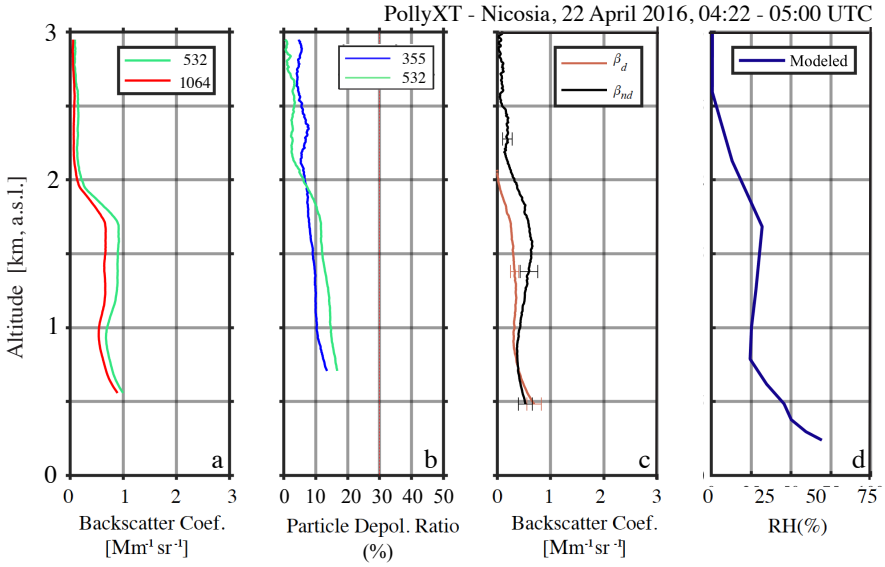

Figure 2.10: Day-time profiles of β (532-, and 1064-nm wavelength) (a) δ^p (355- and 532-nm wavelength) (b) β_d and β_{nd} (c) determined by POLIPHON, as well as RH profiles from WRF–ARW model over Nicosia at 04:00 UTC (d). The 355 nm channel of the LIDAR was discarded due to misalignment.

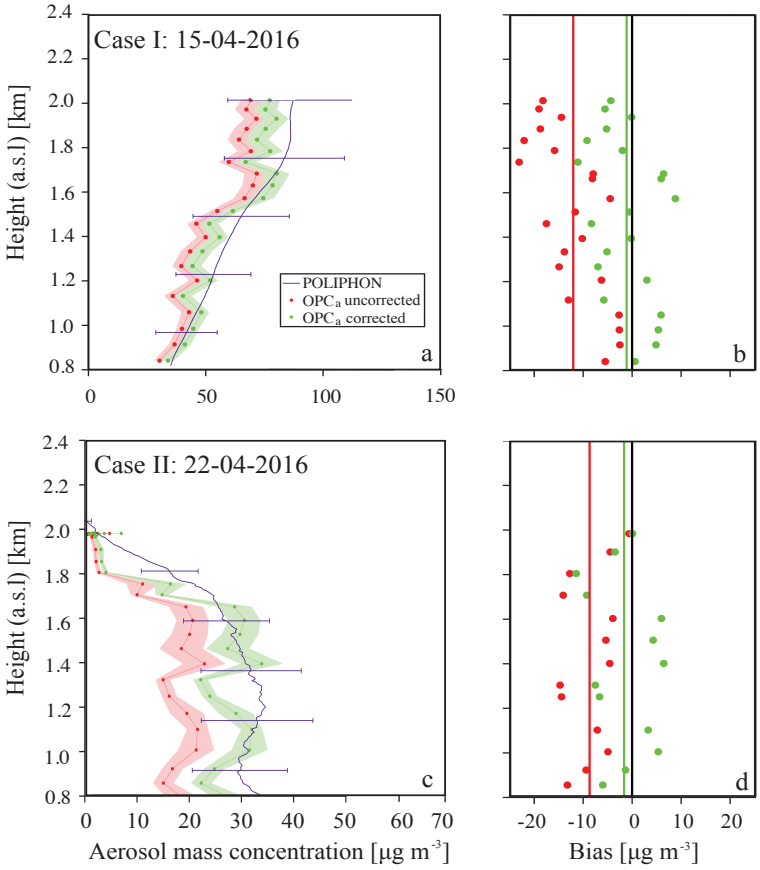

Figure 2.11: Aerosol mass concentration profiles for case study I and II (a, c) and the respective biases (b, d). In plots (a) and (c), the blue solid lines represent the mass concentration derived by the POLIPHON. The mass concentration measured by the OPC$_a$ is plotted in red with the red shaded area representing the uncertainties of the in-situ measurement. The green lines show the mass concentration from the OPC$_a$ corrected for the particles losses. In plots (b) and (d), the red dots show the biases between the values measured by the OPC$_a$ and the LIDAR (OPC$_a$ − LIDAR) before applying the corrections, while the green dots are the biases after corrections. The red and green solid lines show the mean biases before and after correction, respectively.

surements using the formula: $m_{\mathrm{OPC}} = m_{\mathrm{POLIPHON}} \frac{\int_{\mathrm{OPC}_a} dV/d\ln r}{\int_{\mathrm{POLIPHON}} dV/d\ln r}$. This correction significantly improved the agreement between the OPC_a (green curve in Fig. 2.11a) and the LIDAR measurements, constraining the bias range to -11.1 and 8.8 μg m^{-3} which results in a decreased mean bias of -1.1 μg m^{-3}. Further statistical analysis between the LIDAR and the corrected OPC_a measurements showed that our hypothesis that the two observations refer to the same aerosol population is valid. To be more specific, the two-tailed T-test yielded a P-value of 0.70 (assuming equal variances), indicating that the differences between the mean values of the two types of observations are not statistically significant.

The mass concentration profiles determined by the LIDAR and the OPC_a measurements on 22 April 2016 (Fig. 2.11 c) also show a good correlation, with R =0.9. In terms of absolute values, the mass concentrations determined by the OPC_a measurements (green line) are lower compared to those determined by the LIDAR observations for the entire range of altitudes, exhibiting biases in the range from -14.7 to 0.6 μg m^{-3} with a mean value of -8.7 μg m^{-3} (Fig. 2.11 d). The integrated volume size distribution measured by the sunphotomer in Nicosia showed that in this case the OPC_a underestimates the coarse volume fraction by 48%. Upon correction, the mean bias decreases to -1.6 μg m^{-3} and, with the exception of one point at 1.8 km altitude, the mass concentration values from the OPC_a lie within the calculated uncertainty resulting from the POLIPHON algorithm used to invert the LIDAR data (32%). At higher altitudes the mass concentration decreases drastically and OPC_a measurements drop below the POLIPHON uncertainty limits. Also in this case, the two-tailed t-test (assuming equal variances) yielded a p-value of 0.05 indicating marginal statistically insignificant differences between the means of the two types of measurements.

Overall, the airborne in-situ and LIDAR observations are in good agreement both during the observation of a dense as well as of a weak dust event, after the necessary corrections for the OPC_a measurements. In the case of the moderate dust event the volume concentration fraction that is not captured by the OPC range is small and so is the corresponding correction. In contrast, during the weak dust event, the OPC misses almost 50% of the volume size distribution which introduces large measurement ambiguities.

2.4. SUMMARY AND CONCLUSIONS

In this study we compare, for the first time to our knowledge, vertical profiles of the aerosol mass concentrations determined independently by an OPC onboard a UAV and by remote sensing observations using data from a LIDAR and a sunpohotometer. The measurements were performed during two cases of dust events that occurred in the region of the Eastern Mediterranean on 15 and 22 April 2016. During those days, the UAV flew up to ca. 2 km altitude with the OPC measuring the size distributions of sampled aerosol particles having radii in the range 0.15-5 μm, from which the aerosol mass concentration was calculated. The same information was retrieved by the concurrent LIDAR and sunphotometer measurements that were inverted using the POLIPHON method.

During the measurements on 15 April 2016 the dense dust layer extended from 2 to 4 km, while a mixture of dust and almost spherical particles was observed below 2 km. The mass concentration of the coarse mode particles increased from 30 μg m^{-3}, at ca. 0.8

km, to ca. 70 μg m^{-3}, at ca. 1.8 km. Agreement between the in-situ measurements and the LIDAR observations retrieved with the POLIPHON method was very good (R = 0.9), with the in-situ measurements lying within the POLIPHON uncertainty limits (38%), exhibiting a mean bias of -12.0 μg m^{-3} that can be mainly attributed to the difference in the cut-off diameters measured by the two techniques. Corrections applied to account for this difference in the cut-off diameters further enhanced the agreement, decreasing the mean bias to -1.1 μg m^{-3}.

In the measurements carried out on 22 April 2016, a sparse dust layer was observed between 0.8-2 km altitude during the morning hours. Information from the LIDAR measurements and the backtrajectory analysis suggests that this layer was a mixture of desert dust with continental/pollution particles. Despite that, however, agreement between the airborne in-situ and remote sensing measurements in this case was also very good (R = 0.9). In terms of absolute values, the corrected mass concentrations measured by the airborne OPC were equal or lower than those derived from the LIDAR measurements for the entire range of altitudes and exhibited a mean bias of -1.6 μg m^{-3}. The concentrations measured by the airborne OPC were within the calculated uncertainty of POLIPHON.

The measurements reported here indicate that unmanned airborne OPC measurements and LIDAR observations can provide reliable ways to determine coarse mode aerosol mass concentration profiles in the atmospheric column, thereby bridging the gap between in-situ and remote sensing observations. Considering that both methods can provide dense datasets in a cost-effective manner and on a regular basis, this finding paves the way towards their systematic exploitation in climate models.

REFERENCES

[1] U. Lohmann and J. Feichter, *Global indirect aerosol effects: a review,* Atmospheric Chemistry and Physics Discussions **4**, 7561 (2004).

[2] I. C. IPCC, *The physical science basis. contribution of working group i to the fifth assessment report of the intergovernmental panel on climate change,* (2013).

[3] J. D. Klett, *Stable analytical inversion solution for processing lidar returns,* Applied Optics **20**, 211 (1981).

[4] F. G. Fernald, *Analysis of atmospheric lidar observations- some comments,* Applied optics **23**, 652 (1984).

[5] A. Ansmann, M. Riebesell, and C. Weitkamp, *Measurement of atmospheric aerosol extinction profiles with a raman lidar,* Optics letters **15**, 746 (1990).

[6] A. Ansmann, U. Wandinger, M. Riebesell, C. Weitkamp, and W. Michaelis, *Independent measurement of extinction and backscatter profiles in cirrus clouds by using a combined raman elastic-backscatter lidar,* Applied Optics **31**, 7113 (1992).

[7] V. Freudenthaler, M. Esselborn, M. Wiegner, B. Heese, M. Tesche, A. Ansmann, D. Müller, D. Althausen, M. Wirth, A. Fix, *et al.*, *Depolarization ratio profiling at several wavelengths in pure saharan dust during samum 2006,* Tellus B **61**, 165 (2009).

[8] A. Ansmann, M. Tesche, P. Seifert, S. Gross, V. Freudenthaler, A. Apituley, K. Wilson, I. Serikov, H. Linné, B. Heinold, *et al.*, *Ash and fine-mode particle mass profiles from earlinet-aeronet observations over central europe after the eruptions of the eyjafjallajökull volcano in 2010,* Journal of Geophysical Research: Atmospheres **116** (2011).

[9] A. Lopatin, O. Dubovik, A. Chaikovsky, P. Goloub, T. Lapyonok, D. Tanré, and P. Litvinov, *Enhancement of aerosol characterization using synergy of lidar and sun-photometer coincident observations: the garrlic algorithm,* Atmospheric Measurement Techniques **6**, 2065 (2013).

[10] A. Chaikovsky, O. Dubovik, B. Holben, A. Bril, P. Goloub, D. Tanré, G. Pappalardo, U. Wandinger, L. Chaikovskaya, S. Denisov, *et al.*, *Lidar-radiometer inversion code (liric) for the retrieval of vertical aerosol properties from combined lidar/radiometer data: development and distribution in earlinet,* Atmospheric Measurement Techniques **9**, 1181 (2016).

[11] G. Feingold and B. Morley, *Aerosol hygroscopic properties as measured by lidar and comparison with in situ measurements,* Journal of Geophysical Research: Atmospheres **108** (2003).

[12] B. Weinzierl, D. Sauer, M. Esselborn, A. Petzold, A. Veira, M. Rose, S. Mund, M. Wirth, A. Ansmann, M. Tesche, *et al.*, *Microphysical and optical properties of dust and tropical biomass burning aerosol layers in the cape verde region—an overview of the airborne in situ and lidar measurements during samum-2,* Tellus B **63**, 589 (2011).

[13] J. A. Bravo-Aranda, G. Titos, M. J. Granados-Muñoz, J. L. Guerrero-Rascado, F. Navas-Guzmán, A. Valenzuela, H. Lyamani, F. J. Olmo, J. Andrey, and L. Alados-Arboledas, *Study of mineral dust entrainment in the planetary boundary layer by lidar depolarization technique,* Tellus B **67** (2015).

[14] M. J. Granados-Muñoz, J. A. Bravo-Aranda, D. Baumgardner, J. L. Guerrero-Rascado, D. Pérez-Ramírez, F. Navas-Guzmán, I. Veselovskii, H. Lyamani, A. Valenzuela, F. J. Olmo, *et al.*, *A comparative study of aerosol microphysical properties retrieved from ground-based remote sensing and aircraft in situ measurements during a saharan dust event,* Atmospheric Measurement Techniques **9**, 1113 (2016).

[15] B. Rosati, E. Herrmann, S. Bucci, F. Fierli, F. Cairo, M. Gysel, R. Tillmann, J. Größ, G. P. Gobbi, L. Di Liberto, *et al.*, *Studying the vertical aerosol extinction coefficient by comparing in situ airborne data and elastic backscatter lidar,* Atmospheric Chemistry and Physics **16**, 4539 (2016).

[16] P. Kokkalis, V. Amiridis, J. D. Allan, A. Papayannis, S. Solomos, I. Binietoglou, A. Bougiatioti, A. Tsekeri, A. Nenes, P. D. Rosenberg, *et al.*, *Validation of liric aerosol concentration retrievals using airborne measurements during a biomass burning episode over athens,* Atmospheric Research **183**, 255 (2017).

[17] A. Tsekeri, V. Amiridis, F. Marenco, A. Nenes, E. Marinou, S. Solomos, P. Rosenberg, J. Trembath, G. J. Nott, J. Allan, *et al.*, *Profiling aerosol optical, microphysical and hygroscopic properties in ambient conditions by combining in situ and remote sensing,* Atmospheric Measurement Techniques **10**, 83 (2017).

[18] B. Altstädter, A. Platis, B. Wehner, A. Scholtz, N. Wildmann, M. Hermann, R. Käthner, H. Baars, J. Bange, and A. Lampert, *Aladina-an unmanned research aircraft for observing vertical and horizontal distributions of ultrafine particles within the atmospheric boundary layer,* Atmospheric Measurement Techniques **8**, 1627 (2015).

[19] S. Bezantakos, L. Huang, K. Barmpounis, M. Attoui, A. Schmidt-Ott, and G. Biskos, *A cost-effective electrostatic precipitator for aerosol nanoparticle segregation,* Aerosol Science and Technology **49**, iv (2015).

[20] K. Barmpounis, A. Maisser, A. Schmidt-Ott, and G. Biskos, *Lightweight differential mobility analyzers: Toward new and inexpensive manufacturing methods,* Aerosol Science and Technology **50**, 2 (2016).

[21] J. M. Brady, M. D. Stokes, J. Bonnardel, and T. H. Bertram, *Characterization of a quadrotor unmanned aircraft system for aerosol-particle-concentration measurements,* Environmental science & technology **50**, 1376 (2016).

[22] J.-B. Renard, F. Dulac, G. Berthet, T. Lurton, D. Vignelles, F. Jégou, T. Tonnelier, M. Jeannot, B. Couté, R. Akiki, *et al.*, *Loac: a small aerosol optical counter/sizer for ground-based and balloon measurements of the size distribution and nature of atmospheric particles–part 2: First results from balloon and unmanned aerial vehicle flights,* Atmospheric Measurement Techniques **9**, 3673 (2016).

[23] N. Surawski, S. Bezantakos, K. Barmpounis, M. Dallaston, A. Schmidt-Ott, and G. Biskos, *A tunable high-pass filter for simple and inexpensive size-segregation of sub-10-nm nanoparticles,* Scientific Reports **7**, 45678 (2017).

[24] S. Bezantakos, F. Schmidt-Ott, and G. Biskos, *Performance evaluation of the cost-effective and lightweight alphasense optical particle counter for use onboard unmanned aerial vehicles,* Aerosol Science and Technology , 1 (2017).

[25] J. Lelieveld, H. Berresheim, S. Borrmann, P. Crutzen, F. Dentener, H. Fischer, J. Feichter, P. Flatau, J. Heland, R. Holzinger, *et al.*, *Global air pollution crossroads over the mediterranean,* Science **298**, 794 (2002).

[26] J. Taylor, *Introduction to error analysis, the study of uncertainties in physical measurements* (1997).

[27] D. Althausen, R. Engelmann, H. Baars, B. Heese, A. Ansmann, D. Müller, and M. Komppula, *Portable raman lidar pollyxt for automated profiling of aerosol backscatter, extinction, and depolarization,* Journal of Atmospheric and Oceanic Technology **26**, 2366 (2009).

[28] R. Engelmann, T. Kanitz, H. Baars, B. Heese, D. Althausen, A. Skupin, U. Wandinger, M. Komppula, I. S. Stachlewska, V. Amiridis, E. Marinou, I. Mattis, H. Linné, and A. Ansmann, *The automated multiwavelength raman polarization and water-vapor lidar polly^{XT}: the next generation,* Atmospheric Measurement Techniques **9**, 1767 (2016).

[29] C. Böckmann, U. Wandinger, A. Ansmann, J. Bösenberg, V. Amiridis, A. Boselli, A. Delaval, F. De Tomasi, M. Frioud, I. V. Grigorov, *et al.*, *Aerosol lidar intercomparison in the framework of the earlinet project. 2. aerosol backscatter algorithms,* Applied Optics **43**, 977 (2004).

[30] J. Bösenberg and D. J. Brassington, *Instrument development for atmospheric research and monitoring: lidar profiling, DOAS and tunable diode laser spectroscopy*, Vol. 8 (Springer Science & Business Media, 1997).

[31] A. Comerón, F. Rocadenbosch, M. A. López, A. Rodríguez, C. M. noz, D. García-Vizcaíno, and M. Sicard, *Effects of noise on lidar data inversion with the backward algorithm,* Appl. Opt. **43**, 2572 (2004).

[32] F. Rocadenbosch, M. N. M. Reba, M. Sicard, and A. Comerón, *Practical analytical backscatter error bars for elastic one-component lidar inversion algorithm,* Applied optics **49**, 3380 (2010).

[33] D. Whiteman, S. Melfi, and R. Ferrare, *Raman lidar system for the measurement of water vapor and aerosols in the earth?s atmosphere,* Applied Optics **31**, 3068 (1992).

[34] T. Murayama, H. Okamoto, N. Kaneyasu, H. Kamataki, and K. Miura, *Application of lidar depolarization measurement in the atmospheric boundary layer: Effects of dust and sea-salt particles,* Journal of Geophysical Research: Atmospheres **104**, 31781 (1999).

[35] T. Sakai, T. Shibata, S.-A. Kwon, Y.-S. Kim, K. Tamura, and Y. Iwasaka, *Free tropospheric aerosol backscatter, depolarization ratio, and relative humidity measured with the raman lidar at nagoya in 1994–1997: contributions of aerosols from the asian continent and the pacific ocean,* Atmospheric Environment **34**, 431 (2000).

[36] A. Shimizu, N. Sugimoto, I. Matsui, K. Arao, I. Uno, T. Murayama, N. Kagawa, K. Aoki, A. Uchiyama, and A. Yamazaki, *Continuous observations of asian dust and other aerosols by polarization lidars in china and japan during ace-asia,* Journal of Geophysical Research: Atmospheres **109** (2004).

[37] N. Sugimoto and C. H. Lee, *Characteristics of dust aerosols inferred from lidar depolarization measurements at two wavelengths,* Applied optics **45**, 7468 (2006).

[38] B. N. Holben, T. Eck, I. Slutsker, D. Tanre, J. Buis, A. Setzer, E. Vermote, J. Reagan, Y. Kaufman, T. Nakajima, *et al., Aeronet—a federated instrument network and data archive for aerosol characterization,* Remote sensing of environment **66**, 1 (1998).

[39] N. O'Neill, T. Eck, A. Smirnov, B. Holben, and S. Thulasiraman, *Spectral discrimination of coarse and fine mode optical depth,* Journal of Geophysical Research: Atmospheres **108** (2003).

[40] O. Dubovik, M. D. King, *et al., A flexible inversion algorithm for retrieval of aerosol optical properties from sun and sky radiance measurements,* Journal of Geophysical Research **105**, 20673 (2000).

[41] O. Dubovik, A. Sinyuk, T. Lapyonok, B. N. Holben, M. Mishchenko, P. Yang, T. F. Eck, H. Volten, O. Munoz, B. Veihelmann, *et al., Application of spheroid models to account for aerosol particle nonsphericity in remote sensing of desert dust,* Journal of Geophysical Research: Atmospheres **111** (2006).

[42] O. Dubovik, A. Smirnov, B. Holben, M. King, Y. Kaufman, T. Eck, and I. Slutsker, *Accuracy assessments of aerosol optical properties retrieved from aerosol robotic network (aeronet) sun and sky radiance measurements,* Journal of Geophysical Research: Atmospheres **105**, 9791 (2000).

[43] O. Dubovik, B. Holben, T. F. Eck, A. Smirnov, Y. J. Kaufman, M. D. King, D. Tanré, and I. Slutsker, *Variability of absorption and optical properties of key aerosol types observed in worldwide locations,* Journal of the atmospheric sciences **59**, 590 (2002).

[44] T. Eck, B. Holben, J. Reid, O. Dubovik, A. Smirnov, N. O'neill, I. Slutsker, and S. Kinne, *Wavelength dependence of the optical depth of biomass burning, urban, and desert dust aerosols,* Journal of Geophysical Research: Atmospheres **104**, 31333 (1999).

[45] M. Tesche, A. Ansmann, D. Müller, D. Althausen, R. Engelmann, V. Freudenthaler, and S. Groß, *Vertically resolved separation of dust and smoke over cape verde using multiwavelength raman and polarization lidars during saharan mineral dust experiment 2008,* Journal of Geophysical Research: Atmospheres **114** (2009).

[46] R.-E. Mamouri and A. Ansmann, *Potential of polarization lidar to provide profiles of ccn-and inp-relevant aerosol parameters,* Atmospheric Chemistry and Physics **16**, 5905 (2016).

[47] R.-E. Mamouri and A. Ansmann, *Potential of polarization/raman lidar to separate fine dust, coarse dust, maritime, and anthropogenic aerosol profiles,* Atmospheric Measurement Techniques **10**, 3403 (2017).

[48] J. Gasteiger, S. Groß, V. Freudenthaler, and M. Wiegner, *Volcanic ash from iceland over munich: mass concentration retrieved from ground-based remote sensing measurements,* Atmospheric Chemistry and Physics **11**, 2209 (2011).

[49] R. E. Mamouri and A. Ansmann, *Fine and coarse dust separation with polarization lidar,* Atmospheric Measurement Techniques **7**, 3717 (2014).

[50] P. R. Bevington, D. K. Robinson, J. M. Blair, A. J. Mallinckrodt, S. McKay, *et al.*, *Data reduction and error analysis for the physical sciences,* Computers in Physics **7**, 415 (1993).

[51] M. Hess, P. Koepke, and I. Schult, *Optical properties of aerosols and clouds: The software package opac,* Bulletin of the American meteorological society **79**, 831 (1998).

[52] W. C. Skamarock and J. B. Klemp, *A time-split nonhydrostatic atmospheric model for weather research and forecasting applications,* Journal of Computational Physics **227**, 3465 (2008).

[53] G. Rolph, *Real-time environmental applications and display system (ready), noaa air resources laboratory, silver spring, md,* Website (http://www. arl. noaa. gov/ready/hysplit4. html) (2003).

[54] A. Stein, R. R. Draxler, G. D. Rolph, B. J. Stunder, M. Cohen, and F. Ngan, *Noaa's hysplit atmospheric transport and dispersion modeling system,* Bulletin of the American Meteorological Society **96**, 2059 (2015).

[55] G. L. Schuster, M. Vaughan, D. MacDonnell, W. Su, D. Winker, O. Dubovik, T. Lapyonok, and C. Trepte, *Comparison of calipso aerosol optical depth retrievals to aeronet measurements, and a climatology for the lidar ratio of dust,* Atmospheric Chemistry and Physics **12**, 7431 (2012).

[56] A. Nisantzi, R.-E. Mamouri, A. Ansmann, G. Schuster, and D. G. Hadjimitsis, *Middle east versus saharan dust extinction-to-backscatter ratios,* Atmospheric Chemistry and Physics **15**, 7071 (2015).

[57] P. Rosenberg, A. Dean, P. Williams, J. Dorsey, A. Minikin, M. Pickering, and A. Petzold, *Particle sizing calibration with refractive index correction for light scattering optical particle counters and impacts upon pcasp and cdp data collected during the fennec campaign,* Atmospheric Measurement Techniques **5**, 1147 (2012).

[58] A. Petzold, K. Rasp, B. Weinzierl, M. Esselborn, T. Hamburger, A. Dörnbrack, K. Kandler, L. Schütz, P. Knippertz, M. Fiebig, *et al.*, *Saharan dust absorption and refractive index from aircraft-based observations during samum 2006,* Tellus B **61**, 118 (2009).

[59] S. R. Osborne, B. T. Johnson, J. M. Haywood, A. J. Baran, M. A. J. Harrison, and C. L. McConnell, *Physical and optical properties of mineral dust aerosol during the dust and biomass-burning experiment,* Journal of Geophysical Research: Atmospheres **113**, n/a (2008), d00C03.

3

LONG-TERM OBSERVATIONS OF THE BACKGROUND AEROSOL AT CABAUW, THE NETHERLANDS

Long-term measurements of $PM_{2.5}$ mass concentrations and aerosol particle size distributions from 2008 to 2015, as well as hygroscopicity measurements conducted over one year (2008-2009) at Cabauw, The Netherlands, are compiled here in order to provide a comprehensive dataset for understanding the trends and annual variabilities of the atmospheric aerosol in the region. $PM_{2.5}$ concentrations have a mean value of 14.4 $\mu g\ m^{-3}$ with standard deviation 2.1 $\mu g\ m^{-3}$, and exhibit an overall decreasing trend of -0.74 $\mu g\ m^{-3}\ year^{-1}$. The highest values are observed in winter and spring and are associated with a shallower boundary layer and lower precipitation, respectively, compared to the rest of the seasons. The number concentration of the particles smaller than 500 nm has a mean of 9.2×10^3 particles cm^{-3} and standard deviation 4.9×10^3 particles cm^{-3} and shows an increasing trend between 2008 and 2011 while it decreases from 2013 to 2015. It exhibits highest concentrations in spring and summer, despite the increased precipitation, due to the high occurrence of nucleation-mode particles, which most likely are formed elsewhere and are transported to the observation station. Particle hygroscopicity measurements show that, independently of the air mass origin, the particles are mostly externally mixed with the more hydrophobic mode having a mean hygroscopic parameter κ of 0.1 while for the more hydrophilic mode κ is 0.35. The hygroscopicity of the smaller particles investigated (i.e., particles having diameters of 35 nm) appears to increase during the course of the nucleation events, reflecting a change in the chemical composition of the particles.

This chapter have been published in Science of The Total Environment, Mamali et al., Volume 625, 2018, Pages 752-761, https://doi.org/10.1016/j.scitotenv.2017.12.136.

3.1. INTRODUCTION

Epidemiological and medical studies have established that Particulate Matter (PM) pollution has a strong impact on human health (e.g., [1–3]), with elevated ambient $PM_{2.5}$ concentrations being associated with adverse respiratory effects to chronically ill patients and increased mortality rates for people with respiratory problems [4]. In addition, fine particles (i.e., particles with diameters below 1 μm), and especially their smallest fraction that can penetrate deeper in the respiratory tract and reach the alveoli [5], can enter the blood recirculation system and cause cardiovascular deceases [6]. Model studies have shown that $PM_{2.5}$ concentrations correlate well with morbidity and mortality, causing ca. 3.3 million premature deaths annually around the globe [7].

Apart from being related to adverse health effects, airborne particles emitted from natural and anthropogenic sources can affect the climate of our planet at local, regional and global scales. Air-suspended particles affect climate in a direct way by absorbing and scattering incoming solar radiation [8], and indirectly by acting as Cloud Condensation and Ice Nuclei (CCN and IN, respectively; [9]). Both effects result in an overall cooling of the Earth and together can contribute to a forcing of the order of -1 W/m^2 at the top of the atmosphere with an estimated uncertainty of the order of 100% [10]. This high uncertainty results from the high spatial and temporal variability of the atmospheric aerosol as well as from the poor understanding of key physicochemical transformations that the aerosol particles undergo during their lifetime. To better understand their role on climate, and thus to improve the predictability of atmospheric-climate models, we need long-term measurements of the aerosol properties. Apart from the concentration (by mass and number) of airborne particles, information on the temporal variability of their size and chemical composition is highly required for understanding the processes they are involved in.

The Cabauw Experimental Site for Atmospheric Research (CESAR) in The Netherlands is one of oldest stations for atmospheric observations in Europe and one of the core observatories in the global network. CESAR is one of the few observatories where characterization of the atmosphere from the ground up to the top of the atmosphere is taking place by combining in situ sensors installed on the ground and along a 213-m tower, as well as ground-based remote sensing instruments for measuring radiation, wind, turbulence, trace gases, aerosols, and clouds at higher altitudes. Continuous long-term in-situ measurements of the mass concentrations and the number size distributions of atmospheric particles are performed at CESAR since more than a decade. In addition, measurements related to the atmospheric state and various atmosphere-land surface interactions for supporting climate modeling are carried out at CESAR using both in-situ and remote sensing techniques [11].

Here we report $PM_{2.5}$ mass concentration and aerosol size distribution measurements conducted at Cabauw from 2008 to 2015, and analyze their trends and seasonal variability. In addition, we provide aerosol hygroscopicity measurements that took place over almost one year (10 months), and link them with the patterns observed in the recorded size distributions. The rest of the chapter is organized as follows: Section 3.2 describes the instrumentation used for the measurements. Section 3.3 discusses the measurements, including the inter-annual and seasonal variations of $PM_{2.5}$ concentrations and the particle number distributions, as well as the seasonality in particle hygroscopicity.

Finally Section 3.4 summarizes the most important conclusions.

3.2. INSTRUMENTATION AND METHODS

3.2.1. THE CABAUW EXPERIMENTAL SITE FOR ATMOSPHERIC RESEARCH (CESAR)

CESAR is a rural site in a region that is one of the most populated areas in Europe [12]. The station, located 50 km away from the coast, is surrounded by grassland and agricultural pastures, and is influenced by maritime and continental environments. The terrain in the region is flat, varying from -3 to 5 m a.s.l. within a radius of 45 km. Figure 3.1 shows the location of the station and the frequency of the different wind directions based on measurements recorded between 2008 and 2015 at the tower of the station. The site most often receives continental air masses from Southern Europe (40%), with the predominant wind directions being Southwestern (SW), advecting polluted air masses that pass over the neighboring city of Rotterdam. Clean air masses are associated with Northern (N) air originating from the North Sea or Scandinavia only if they do not follow trajectories over Amsterdam and Utrecht; i.e., the other two major neighboring cities to CESAR. Considering that the site mostly receives air masses passing over close-by cities and a dense highway grid located within a radius of 45 km, the station is representative of the wider region.

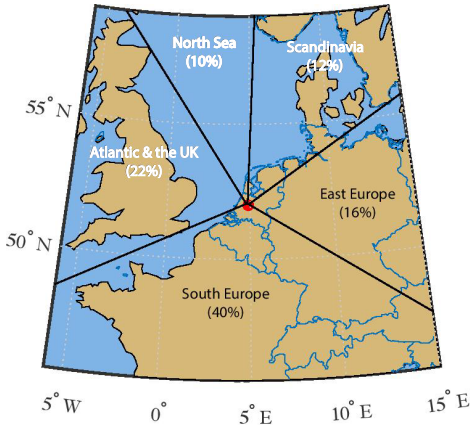

Figure 3.1: Location of the CESAR and annual relative frequency of the wind directions observed at the site during the study period.

3.2.2. INSTRUMENTATION

A low-volume sampler operated at a flow rate of 2.3 m^3 h^{-1} and equipped with a $PM_{2.5}$ sampling head (complying with the standards [13]) was deployed to measure the mass concentration of particles smaller than 2.5 μm on quartz filters (Whatman QM-A). All

$PM_{2.5}$ measurements were performed by the Dutch National Institute of Public Health and the Environment (RIVM) at the Cabauw Wielsekade station (500 m away from the tower) where air was sampled at a height of 4 m a.s.l.. The samples were collected every 24 hours, and the mass of the particles deposited on the filters was determined gravimetrically [14]. All the filters were conditioned at 20 ± 1 °C and 50 ± 5% RH for at least 48 hours before weighing [15]. $PM_{2.5}$ measurements were performed on a daily basis during 2009 and 2015, while for the rest of the years investigated in this work data were available every second day. During days without $PM_{2.5}$ measurements, the quartz filters were replaced by teflon or tissuquartz filters used for metal Elemental or Organic Carbon analysis, respectively.

A Scanning Mobility Particle Sizer (SMPS; TSI Model 3034) was used to measure the size distributions of the particles having diameters in the range 9.37 - 516 nm. The SMPS consisted of an impactor, a charger, a Differential Mobility Analyzer (DMA) and a Condensation Particle Counter (CPC). Inversion of the collected data was performed with the algorithm described by 16. Although the SMPS data used for this analysis cover the period from 2008 to 2015, the data from January to December 2012 were discarded due to high noise levels.

A Hygroscopic Tandem DMA (HTDMA) system was deployed in the framework of the EUCAARI IMPACT campaign to determine the hygroscopicity of the particles observed from May 2008 to February 2009 at CESAR. In brief, the system consists of two DMAs (cf. [17], for details) and a CPC (TSI Model 3772; [18]). To reduce the humidity below 20% and comply with the EUSAAR standards [19], a custom-made Nafion drying system was used upstream the HTDMA, in addition to the sample drying system of the station. In the HTDMA, the polydisperse aerosol sample was first charge neutralized (by passing through a ^{85}Kr-source aerosol neutralizer) and then passed through the first DMA that selected particles of specific dry sizes (35, 50, 75, 110 and 165 nm) before being exposed at a constant RH of 90% in the humidifier of the system. The size distribution of the humidified particles was measured by the second DMA and a CPC. Both DMAs used sheath flows in closed loops [20], whereas the measurement time for each particle size was 5 min. Values of the hygroscopic parameter κ, which are discussed in the following section, were determined by the HTDMA measurements [21].

Both the SMPS and the HTDMA sampled air at 60 m a.s.l. through a specially-designed inlet system that consisted of four parts: (a) 4 PM_{10} inlets, (b) a Nafion-tube system that dried the aerosol stream to relative humidity values (RH) below 40%, (c) a 60-m stainless steel pipe and (d) a manifold that splits the flow to the instrument suite [22]. The total flow through the 60-m long inlet pipe was maintained at about 60 l min^{-1}, which was the highest flow warranting laminar flow ($Re \approx 2000$), from which the SMPS and the HTDMA were sampling at a flow rate of 1 l min^{-1} each. For the SMPS data, corrections were applied to account for the diffusional losses of the particles on the walls of the 60-m sampling line [23].

Meteorological measurements of wind direction, wind speed, temperature and relative humidity at 40 m altitude were used in the analysis. In addition, back-trajectories of the air masses arriving at the station were calculated by the NOAA HYSPLIT model [24, 25].

3.3. RESULTS AND DISCUSSION

3.3.1. PARTICLE MASS AND NUMBER CONCENTRATIONS

$PM_{2.5}$ INTRA-ANNUAL VARIATION

Fig. 3.2 shows $PM_{2.5}$ daily concentrations measured at Cabauw from January 2008 to December 2015. The measurements exhibit an overall decreasing trend with a slope of $-0.74\ \mu g\ m^{-3}\ year^{-1}$, calculated based on the yearly mean values. This trend is partly (28%) due to the absence of extreme mass concentrations of $PM_{2.5} > 50\ \mu g\ m^{-3}$ from 2011 onwards, which are more frequent under Eastern winds (cf. Fig. 3.3; left figure). Analysis excluding these extreme values still showed a negative trend with a slope of $-0.54\ \mu g\ m^{-3}\ year^{-1}$, suggesting that the overall decrease is mainly attributed to the reduction of the background aerosol concentration. Despite the decreasing trend, all the yearly averages exceed the annual $PM_{2.5}$ limit of $10\ \mu g\ m^{-3}$ of the World Health Organization (WHO).

Apart from the annual mean values, also the number of days with $PM_{2.5}$ concentrations higher than the WHO daily limit of $25\ \mu g\ m^{-3}$ decreased substantially over the study period, especially in winter (data not shown). The majority of the limit exceedances are associated with stable atmospheric conditions (i.e. Convective Available Potential Energy (CAPE) ≈ 0; [26]), which aid the built-up of pollution. As shown in Fig. 3.3 (see right figure) those days are mostly associated with winds from the East (E; ca. 65% of the cases), advecting air masses that pass over the heavily industrialized Ruhr area in Germany, and from the South (S, ranging from SE to SW; ca. 20% of the cases), traveling over France and Belgium before reaching Cabauw. Only in few occasions (ca. 15% of the cases) the air masses had marine origin and traveled from the SW over the Rotterdam and Antwerp harbor areas.

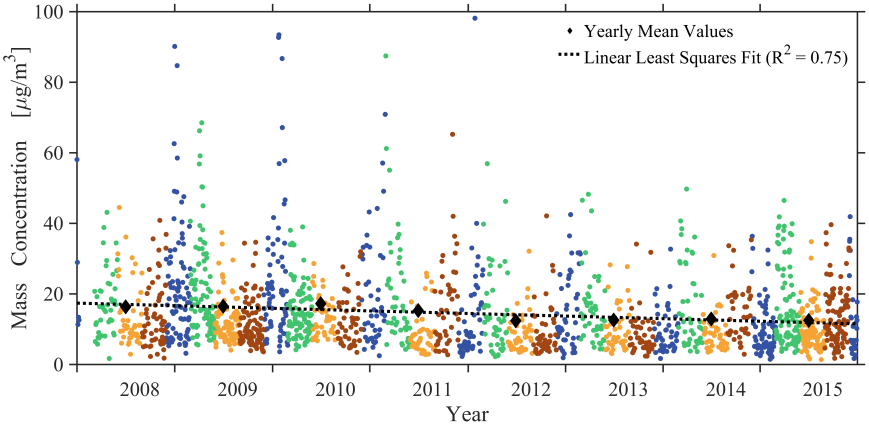

Figure 3.2: $PM_{2.5}$ daily concentrations measured at Cabauw from January 2008 to December 2015. Daily measurements are represented by dots color-coded based on the different seasons: blue for winter including the months December, January and February, green for spring including the months of March, April and May, yellow for summer including the months of June, July and August and brown for autumn including the months of September, October and November. The red line shows the $PM_{2.5}$ trend calculated based on the yearly mean values (red hexagons).

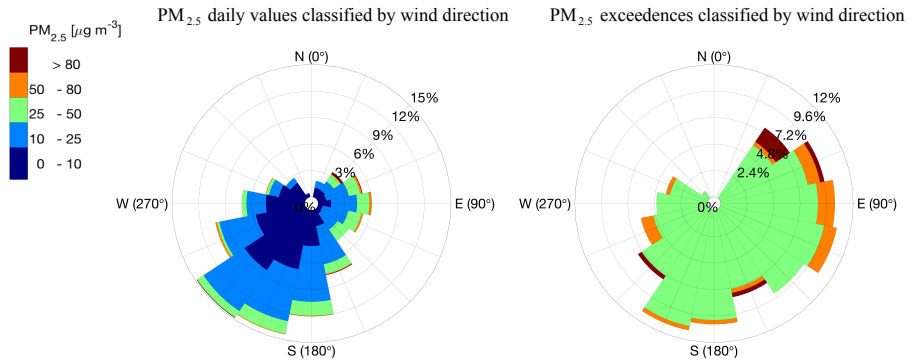

Figure 3.3: $PM_{2.5}$ values (left) and $PM_{2.5}$ limit exceedances (right) segregated based on wind direction.

The overall decreasing trends of $PM_{2.5}$ (both in terms of annual mean concentration and number of daily limit exceedance days) can be attributed to the more stringent European regulations for industrial emissions [27] and by the more advanced emission treatment technologies introduced in the transportation sector (it should be noted here that industry and transportation are two of the main contributors of $PM_{2.5}$ in The Netherlands and its neighboring countries; [28, 29]). This hypothesis can be further supported by the similar decreasing pattern observed in the carbon monoxide (CO) measurements (cf. Fig. 3.4) which is mainly emitted from biomass burning, combustion and a number of industrial activities. The inter-annual variability of atmospheric factors influencing particle concentration (e.g., rain height, temperature, incoming solar radiation, frequency and persistence of cold days < 3 °C) showed no statistically significant trends, suggesting that the reduced emissions are the main driver of the decreasing trend of $PM_{2.5}$.

$PM_{2.5}$ Seasonal Variation

The highest $PM_{2.5}$ concentrations throughout the study period were observed in winters and springs, with average values of 19.0 and 15.0 μg m^{-3}, respectively, whereas the lowest concentrations were observed in summers and autumns, having respective mean values of 9.1 and 10.8 μg m^{-3}. In general, high emissions from combustion sources (i.e., transportation and residential heating) in winter and autumn, and from agricultural activities in spring and summer, are the main contributors to this seasonal variation [30].

Apart from the local sources, $PM_{2.5}$ seasonal variability is also affected by the regional meteorological conditions including the variations in the wind speed that influences horizontal transport, in Boundary Layer Height (BLH) which is related to the dilution of the pollutants, and in precipitation that is the most important sink of PM pollution. Interestingly, only weak anti-correlation between wind speed and $PM_{2.5}$ concentrations (linear Pearson and non-linear Kendall correlation coefficient had respective values of $R_{Pearson}$ = -0.32 and $\tau_{Kendall}$ = -0.27; [31]) was observed despite the high wind speeds occurring in The Netherlands, suggesting that vertical dispersion (rather than natural ventilation) is the main process of dilution. Our analysis showed that the seasonal variability of the BLH influences the $PM_{2.5}$ concentrations which is in-line with previous

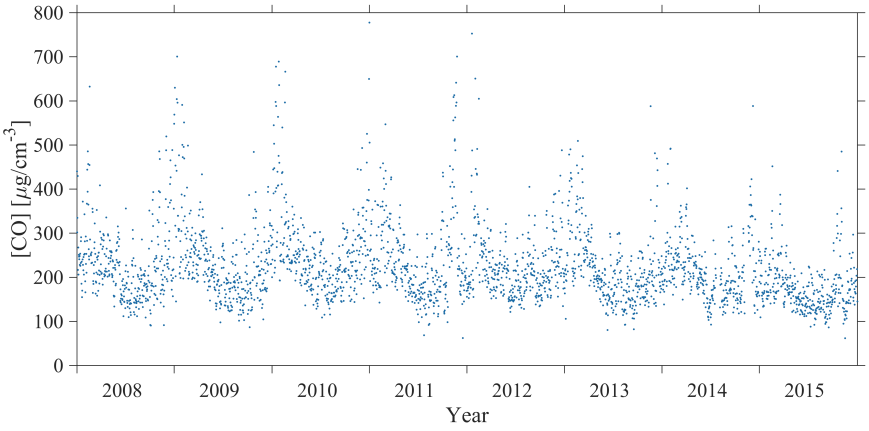

Figure 3.4: CO daily average concentrations measured at Cabauw from January 2008 to December 2015.

studies [32]. However, the low BLHs observed during winter cannot alone justify the higher $PM_{2.5}$ concentrations, and thus additional factors certainly contribute towards their seasonality. The rainfall intensity showed an anti-correlation with $PM_{2.5}$ ($R_{Pearson}$ = -0.68, $\tau_{Kendall}$ = -0.51, based on monthly average values) with the highest $PM_{2.5}$ concentrations observed in April, which is the driest month of the year (cf. Fig. 3.5 b).

PARTICLE NUMBER CONCENTRATIONS

Figure 3.6 shows the number concentration of particles having diameters between 30 and 500 nm (N_{30-500}) measured at Cabauw from January 2008 to December 2015 (the measurements during 2012 were discarded due to high noise level). The mean number concentration of all years was 9.2×10^3 particles cm^{-3} with a standard deviation of 4.9×10^3 particles cm^{-3}. In contrast to the monotonic decrease of the $PM_{2.5}$ values, the particle number concentrations show an increasing trend of 8.1 % $year^{-1}$ from 2008 to 2011 (calculated from the yearly mean values) and a decreasing trend of -11.7 % $year^{-1}$ between 2013 and 2015. The predominant driver for these trends should be the aerosol sources since no corresponding changes were observed in the meteorological conditions in this period. More specifically, in terms of rainfall, which is the major aerosol sink, no significant drop was recorded in years 2011 and 2013 when the highest N_{30-500} values were measured. $PM_{0.5}$ estimated by the number concentration measurements assuming a constant particle density of 1.5 g cm^{-3} (data not shown) exhibit the same trend with the N_{30-500}, suggesting that the decreasing trend of the $PM_{2.5}$ is driven by a decrease of particles with diameters larger than 0.5 μm.

Seasonally, N_{30-500} exhibits a strong anti-correlation with rainfall from January to June ($R_{Pearson} = -0.78$; Fig. 3.5), but in July and August, when the rain height reaches its maximum, the number of particles does not decrease, indicating that aerosol sources are also higher during this period. The additional sources of particles in the warm period are possibly the new particle formation (NPF) events (see Section 3.3.2).

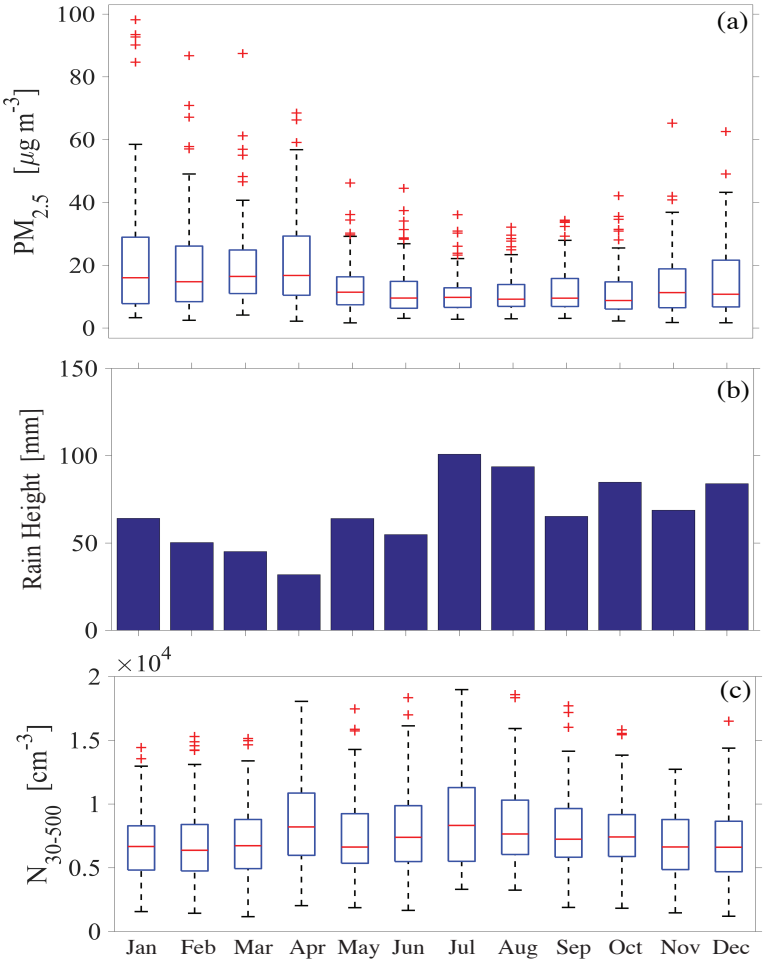

Figure 3.5: (a) Monthly averages of $PM_{2.5}$ concentrations from 2008 to 2015. The box plots indicate the median (red line) and the 25% and 75% percentile, whereas the red crosses are the maximum values observed in every month; (b) rainfall intensity and (c) seasonal variability of N_{30-500} from 2008 to 2015 (Due to discontinuities of the SMPS data during the entire study period, only the data between January 2008-December 2011 and January 2013-December 2015, were considered in the analysis)

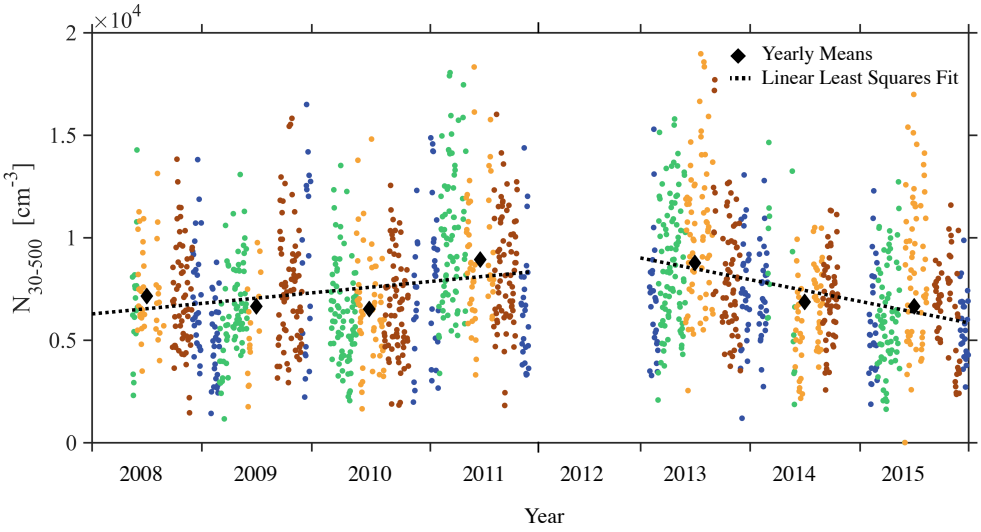

Figure 3.6: N_{30-500} concentrations measured at Cabauw from January 2008 to December 2015. Daily measurements are represented by dots color-coded based on the different seasons (winter (DJF) - blue, spring (MAM) - green, summer (JJA) - yellow, autumn (SON) - brown). The black dotted line shows the $PM_{2.5}$ trend calculated based on the yearly mean values (black diamonds).

3.3.2. AEROSOL PARTICLE SIZE DISTRIBUTIONS

DIURNAL AND SEASONAL VARIATION

Figure 3.7 shows the diurnal variation of the mean particle number size distributions in the different seasons. The size distribution count median diameter (CMD) and geometric standard deviation of the background aerosol are ca. 55 nm and 1.81 (average of the entire study period), respectively. The diurnal variabilities in winter and autumn are very similar, with pronounced peaks observed during the late morning and evening hours corresponding to the traffic and residential heating peaks. Interestingly, in spring and summer, the distributions shift to smaller sizes after 12:00 UTC as a result of the frequent NPF events occurring during these periods. A comparison between weekends and weekdays shows that the number concentration decreases by ca. 15% during the weekends for all seasons. In winter and autumn the peaks of the size distributions are less pronounced during the weekends as a result of the lower traffic density. Weekends during spring and summer exhibit intensified midday peaks due to more frequent NPF events (see discussion further below), which can be explained by the lower condensational sink as depicted in Fig. 3.8 (cf. similar observation in the measurements reported by Siakavaras et al. [33]). In an intra-annual basis, the annual mean CMD fluctuated slightly (within < 10%), while the shape of the size distribution showed no significant changes.

NEW PARTICLE FORMATION EVENTS

The particle number size distribution measurements show that numerous NPF events took place during the study period. To discriminate between an "event-day" and a "non-

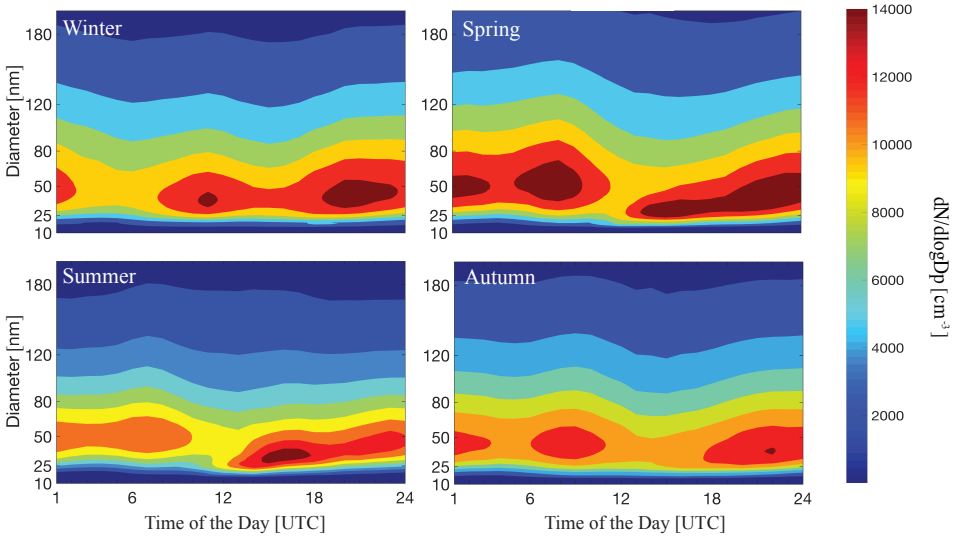

Figure 3.7: Diurnal variation of the mean number size distributions in the different seasons. The color shading represents the particle concentration.

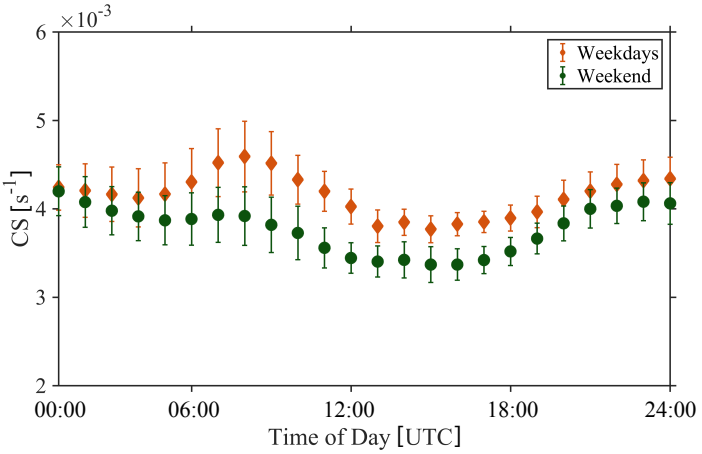

Figure 3.8: Diurnal evolution of the condensational sink in weekdays (error bars correspond to 1 standard deviation).

event" day, we used the procedure described by Dal Maso et al. [34]. In brief, we first examined the data visually, based on the 24-h (midnight to midnight) contour plots of the size distributions. A day was characterized as an event-day if the size distribution exhibited a new mode corresponding to particles smaller than 25 nm, followed by growth which lasted for several hours; otherwise it was labeled as a "non-event" day. This classification showed that NPF events occur at Cabauw throughout the year but they are

Table 3.1: Number of new particle formation events recorded each month for the years 2010 and 2011.

Month	NPF events (2010)	NPF events (2011)
January	0	-
February	0	2
March	2	5
April	5	8
May	9	10
June	13	11
July	6	3
August	2	7
September	2	7
October	3	4
November	2	1
December	2	0

pronounced during spring and summer as has been observed in climatological studies at different locations in Europe [35, 36]. Our analysis focused on measurements from January 2010 to December 2011, when measurements down to 9.6 nm were available. Table 3.1 summarizes the number of NPFs for each month. The fraction of the number of "event-days" to the total number of (measurement) days was 20% in 2010 and 24% in 2011. All the events took place during daytime between 08:00 and 14:00 UTC, with the majority being observed under cloud free conditions. These observations are in line with those reported by Manninen et al. [37], who investigated nucleation events and the first steps of growth, at many observatories in Europe, including Cabauw, using ion spectrometer measurements. Back-trajectory analysis showed that NPF events are mostly related to marine air masses from the NW, N, W and SW (80%). These clean air masses having low particle number concentrations, and thus low condensational sinks, most often pass over cities (e.g. Amsterdam, Rotterdam) where they get enriched with gaseous pollutants which act as precursors for NPF. The rest of the events (20%) were recorded when air from the E and SE, that carry polluted air from Central Europe, reached Cabauw.

Characteristic NPF events, associated with air masses from the North Sea, are shown in Fig. 3.9. Solar radiation in the morning triggers the photochemical formation of new particles which grow to the detectable sizes within ~3-4 h. A steep increase in the number concentration of the smaller particles (having diameters up to 25 nm) was observed around 08:00-10:00 UTC. The small, newly formed particles slowly increase in size reaching that of the background aerosol sizes late at night.

It should be noted here that the smallest particles for which increased concentrations were observed during the events had diameters of ca. 11 nm (note that the SMPS can measure from 9.6 nm and higher), suggesting that the fresh particles were formed elsewhere and were advected to the site. This, however, is valid provided that the sub-11-nm channels of the SMPS do not underestimate the corresponding particle number concentrations significantly, and that the particles grow slow enough so that the instrument time resolution allows for capturing their growth.

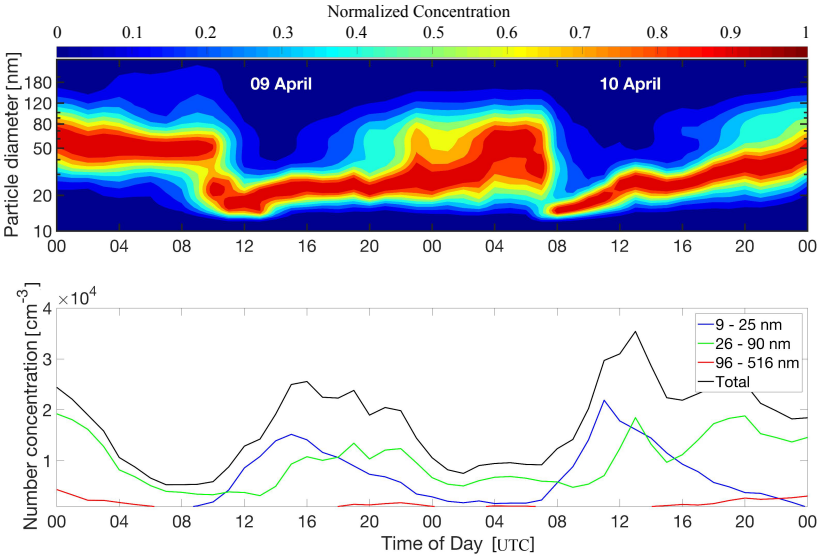

Figure 3.9: Evolution of the particle size distributions during two consecutive days, (9 and 10 April 2011) with new particle formation events. The upper panel shows hourly measurements of the aerosol size distribution (normalized by the maximum value), whereas the lower panel shows the number concentrations of the particles for four size ranges: 9-25 nm, 26-90 nm, 96-516 nm and 9-516 nm (total).

3.3.3. AEROSOL PARTICLE HYGROSCOPICITY

The hygroscopicity parameter κ is a measure of the affinity of the aerosol particles to water. Relatively high κ values >1 correspond to the highly hygroscopic inorganic species (e.g. sodium chloride; [38]) while oxidized organic compounds found in the atmosphere have κ values in the range 0.01-0.3. In the case of multicomponent aerosol particles κ can be estimated assuming that the total volume of water is equal to the sum of the water associated to the individual components [38] and can be calculated as $\kappa_{mixed} = \sum_i \varepsilon_i \kappa_i$, where ε_i is the volume fraction of each component having hygroscopic parameter κ_i.

Figure 3.10 shows the diurnal pattern of the seasonally averaged κ distributions for particles having dry sizes of 165 and 35 nm. For all the particle sizes κ was below 0.5, suggesting the co-existence of organic and inorganic compounds in the aerosol phase during all seasons. The larger particles (i.e., those having dry diameter of 165 nm) show a constant diurnal pattern in all seasons. In winter and autumn the 165-nm particles exhibit an external mixing state with two distinct modes (85% of the days): one corresponding to the background aerosol with $\kappa \approx 0.4$ and a very hydrophobic mode with κ less than 0.1. The presence of this less hygroscopic mode becomes more dominant during periods with intense anthropogenic activities (i.e., traffic in the morning, between 06:00-12:00 UTC, and in the late evening, between 17:00-22:00 UTC, together with residential heating). In spring and summer, when the contribution of heating is minimum, the fraction of the less hygroscopic particles decreases markedly, resulting in an internally mixed aerosol with a mean κ of ca. 0.3 throughout the day, which suggests a strong

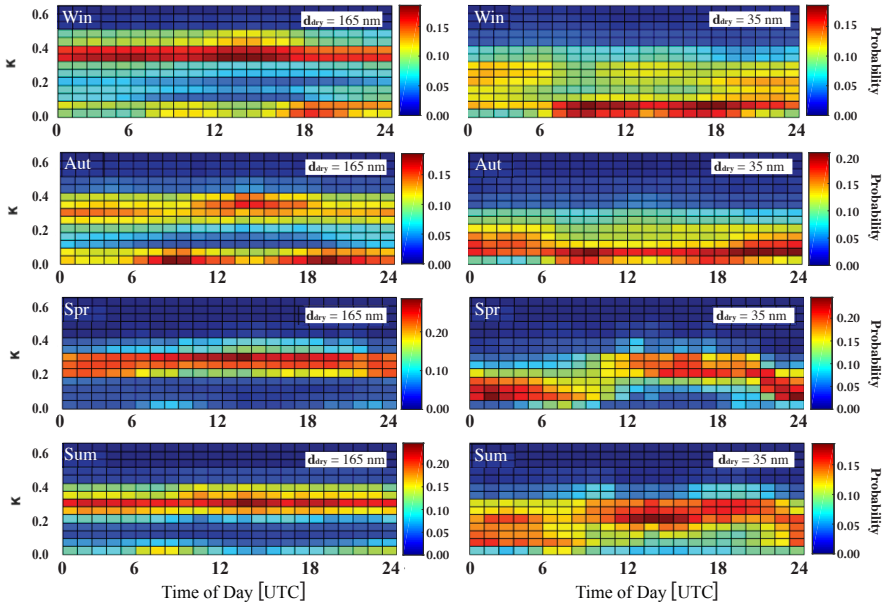

Figure 3.10: Diurnal variation of the κ probability distributions of particles having dry diameters of 165 nm (left) and 35 nm (right).

influence from organic compounds.

The smaller particles (i.e., those having dry diameters of 35 nm) exhibit different diurnal patterns each season compared to the larger particles. In winter and autumn, when particles are emitted from anthropogenic sources between 07:00 and 19:00 UTC, their κ values are below 0.1. At night the distributions widen and the mean κ value is ca. 0.2. In spring and summer the distribution follows a different pattern: κ is 0.3 between 11:00 and 21:00 UTC but decreases to 0.15 during the night. The time of the shift to higher κ values coincides with the initiation of the NPF events. At night, when these processes seize, κ shifts back to background values (i.e., around 0.1). The day-by-day analysis of the diurnal κ distributions showed that the seasonally averaged patterns (cf. Fig. 3.10) are representative for more than 85% of the days for winter, spring and summer. However, in autumn, some days exhibit a different pattern (e.g. narrower κ distributions) and the percentage of the days that resemble the seasonally averaged patterns drops to 60%.

Fig. 3.11 shows the κ probability distribution function for air masses originating from the North Sea (marine origin) and Central Europe (continental origin). In all cases, the distributions are bimodal, with the smaller dry particles (35 nm in diameter) having a more pronounced hydrophobic mode and the larger particles (75 and 165 nm) a more pronounced hydrophilic mode. This similarity in the κ values when air masses from marine or continental origins reach the station indicates that particle hygroscopicity is mainly influenced by local sources.

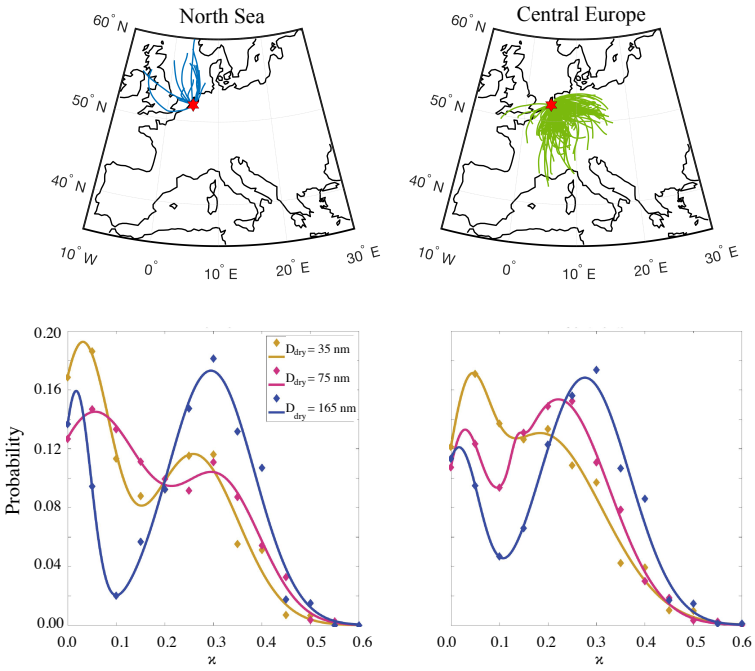

Figure 3.11: Probability distributions of κ for different dry particle sizes carried to the station by marine (left) and continental (right) air masses.

3.4. CONCLUSIONS

In this study we report on a 8-year-long dataset (2008-2015) of aerosol particle mass concentrations ($PM_{2.5}$) and size distributions, as well as on a 10-month record of aerosol hygroscopicity at the CESAR site in The Netherlands. The yearly mean $PM_{2.5}$ concentrations showed a decreasing trend that can be attributed to more stringent regulations to industrial emissions and to the advanced emission treatment technologies introduced in the transportation sector over the past decade. $PM_{2.5}$ concentrations exhibit a clear seasonal variability which is primarily affected by the higher emissions and to a lesser extent by meteorological conditions such as the BLH and precipitation.

In contrast to the $PM_{2.5}$, the number concentration of particles having diameters in the range 30-500 nm showed an increasing trend between 2008 and 2011 and an opposite trend from 2013 to 2015, with N_{30-500} values in 2015 being at the same level with those in 2008, raising questions on whether air quality actually improves as the $PM_{2.5}$ measurements suggest. Seasonally, N_{30-500} was higher in spring and summer mostly due to the production of new particles by nucleation. The diurnal variation of the number concentration in winter and autumn shows pronounced peaks in the late morning and evening hours corresponding to the traffic and residential heating peaks. The measurements also show a shift towards smaller particle sizes in spring and summer, supporting that the particle number concentrations during these seasons are strongly influenced by

the NPF events.

The hygroscopic parameter κ, for all sizes measured in this work suggest the presence of organics in the particle phase. The freshly emitted smaller particles (35 nm) are most often externally mixed compared to the chemically aged larger particles (165 nm). The diurnal patterns of the seasonally averaged κ distributions of the larger particles showed constant values throughout the day while the smaller particles exhibited diurnal variations. The 165-nm particles are mostly internally mixed in spring and summer whereas in autumn and winter the κ distributions are bimodal with the more hydrophobic peak being temporarily associated to traffic and residential heating. The smaller particles are externally mixed during all seasons and are also influenced by anthropogenic activities in the cold season as suggested be the reduced κ values during the day. In spring and summer, new particles formation events and photochemical aging are affecting the κ distribution, which is shifted to higher values during the day. Air masses of different origins (continental and marine) exhibit similar κ distributions for all sizes signifying the dominance of the local sources to particles hygroscopicity.

ACKNOWLEDGEMENTS

We extend special appreciation to Mr. Rob Zwartjes of Rijksinstituut voor Volksgezondheid en Milieu (RIVM) for providing useful information about the PM measurements, to Mrs. Ann-Mari Fjæraa of the Norwegian Institute for Air Research (NILU) for providing level 0 SMPS data for quality check, to Dr. Ari Asmi and Prof. Dr. Alfred Wiedensohler for providing valuable information regarding the SMPS measurements.

REFERENCES

[1] US-EPA, *Air quality criteria for particulate matter,* (2004).

[2] I. C. A. Pope and D. W. Dockery, *Health effects of fine particulate air pollution: lines that connect,* Journal of the air & waste management association **56**, 709 (2006).

[3] A. A. Baccarelli, N. Hales, R. T. Burnett, M. Jerrett, C. Mix, D. W. Dockery, and C. A. Pope III, *Particulate air pollution, exceptional aging, and rates of centenarians: A nationwide analysis of the united states, 1980–2010,* Environmental health perspectives **124**, 1744 (2016).

[4] H.-E. Wichmann and A. Peters, *Epidemiological evidence of the effects of ultrafine particle exposure,* Philosophical Transactions of the Royal Society of London A: Mathematical, Physical and Engineering Sciences **358**, 2751 (2000).

[5] B. Asgharian, O. Price, M. Oldham, L.-C. Chen, E. Saunders, T. Gordon, V. Mikheev, K. Minard, and J. Teeguarden, *Computational modeling of nanoscale and microscale particle deposition, retention and dosimetry in the mouse respiratory tract,* Inhalation toxicology **26**, 829 (2014).

[6] R. Zlotkowska, *Adverse health effects of the exposure to the spherical aerosol particles, including ultra-fine particles,* Synergic Influence of Gaseous, Particulate, and Biological Pollutants on Human Health , 109 (2015).

[7] J. Lelieveld, J. Evans, M. Fnais, D. Giannadaki, and A. Pozzer, *The contribution of outdoor air pollution sources to premature mortality on a global scale,* Nature **525**, 367 (2015).

[8] V. Ramanathan, P. Crutzen, J. Kiehl, and D. Rosenfeld, *Aerosols, climate, and the hydrological cycle,* science **294**, 2119 (2001).

[9] U. Lohmann and J. Feichter, *Global indirect aerosol effects: a review,* Atmospheric Chemistry and Physics **5**, 715 (2005).

[10] S. Solomon, *Climate change 2007-the physical science basis: Working group I contribution to the fourth assessment report of the IPCC*, Vol. 4 (Cambridge University Press, 2007).

[11] H. Russchenberg, F. Bosveld, D. Swart, H. ten Brink, G. de Leeuw, R. Uijlenhoet, B. Arbesser-Rastburg, H. van der Marel, L. Ligthart, R. Boers, *et al.*, *Ground-based atmospheric remote sensing in the netherlands: European outlook,* IEICE Transactions on Communications **88**, 2252 (2005).

[12] F. J. Gallego, *A population density grid of the european union,* Population and Environment **31**, 460 (2010).

[13] C. A. EN 12341, *Determination of the pm10 fraction of suspended particulate matter–reference method and field test procedure to demonstrate reference equivalence of measurement methods,* European Committee for Standardization (European Standard EN 12341), Brussels, 1998 .

[14] E. Triantafyllou, E. Diapouli, E. Tsilibari, A. Adamopoulos, G. Biskos, and K. Eleftheriadis, *Assessment of factors influencing pm mass concentration measured by gravimetric & beta attenuation techniques at a suburban site,* Atmospheric Environment **131**, 409 (2016).

[15] *Cen 14907 ambient air quality; standard gravimetric measurement method for the determination of the $pm_{2.5}$ mass fraction of suspended particulate matter.* (2005).

[16] A. Wiedensohler, W. Birmili, A. Nowak, A. Sonntag, K. Weinhold, M. Merkel, B. Wehner, T. Tuch, S. Pfeifer, M. Fiebig, *et al., Mobility particle size spectrometers: harmonization of technical standards and data structure to facilitate high quality long-term observations of atmospheric particle number size distributions,* Atmospheric Measurement Techniques **5**, 657 (2012).

[17] W. Winklmayr, G. Reischl, A. Lindner, and A. Berner, *A new electromobility spectrometer for the measurement of aerosol size distributions in the size range from 1 to 1000 nm,* Journal of Aerosol Science **22**, 289 (1991).

[18] M. R. Stolzenburg and P. H. McMurry, *An ultrafine aerosol condensation nucleus counter,* Aerosol Science and Technology **14**, 48 (1991).

[19] J. Duplissy, M. Gysel, S. Sjogren, N. Meyer, N. Good, L. Kammermann, V. Michaud, R. Weigel, S. M. dos Santos, C. Gruening, *et al., Intercomparison study of six htdmas: results and recommendations,* Atmospheric Measurement Techniques (2009).

[20] V. Jokinen and J. M. Mäkelä, *Closed-loop arrangement with critical orifice for dma sheath/excess flow system,* Journal of Aerosol Science **28**, 643 (1997).

[21] A. Bougiatioti, S. Bezantakos, I. Stavroulas, N. Kalivitis, P. Kokkalis, G. Biskos, N. Mihalopoulos, A. Papayannis, and A. Nenes, *Biomass-burning impact on ccn number, hygroscopicity and cloud formation during summertime in the eastern mediterranean,* Atmospheric Chemistry and Physics **16**, 7389 (2016).

[22] P. Zieger, E. Weingartner, J. Henzing, M. Moerman, G. d. Leeuw, J. Mikkilä, M. Ehn, T. Petäjä, K. Clémer, M. v. Roozendael, *et al., Comparison of ambient aerosol extinction coefficients obtained from in-situ, max-doas and lidar measurements at cabauw,* Atmospheric chemistry and physics **11**, 2603 (2011).

[23] J. Henzing, *Interactive comment on: "number size distributions and seasonality of submicron particles in europe 2008–2009" by a. asmi et al,* Atmos. Chem. Phys. Discuss **11**, C3137 (2011).

[24] R. R. Draxler and G. Hess, *An overview of the hysplit_4 modelling system for trajectories,* Australian meteorological magazine **47**, 295 (1998).

[25] R. R. Draxler and G. Rolph, *Hysplit (hybrid single-particle lagrangian integrated trajectory) model access via noaa arl ready website (http://www. arl. noaa. gov/ready/hysplit4. html). noaa air resources laboratory, silver spring,* (2003).

[26] J. H. Seinfeld and S. N. Pandis, *Atmospheric chemistry and physics: from air pollution to climate change* (John Wiley & Sons, 2016).

[27] Directive, *2008/1/ec of the european parliament and of the council of 21 december 2007 on industrial emissions (integrated pollution prevention and control).* (2008).

[28] J. Matthijsen, H. M. Brink, M. Abels, and C. Frink, *PM2. 5 in the Netherlands: Consequences of the New European Air Quality Standards* (Netherlands Environmental Assessment Agency, 2007).

[29] EMEP, *Emep/ceip 2014 present state of emission data,* (2014).

[30] A. Manders-Groot, A. Segers, S. Jonkers, M. Schaap, R. Timmermans, C. Hendriks, R. Sauter, Wichink Kruit, E. van der Swaluw, H. Eskes, *et al.*, *Lotos-euros v2. 0 reference guide,* (2016).

[31] R. O. Gilbert, *Statistical methods for environmental pollution monitoring* (John Wiley & Sons, 1987).

[32] S. Pal, T. Lee, S. Phelps, and S. D. Wekker, *Impact of atmospheric boundary layer depth variability and wind reversal on the diurnal variability of aerosol concentration at a valley site,* Science of The Total Environment **496**, 424 (2014).

[33] D. Siakavaras, C. Samara, M. Petrakakis, and G. Biskos, *Nucleation events at a coastal city during the warm period: Kerbside versus urban background measurements,* Atmospheric Environment **140**, 60 (2016).

[34] M. Dal Maso, M. Kulmala, I. Riipinen, R. Wagner, T. Hussein, P. P. Aalto, and K. E. Lehtinen, *Formation and growth of fresh atmospheric aerosols: eight years of aerosol size distribution data from smear ii, hyytiala, finland,* Boreal Environment Research **10**, 323 (2005).

[35] W. Birmili, A. Wiedensohler, J. Heintzenberg, and K. Lehmann, *Atmospheric particle number size distribution in central europe- statistical relations to air masses and meteorology,* Journal of Geophysical Research. D. Atmospheres **106**, 32 (2001).

[36] J. Boulon, K. Sellegri, H. Venzac, D. Picard, E. Weingartner, G. Wehrle, M. Collaud Coen, R. Bütikofer, E. Flückiger, U. Baltensperger, *et al.*, *New particle formation and ultrafine charged aerosol climatology at a high altitude site in the alps (jungfraujoch, 3580 m asl, switzerland),* Atmospheric Chemistry and Physics **10**, 9333 (2010).

[37] H. Manninen, T. Nieminen, E. Asmi, S. Gagné, S. Häkkinen, K. Lehtipalo, P. Aalto, M. Vana, A. Mirme, S. Mirme, *et al.*, *Eucaari ion spectrometer measurements at 12 european sites–analysis of new particle formation events,* Atmospheric Chemistry and Physics **10**, 7907 (2010).

[38] M. Petters and S. Kreidenweis, *A single parameter representation of hygroscopic growth and cloud condensation nucleus activity,* Atmospheric Chemistry and Physics **7**, 1961 (2007).

4

RADIATIVE FORCING OF NUCLEATION IN THE NETHERLANDS

New particle formation events induced by natural and anthropogenic precursor gases in the atmosphere can contribute up to 50% of the global cloud droplet condensation nuclei, and are therefore thought to always enhance the shortwave radiative cooling from warm clouds. The effectiveness of these events in enhancing radiative cooling, however, depends on the evolution of the size distribution of the aerosol particles and the resulting population of cloud droplets that can form and modulate cloud optical depth over time. Here we use year-long observations of ground-based particle size distributions and hygroscopicity of the atmospheric aerosol – conducted in a region strongly affected by anthropogenic emissions – together with vertical velocities of the air masses in order to determine the number concentration of cloud droplets under typical updraft conditions. The resulting mean diurnal evolution in cloud droplet concentrations, and the consequent radiative forcing associated with the new particle formation events, are then compared with associated profiles during non-event days. We find that new particle formation actually decreases the number of droplets that can be formed throughout the course of the event days, causing a warming effect that ranges between 0.6 and 1.6 W m^{-2} compared to non-event days (in daily means). This counterintuitive observation is a result of the shift of the aerosol distribution to smaller sizes and the slow particle growth to CCN-relevant sizes during the events. Eventually, droplet number does increase above pre-event levels but only during the late evening or the night hours when solar radiation is low or absent. This behaviour is not unique to our study region, suggesting that it is a persistent effect of atmospheric new particle formation, which may carry important implications for their impact on weather and climate.

4.1. INTRODUCTION

Atmospheric aerosol particles affect the radiative balance of the Earth directly by scattering and absorbing solar radiation, and indirectly through their role as Cloud Condensation Nuclei (CCN) in cloud droplet formation [1–5]. The microphysical and radiative properties of clouds strongly depend on the fraction of atmospheric particles that can act as CCN (cloud albedo effect). The higher the concentration of CCN, the higher the concentration and the smaller the size of the resulting droplets formed in the clouds [6, 7], which, in turn, strongly affects cloud reflectance and consequently the atmospheric radiative balance [8, 9]. At the same time, the smaller the cloud droplets, the lower their chance of growing to precipitable sizes, and consequently the lower the probability of the clouds to produce rain (aerosol second indirect effect) [10, 11]. This also affects cloud lifetime [12], and thus the overall atmospheric radiation budget.

Airborne particles are either emitted directly from anthropogenic or natural sources (primary particles) [13], or formed by nucleation of precursor gaseous species (secondary particles) [14]. Once formed in the atmosphere, secondary aerosol particles start to grow, reaching CCN sizes (typically $\gtrapprox$ 100 nm in size) after several hours or even over consecutive days in some cases [15]. Due to the variable dynamic evolution of secondary particles, and the fact that not all of them grow enough to act as CCN, quantifying the extent to which new particle formation (NPF) events affect the microphysical properties of clouds and the associated radiative cooling remains subject to considerable uncertainty. What is more, the expected appearance of the additional cloud droplets during the course of the events (compared to the non-event days) can strongly influence their cooling ability as this is related to the radiation intensity available at the time the clouds are formed or modulated.

A number of studies assessing the contributions of NPF events to the CCN budget using long-term observations has shown that these vary from region to region depending on the particle sources and the ambient conditions. For instance, the frequency of NPF events in pristine environments is typically low, thereby providing a minor source of CCN [16]. In polluted environments, on the other hand, NPF events can be rather frequent (occurring up to 40% of the days on an annual basis), therefore having a significant impact on the concentration of CCN [17, 18]. In either case, identifying the most important precursor gaseous species that lead to NPF events and understanding the new particle formation mechanisms in every case is challenging and therefore requires combination of field, laboratory and modelling studies [19, 20].

On a global scale, NPF has been estimated to contribute as much as ca. 50% of the CCN to low-level clouds, thereby having potential to act as an important climate regulator according to modeling studies [21]. Despite our ability of assessing the contribution of NPF to the CCN budget at both regional and global scales, however, only very recent studies have started linking them with changes of cloud properties (primarily cloud droplet concentration) and the resulting radiative forcing using computational modelling tools[21–24].

Here we use a combination of observations and models to assess the impacts of NPF events on cloud formation, and consequently on the atmospheric radiation budget, in a region that is highly influenced by anthropogenic activities. More specifically, we use year-long measurements of aerosol size distribution measurements and information of

aerosol hygroscopicity from observations conducted at the Cabauw monitoring station in the Netherlands (Fig. 4.1). These measurements are provided as input to a state-of-the-art cloud droplet formation parametric model [25] in order to predict the resulting cloud droplet number concentrations under typical updraft conditions. We then evaluate the climatological impact by determining how the evolution in the cloud number concentrations during the course of the NPF events, affect the radiative properties of the clouds and determine the associated forcing, which we directly compare with associated values determined during non-event days.

4.2. INSTRUMENTATION AND METHODS

The Cabauw Experimental Site for Atmospheric Research (CESAR) is situated at a rural location in one of the most populated areas in Europe [26]. It is located 50 km from the coast in an area surrounded by grassland and agricultural pasture, and is influenced by maritime and continental air masses. The site most often receives continental air masses from Southern Europe (40%), with the predominant wind directions being Southwestern (SW), advecting polluted air masses that pass over the neighboring city of Rotterdam [27]. Clean marine air masses are associated with Northern (N) air originating from the North Sea (10%) or Scandinavia (12%) only if they do not follow trajectories over Amsterdam and Utrecht; i.e., the other two major neighboring cities to CESAR. Considering that the site mostly receives air masses passing over close-by cities and a dense highway grid located within a radius of 45 km, the station is representative of the wider region. Fig 4.1 shows the location of the station and a picture (inset) of its tower.

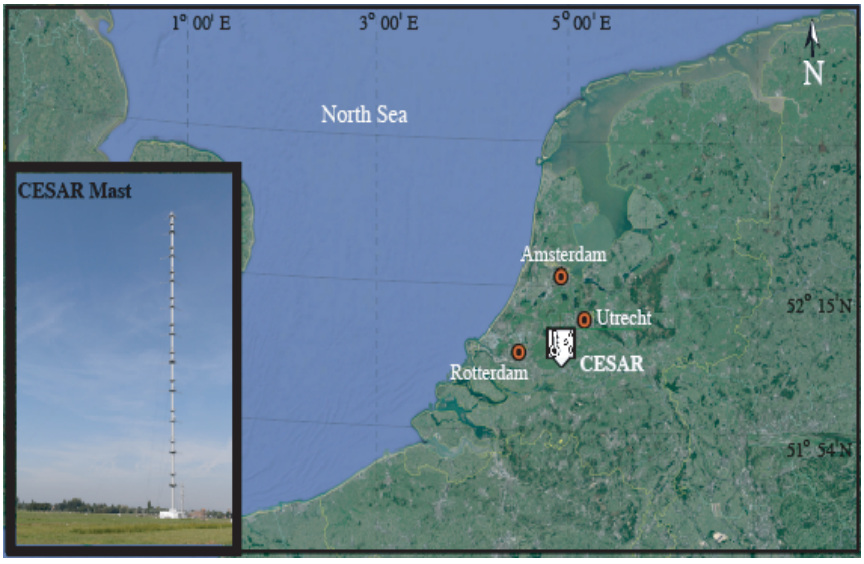

Figure 4.1: Location of CESAR and of the major cities in the vicinity. The inset shows the CESAR mast of 213 m (courtesy of Erwin de Beus).

4.2.1. AEROSOL SIZE DISTRIBUTION MEASUREMENTS

A Scanning Mobility Particle Sizer (SMPS; TSI Model 3034) was used to measure the size distribution of the particles having diameters in the range 9.37 - 516 nm with 5 minutes time resolution (the data presented here are hourly averages). In our analysis we used data spanning the period from February to December 2011. Inversion of the collected data was performed with the algorithm described by Wiedensohler et al. [28]. The instrument was sampling air from 60 m above sea level through a specially-designed inlet system that consists of four parts: (a) 4 PM_{10} inlets, (b) a Nafion-tube system that dried the aerosol stream to relative humidity (RH) values below 40%, (c) a 60-m stainless steel pipe and (d) a manifold that split the flow to the instrument suite [29]. The total flow through the 60-m long inlet pipe was maintained at about 60 l min^{-1}, which was the highest flow warranting laminar flow ($Re \approx 2000$), from which the SMPS was sampling at a flow rate of 1 l min^{-1}. To account for the diffusional losses of the particles on the walls of the 60-m sampling line corrections articulated by Henzing et al.[30] were applied.

4.2.2. CLOUD DROPLET NUMBER CONCENTRATION CALCULATION

NPF events can increase the number concentration of atmospheric particles significantly. Under favorable atmospheric conditions (e.g. availability of precursor vapors, low condensational sink) these new particles grow to larger diameters reaching cloud condensation nuclei sizes (ca. 80-150 nm depending on aerosol hygroscopicity and ambient supersaturation levels) within a few hours to 1-2 days. During the height development of the diurnal boundary layer, these air masses near the surface will ascend to higher atmospheric levels. While rising, the air expands and cools, and the relative humidity (RH) of the air parcel increases. If the air parcel reaches a critical supersaturation level, the particles activate and form cloud droplets. Clouds formed during days with and without NPF events can have different microphysical properties as a result of the differences in the particle size distribution and composition. Higher CCN numbers result in higher droplet number concentrations (N_d) and smaller cloud drop diameters, which in turn will affect the cloud reflectance [6].

Recent studies have examined the impact of NPF events on CCN concentration by calculating their number at different supersaturation levels using cloud condensation nuclei counters [17, 31, 32]. However, this approach does not take into account the feedback of the CCN on cloud supersaturation that develops in cloudy updrafts. Here we utilized the mechanistic cloud droplet formation parameterization described by Morales et al. [25] that captures this complexity by efficiently calculating the maximum supersaturation (S_{max}) that would form in a cloudy updraft and the respective N_d. This model uses as input the aerosol size distribution, updraft velocity (w), aerosol composition (expressed by the hygroscopicity parameter κ; [33]) and initial thermodynamic variables (pressure, temperature at the ground level) of the air parcel.

The SMPS aerosol size distribution measurements were used as input in the cloud parameterization yielding the S_{max} and N_d values with 1 hour time resolution. Observations at the CESAR site with a Doppler lidar (data not shown) suggest that an updraft velocity value w = 0.4 ms^{-1} is representative of boundary layer cloud formation in the area. A climatology of the aerosol hygroscopicity parameter at CESAR [27] showed that the κ of the CCN-relative size particles (75 nm and 110 nm) is relatively constant throughout

the year having a value of 0.20 ± 0.06. This value was used as input in the cloud drop parameterization to represent the particles' chemical composition.

4.2.3. RADIATIVE TRANSFER CALCULATIONS

To quantify the radiative forcing of the NPF events we utilized a radiative transfer scheme based on the Rapid Radiation Transfer Model for GCMs (RRTMG; [34, 35]), which calculates upward and downward fluxes of the short-wave and long-wave radiation from the ground up to 80 km using 137 levels in a single column. This scheme underlies the radiation computations in the model used by the European Centre for Medium Range Weather Forecasts (ECMWF; [36]). The input meteorological parameters used for the model runs (cloud cover, temperature, humidity) were obtained from the ERA5 reanalysis data [37], whereas monthly-mean climatology data were fed into the code for the main trace gases (CO_2, O_3, CH_4, N_2O, $CFCl_3$ and CF_2Cl_2). Cloud dynamics were not taken into account in this analysis.

Interactions of the radiation with clouds were taken into account by using values of cloud fraction as well as the liquid, ice and snow water contents from the cloud scheme. Because the cloud droplet parameterisation model used here calculates only the concentration and not the size of the droplets in the clouds, we parametrized their mean effective radius (r_e) using the following diagnostic formulation [38]:

$$r_e = \left(\frac{3\,\mathrm{LWC}}{4\pi\rho_w k N_d}\right)^{1/3} , \tag{4.1}$$

where LWC is the liquid water content of the cloud given by the ERA5 data, ρ_w is the liquid water density, N_d is the cloud drop number concentration and k is a constant ($k = 0.67 \pm 0.07$ for continental air masses).

In the original version of the code, the parametrization uses prescribed concentrations cloud condensation nuclei (CCN) from monthly-mean climatology data and the cloud LWC from the ERA5 data. For the purposes of this study the code was modified such that it uses as input N_d values calculated by the cloud drop parametrization described above. The hourly mean N_d values of the NPF and non-NPF days were fed into the radiation code to calculate the radiative forcing induced by the nucleation events at the bottom of the atmosphere (BOA) according to:

$$\Delta F_{BOA} = (\, F_{BOA}^{NPF}\downarrow - F_{BOA}^{NPF}\uparrow\,) - (\, F_{BOA}^{non-NPF}\downarrow - F_{BOA}^{non-NPF}\uparrow\,) , \tag{4.2}$$

where F^{NPF} and $F^{non-NPF}$ refer to the radiative fluxes during the NPF and the non-NPF days, respectively, whereas the arrows ($\downarrow\uparrow$) indicate downward and upward fluxes. With this convention, a plus sign of ΔF implies a warming effect and thus a positive radiative forcing at the BOA.

4.3. RESULTS AND DISCUSSION

To assess the effect of NPF events on the cloud drop number concentration, first we categorized each day based on whether NPF events occurred or not using the aerosol size distribution measurements. Initially, we performed a visual examination of the data using 24-h (midnight to midnight) contour plots of the size distributions (cf. Figure 4.2).

Then, we categorized the days into three classes: (a) days with NPF and growth during which the size distributions exhibited a new mode corresponding to particles smaller than 25 nm that was followed by an uninterrupted growth for several hours (Type A), (b) days that the aerosol size distribution showed signs of particles growth but there was no sudden and significant concentration increase in the nucleation mode particles, or days with elevated concentration of nucleation mode particles the exhibit a complex evolution of the size distribution (Type B), (c) non-event days during which the mean size of the particles varied marginally (Type C).

NPF events at the Cabauw station are more pronounced during spring and summer compared to the other seasons, which is in accordance with previous studies reporting measurements carried out in the region [27, 39]. For the period examined here, 13% where classified as events days (Type A or Type B) and 7% of the days were characterized as event days with particle growth (Type - A only; cf. Table 4.1 for the absolute numbers). A characteristic feature of the NPF events observed at Cabauw is that they exhibit an increase in the number concentration of nucleation-mode particles that have already grown to ca. 13 nm (note that the lower detection limit of the particle size distribution measurements used in this study is 9.37 nm) followed by a linear growth with an apparent mean growth rate of 2.5 nm h^{-1}. The fact that we do not observe an increase in the number concentration of particles having diameters in the sub-13-nm range suggests that the new particles have been formed upwind and grown while being advected to the monitoring station, as has been observed in previous cases [40, 41]. This is corroborated by the observed linear growth of the particles, which is the result of their physical growth rate, the wind speed and the distance from the point where the NPF events manifested upwind.

The size distribution measurements, together with information on the hygroscopicity of the CCN active particles [27] and updraft velocities in the region derived from Doppler lidar measurements at the Cabauw station, was then used as input to the parametrization model [25] in order calculate the cloud drop number concentration (N_d) resulting from the ascending parcels (cf. Section 4.2.2).

Table 4.1: Number of days classified according to NPF occurence/non-occurrence in 2011.

Category	**Number of days**
NPF - Type A	16
NPF - Type B	15
No NPF - Type C	207
Total number of days	**238**

4.3.1. DIURNAL IMPACT OF NUCLEATION ON N_d

Figure 4.2 shows the evolution of the aerosol particle size distribution measurements recorded on 10 April 2011, which is a representative day with an NPF event and the wind blowing constantly from the North-East (N-E) quadrant, together with the associated N_d values. The air-masses during that day, and for all event days with similar synoptic

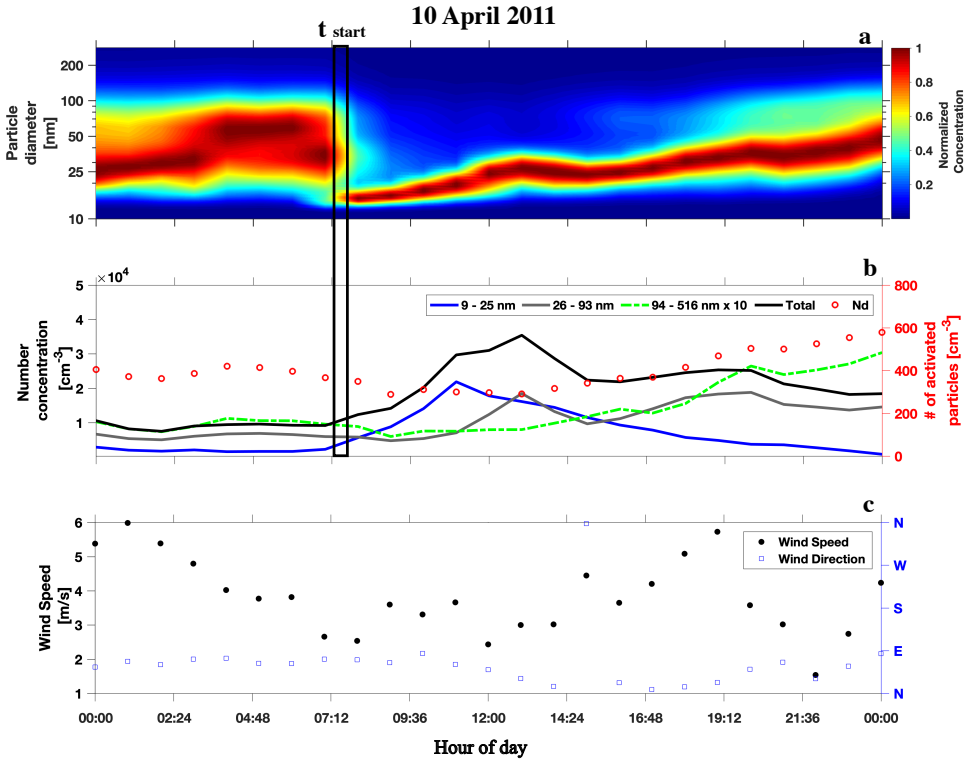

Figure 4.2: Evolution of the recorded aerosol particle size distribution, of the calculated cloud droplet concentrations associated to these ascending aerosol parcels and of meteorological conditions during a representative NPF event on 10 April 2011 when the wind direction was from the N-E quadrant. (a) Aerosol size distributions normalized by the peak number concentration for each measurement, (b) number concentrations of cloud droplets (N_d; red circles) predicted by the parameterization model, and of the measured aerosol particles having diameters in different size ranges: 9-25 nm (blue), 26-95 nm (grey), 96-516 nm (green), 9-516 nm (black), and of (c) wind speed (black squares) and wind direction (blue squares).

conditions, pass over the vicinity of the cities of Utrecht or Amsterdam 4 to 6 h before reaching the monitoring site (cf. Fig. 4.3).

To determine the effect of NPF events on the diurnal variation of the N_d we compare the mean evolution of the normalized cloud droplet concentration $N_d(t)/N_d(t_{start})$, where $N_d(t)$ is the droplet number concentration determined at time t during the course of the event, and $N_d(t_{start})$ at the start of the event during the event and the non-event days. The time is also normalized in order to serve the comparison of the evolution in N_d during event and non-event days. For each event day t_{start} is determined as the time when the number concentration of the nucleation mode particles start to increase dramatically (cf. Fig. 4.2 b) and an additional reference time, denoted as t_{end}, is the time when the cloud drop number concentration returns to the $N_d(t)/N_d(t_{start})$ value of unity. The same approach was used for the non-event days. It has to be noted here

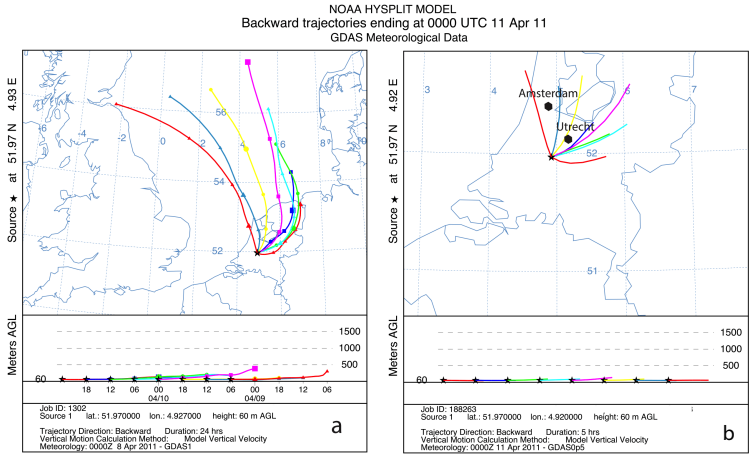

Figure 4.3: Back-trajectories of the NPF case studies shown in Figure 4.2. Trajectories in plot (a) trace the air-masses up to 24-h back in time, while plot (b) shows the same trajectories up to 5-h back in time. The two major cities (Amsterdam and Utrecht) that have probably influenced the particulate and gas signature of the air-masses are shown with the black polygons.

that from the 10 out of the 16 NPF days of Type A were used in this analysis as for the rest of the NPF days the diurnal variation of the N_d were obscured by the background aerosols.

Interestingly, N_d values calculated during the non-event days are higher than those determined when NPF events were observed as shown in Fig. 4.4. This counterintuitive observation can be partly explained by the fact that the fraction of large pre-existing particles acting as CCN in the atmospheric aerosol is lower during the event days. In fact, low concentrations of large particles prior to the nucleation events is a prerequisite for NPF to occur, as they provide a low enough condensational sink [14]. Another reason for the reduced N_d values on the event days can be that the growth of the large pre-existing particles to CCN-relevant sizes is reduced owing to the redistribution of aerosol mass to smaller sizes during the formation and growth of the new particles.

Eventually N_d values do increase above pre-event levels but only during the late evening or the night hours (cf. Fig. 4.4 b) when solar radiation is low or absent. This pattern is the same regardless of the wind direction, which attributes a strong generality to the observations. It should be noted that the observed effects are of regional importance as the low condensational sink periods last for several hours (typically > 10 h), and the windspeed recorded during the NPF events can be as high as 15 km h^{-1}. This means that the dimensions of the air masses that yield NPF and consequently low concentrations of cloud droplets can be up to ca. 100 km across, which expands the importance of our finding beyond the vicinity of our site.

Similar behavior has recently been reported in the literature by Kalkavouras et al. [24] who examined nucleation events at a remote background site of the Eastern Mediterranean (Finokalia). The combined results in Fig. 4.5 show that the decrease in the

$N_d(t)/N_d(t_{start})$ numbers is more pronounced in Finokalia compared to Cabauw because the background aerosol number concentrations in the former site are lower because droplet formation is more sensitive to aerosol (CCN) fluctuations. Nevertheless, the overall pattern is remarkably similar, providing a first indication that this is a persistent feature of new particle formation events on N_d that may carry important implications on the impact of particle formation events on regional weather and climate.

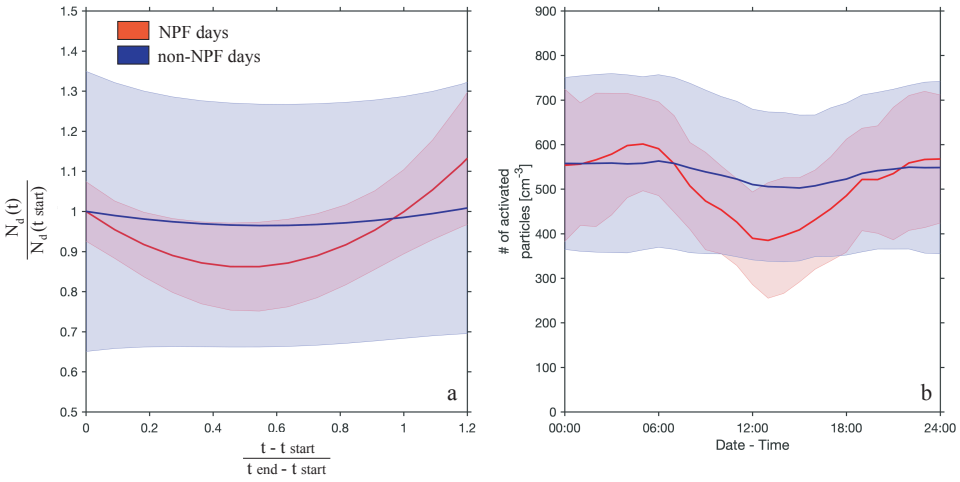

Figure 4.4: (a) Mean diurnal variation of normalized N_d during NPF event (in red) and non-event (in blue) days, and (b) mean diurnal variation of absolute N_d values determined during NPF event (in red) and non-event (in blue) days. The shaded areas indicate $\pm\,\sigma$.

4.3.2. RADIATIVE FORCING OF NPF EVENTS IN THE NETHERLANDS

To determine the indirect radiative forcing (cloud albedo effect) caused by the changes of the cloud droplet number concentration due to the NPF events, we use the RRTMG, modified in order to use the estimated mean evolution of the N_d values during the event and non-event days as input. Representative clouds observed during the event and non-event days were selected to run these calculations (cf. Fig. 4.6).

For the characteristic clouds occurring during the period that the NPF events are observed, the radiative forcing of the NPF events ranges from -0.5 to 4.9 W m^{-2} with a diurnal mean of 0.6 W m^{-2}. For characteristic clouds that occur during non-event days, the estimated forcing is higher and ranges from -0.3 to 9.1 W m^{-2} with a mean of 1.5 W m^{-2}. In both cases the diurnal mean radiative forcing is positive, meaning that the nucleation events enhance the incoming solar radiation at a regional scale. The difference in the amount of forcing between event and non-event days underlines the sensitivity of the system through variations of the cloud optical thickness.

The characteristic cloud during the NPF events is optically thinner and has a shorter lifetime than the boundary layer clouds we observe during non-NPF events, causing a

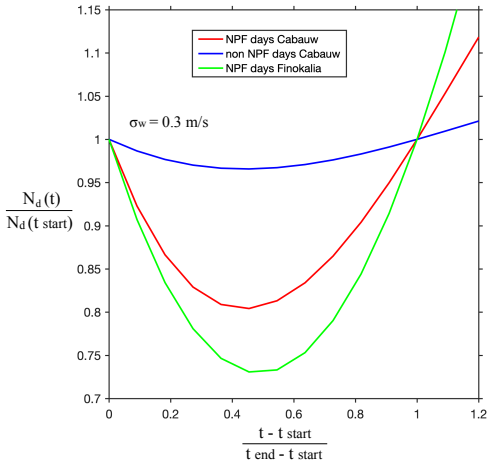

Figure 4.5: Diurnal variation of N_d during NPF event (red line - Cabauw, green line - Finokalia) and non-event (blue-line) days (normalized and fitted data for $\sigma_w = 0.3$ m s^{-2}).

higher positive forcing when the latter is considered in the calculations. In addition to that, the increase in N_d resulting from the NPF events becomes higher than that observed during the non-event days only in the late evening or night hours. Although this increase could affect the cloud droplet concentrations over the day after the NPF event, we observe that the N_d values drop again during the night as a result of the lower aerosol number concentration (both for primary and secondary particles), starting at the same levels (ca. 550 droplets cm^{-3}). This observation makes the event and the non-event days highly comparable, attributing a high generality to the estimations of the radiative properties of the resulting clouds.

The abovementioned effects are clearly illustrated in Fig. 4.7 where the short-wave downward (SWD) radiation at the bottom of the atmosphere is shown for the characteristic clouds during NPF days (Fig. 4.7 a) and clouds for days without NPF events (Fig. 4.7 b). For illustrative purposes we present the SWD radiation using a relatively low cloud droplet number concentration of 70 m^{-3}, which is in the range used in many atmospheric models, and an N_d value representative of the Cabauw site (580 m $^{-3}$). Comparison of the SWD radiation lines that correspond to the different N_d values demonstrates the sensitivity of the radiation code to the cloud droplet number concentration. As expected, higher N_d values decrease the SWD radiation because, when the liquid water path is constant, the cloud droplet radius decreases which results in a higher cloud albedo. (The liquid water path measurements, from the Cabauw site, for the NPF characteristic cloud are given in Fig. 4.8 (the respective measurements for the characteristic cloud during days without NPF were not available.)

Comparing the radiation code outcomes with actual measurement of the SWD radiation at the Cabauw site we see that there is a good agreement between the two. Large deviation at certain times of the day are probably caused by the large variance of the ra-

diation measurements. During cloud free conditions the radiation code results and the radiation measurements are in very good agreement as shown in Fig. 4.9.

In summary, here we examined the effect of new particle formation events on the cloud drop number concentration (N_d) and the associated indirect radiative forcing in a region that is highly affected by anthropogenic activity. Our results show that N_d values are lower during the course of the NPF events compared to those during the non-event days. This observation can be explained by the reduced concentration of background particles, which is a prerequisite for NPF to occur, and the fact that the N_d values associated to the NPF event days increase substantially only after the end of the event (defined here as the time when the droplet number concentration reaches the value at the start of the event), in the late evening and the night hours that solar radiation is low or absent. As a result, NPF events are associated with radiative warming; a conclusion that is counter-intuitive to the expected/assumed impact associated to the increase of CCN during NPF events.

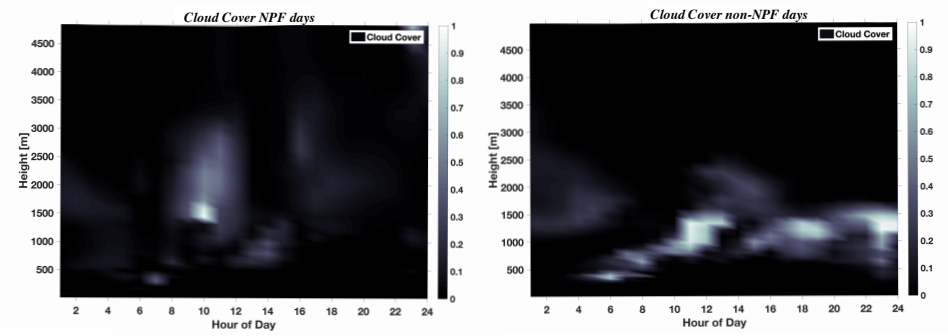

Figure 4.6: Charecteristic cloud cover at Cabauw during NPF and non-NPF days.

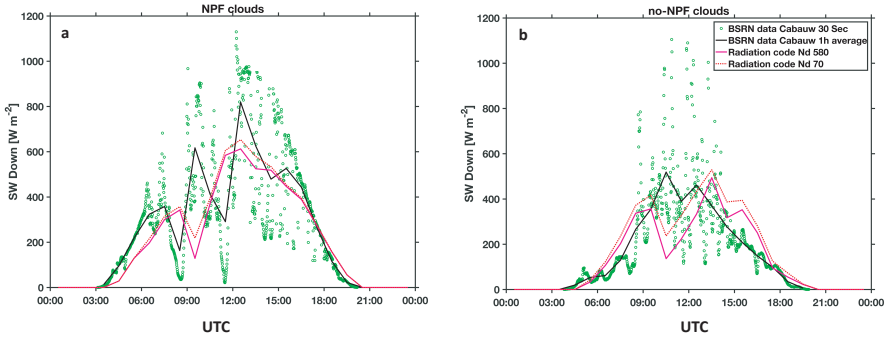

Figure 4.7: Short-wave downward (SWD) radiation at the BOA for characteristic cloud during NPF days (a) and characteristic cloud during days without NPF (b). The red dotted line shows the SWD radiation calculated by the radiation code using as input N_d value of 70 m^{-3} while the magenda line is the SWD for N_d equal to 580 m^{-3}. The green circles are radiation measurements from the Cabauw site and the black line is their average over 1 h intervals.

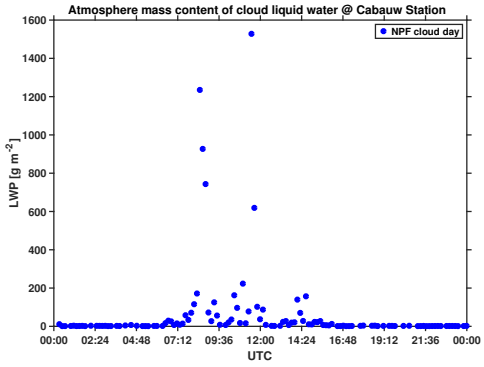

Figure 4.8: Liquid water path measurements from the Cabauw site using a microwave radiometer.

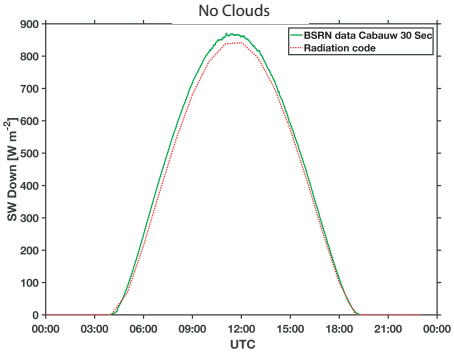

Figure 4.9: Short-wave downward (SWD) radiation at the Cabauw site measured (green line) and estimated by the radiation code (red dotted line).

REFERENCES

[1] S. Twomey, *Pollution and the planetary albedo,* Atmospheric Environment **8**, 1251 (1974).

[2] R. J. Charlson, S. Schwartz, J. Hales, R. D. Cess, J. J. Coakley, J. Hansen, and D. Hofmann, *Climate forcing by anthropogenic aerosols,* Science **255**, 423 (1992).

[3] V. Ramanathan, P. J. Crutzen, J. T. Kiehl, and D. Rosenfeld, *Aerosols, climate, and the hydrological cycle,* Science **294**, 2119 (2001), https://science.sciencemag.org/content/294/5549/2119.full.pdf .

[4] O. Boucher, D. Randall, P. Artaxo, C. Bretherton, G. Feingold, P. Forster, V.-M. Kerminen, Y. Kondo, H. Liao, U. Lohmann, P. Rasch, S. Satheesh, S. Sherwood, S. B, and Z. XY, *In: The physical science basis. climate change 2013: The physical science basis. contribution of working group i to the fifth assessment report of the intergovernmental panel on climate change,* in *The Physical Science Basis. Climate Change 2013: The Physical Science Basis. Contribution of Working Group I to the Fifth Assessment Report of the Intergovernmental Panel on Climate Change* (Cambridge University Press, 2013) pp. 571–657.

[5] D. Rosenfeld, M. O. Andreae, A. Asmi, M. Chin, G. de Leeuw, D. P. Donovan, R. Kahn, S. Kinne, N. Kivekäs, M. Kulmala, *et al.*, *Global observations of aerosol-cloud-precipitation-climate interactions,* Reviews of Geophysics **52**, 750 (2014).

[6] S. Twomey, *The influence of pollution on the shortwave albedo of clouds,* Journal of the Atmospheric Sciences **34**, 1149 (1977).

[7] P. Reutter, H. Su, J. Trentmann, M. Simmel, D. Rose, S. S. Gunthe, H. Wernli, M. O. Andreae, and U. Pöschl, *Aerosol- and updraft-limited regimes of cloud droplet formation: influence of particle number, size and hygroscopicity on the activation of cloud condensation nuclei (ccn),* Atmospheric Chemistry and Physics **9**, 7067 (2009).

[8] J. Ching, R. A. Zaveri, R. C. Easter, N. Riemer, and J. D. Fast, *A three-dimensional sectional representation of aerosol mixing state for simulating optical properties and cloud condensation nuclei,* Journal of Geophysical Research: Atmospheres **121**, 5912 (2016).

[9] J. H. Seinfeld, C. Bretherton, K. S. Carslaw, H. Coe, P. J. DeMott, E. J. Dunlea, G. Feingold, S. Ghan, A. B. Guenther, R. Kahn, *et al.*, *Improving our fundamental understanding of the role of aerosol- cloud interactions in the climate system,* Proceedings of the National Academy of Sciences **113**, 5781 (2016).

[10] B. A. Albrecht, *Aerosols, cloud microphysics, and fractional cloudiness,* Science **245**, 1227 (1989), https://science.sciencemag.org/content/245/4923/1227.full.pdf .

[11] D. Rosenfeld, Y. Zhu, M. Wang, Y. Zheng, T. Goren, and S. Yu, *Aerosol-driven droplet concentrations dominate coverage and water of oceanic low-level clouds,* Science **363** (2019), 10.1126/science.aav0566, https://science.sciencemag.org/content/363/6427/eaav0566.full.pdf .

[12] B. Stevens and G. Feingold, *Untangling aerosol effects on clouds and precipitation in a buffered system,* Nature **461**, 607 (2009).

[13] P. Paasonen, K. Kupiainen, Z. Klimont, A. Visschedijk, H. A. C. Denier van der Gon, and M. Amann, *Continental anthropogenic primary particle number emissions,* Atmospheric Chemistry and Physics **16**, 6823 (2016).

[14] M. Kulmala, H. Vehkamäki, T. Petäjä, M. D. Maso, A. Lauri, V.-M. Kerminen, W. Birmili, and P. McMurry, *Formation and growth rates of ultrafine atmospheric particles: a review of observations,* Journal of Aerosol Science **35**, 143 (2004).

[15] M. Dal Maso, M. Kulmala, I. Riipinen, R. Wagner, T. Hussein, P. P. Aalto, and K. E. Lehtinen, *Formation and growth of fresh atmospheric aerosols: eight years of aerosol size distribution data from smear ii, hyytiala, finland,* Boreal Environment Research **10**, 323 (2005).

[16] H. Lihavainen, V.-M. Kerminen, M. Komppula, J. Hatakka, V. Aaltonen, M. Kulmala, and Y. Viisanen, *Production of "potential" cloud condensation nuclei associated with atmospheric new-particle formation in northern finland,* Journal of Geophysical Research: Atmospheres **108** (2003).

[17] C. D. de España, A. Wonaschütz, G. Steiner, B. Rosati, A. Demattio, H. Schuh, and R. Hitzenberger, *Long-term quantitative field study of new particle formation (npf) events as a source of cloud condensation nuclei (ccn) in the urban background of vienna,* Atmospheric Environment **164**, 289 (2017).

[18] A. Laaksonen, A. Hamed, J. Joutsensaari, L. Hiltunen, F. Cavalli, W. Junkermann, A. Asmi, S. Fuzzi, and M. C. Facchini, *Cloud condensation nucleus production from nucleation events at a highly polluted region,* Geophysical Research Letters **32** (2005).

[19] M. Kulmala, T. Petäjä, M. Ehn, J. Thornton, M. Sipilä, D. Worsnop, and V.-M. Kerminen, *Chemistry of atmospheric nucleation: On the recent advances on precursor characterization and atmospheric cluster composition in connection with atmospheric new particle formation,* Annual Review of Physical Chemistry **65**, 21 (2014), pMID: 24245904, https://doi.org/10.1146/annurev-physchem-040412-110014 .

[20] E. M. Dunne, H. Gordon, A. Kürten, J. Almeida, J. Duplissy, C. Williamson, I. K. Ortega, K. J. Pringle, A. Adamov, U. Baltensperger, P. Barmet, F. Benduhn, F. Bianchi, M. Breitenlechner, A. Clarke, J. Curtius, J. Dommen, N. M. Donahue, S. Ehrhart, R. C. Flagan, A. Franchin, R. Guida, J. Hakala, A. Hansel, M. Heinritzi, T. Jokinen, J. Kangasluoma, J. Kirkby, M. Kulmala, A. Kupc, M. J. Lawler, K. Lehtipalo, V. Makhmutov, G. Mann, S. Mathot, J. Merikanto, P. Miettinen, A. Nenes, A. Onnela, A. Rap, C. L. S. Reddington, F. Riccobono, N. A. D. Richards, M. P. Rissanen, L. Rondo, N. Sarnela, S. Schobesberger, K. Sengupta, M. Simon, M. Sipilä, J. N. Smith, Y. Stozkhov, A. Tomé, J. Tröstl, P. E. Wagner, D. Wimmer, P. M. Winkler, D. R. Worsnop, and K. S. Carslaw, *Global atmospheric particle formation from cern cloud measurements,* Science **354**, 1119 (2016), https://science.sciencemag.org/content/354/6316/1119.full.pdf .

[21] H. Gordon, J. Kirkby, U. Baltensperger, F. Bianchi, M. Breitenlechner, J. Curtius, A. Dias, J. Dommen, N. M. Donahue, E. M. Dunne, *et al.*, *Causes and importance of new particle formation in the present-day and preindustrial atmospheres,* Journal of Geophysical Research: Atmospheres **122**, 8739 (2017).

[22] H. Gordon, K. Sengupta, A. Rap, J. Duplissy, C. Frege, C. Williamson, M. Heinritzi, M. Simon, C. Yan, J. Almeida, *et al.*, *Reduced anthropogenic aerosol radiative forcing caused by biogenic new particle formation,* Proceedings of the National Academy of Sciences **113**, 12053 (2016).

[23] R. C. Sullivan, P. Crippa, H. Matsui, L. R. Leung, C. Zhao, A. Thota, and S. C. Pryor, *New particle formation leads to cloud dimming,* NPJ Climate and Atmospheric Science **1**, 9 (2018).

[24] P. Kalkavouras, A. Bougiatioti, N. Kalivitis, I. Stavroulas, M. Tombrou, A. Nenes, and N. Mihalopoulos, *Regional new particle formation as modulators of cloud condensation nuclei and cloud droplet number in the eastern mediterranean,* Atmospheric Chemistry and Physics **19**, 6185 (2019).

[25] R. Morales Betancourt and A. Nenes, *Droplet activation parameterization: The population-splitting concept revisited,* Geoscientific Model Development **7**, 2345 (2014).

[26] F. J. Gallego, *A population density grid of the european union,* Population and Environment **31**, 460 (2010).

[27] D. Mamali, J. Mikkilä, B. Henzing, R. Spoor, M. Ehn, T. Petäjä, H. Russchenberg, and G. Biskos, *Long-term observations of the background aerosol at cabauw, the netherlands,* Science of the Total Environment **625**, 752 (2018).

[28] A. Wiedensohler, W. Birmili, A. Nowak, A. Sonntag, K. Weinhold, M. Merkel, B. Wehner, T. Tuch, S. Pfeifer, M. Fiebig, *et al.*, *Mobility particle size spectrometers: harmonization of technical standards and data structure to facilitate high quality long-term observations of atmospheric particle number size distributions,* Atmospheric Measurement Techniques **5**, 657 (2012).

[29] P. Zieger, E. Weingartner, J. Henzing, M. Moerman, G. d. Leeuw, J. Mikkilä, M. Ehn, T. Petäjä, K. Clémer, M. v. Roozendael, *et al.*, *Comparison of ambient aerosol extinction coefficients obtained from in-situ, max-doas and lidar measurements at cabauw,* Atmospheric chemistry and physics **11**, 2603 (2011).

[30] J. Henzing, *Interactive comment on: "number size distributions and seasonality of submicron particles in europe 2008–2009" by a. asmi et al,* Atmos. Chem. Phys. Discuss **11**, C3137 (2011).

[31] V.-M. Kerminen, M. Paramonov, T. Anttila, I. Riipinen, C. Fountoukis, H. Korhonen, E. Asmi, L. Laakso, H. Lihavainen, E. Swietlicki, *et al.*, *Cloud condensation nuclei production associated with atmospheric nucleation: a synthesis based on existing literature and new results,* Atmospheric Chemistry and Physics **12**, 12037 (2012).

[32] N. Kalivitis, V.-M. Kerminen, G. Kouvarakis, I. Stavroulas, A. Bougiatioti, A. Nenes, H. Manninen, T. Petäjä, M. Kulmala, and N. Mihalopoulos, *Atmospheric new particle formation as a source of ccn in the eastern mediterranean marine boundary layer,* Atmospheric Chemistry and Physics **15**, 9203 (2015).

[33] M. Petters and S. Kreidenweis, *A single parameter representation of hygroscopic growth and cloud condensation nucleus activity–part 2: Including solubility,* Atmospheric Chemistry and Physics **8**, 6273 (2008).

[34] ECMWF, *Ecmwf, 2017. era5 data documentation. european centre for medium-range weather forecast (ecmwf),* (2017).

[35] J. Morcrette, H. Barker, J. Cole, M. Iacono, and R. Pincus, *Impact of a new radiation package, mcrad, in the ecmwf integrated forecasting system,* Monthly weather review **136**, 4773 (2008).

[36] E. J. Mlawer, S. J. Taubman, P. D. Brown, M. J. Iacono, and S. A. Clough, *Radiative transfer for inhomogeneous atmospheres: Rrtm, a validated correlated-k model for the longwave,* Journal of Geophysical Research: Atmospheres **102**, 16663 (1997).

[37] M. J. Iacono, J. S. Delamere, E. J. Mlawer, M. W. Shephard, S. A. Clough, and W. D. Collins, *Radiative forcing by long-lived greenhouse gases: Calculations with the aer radiative transfer models,* Journal of Geophysical Research: Atmospheres **113** (2008).

[38] G. Martin, D. Johnson, and A. Spice, *The measurement and parameterization of effective radius of droplets in warm stratocumulus clouds,* Journal of the Atmospheric Sciences **51**, 1823 (1994).

[39] H. E. Manninen, T. Nieminen, E. Asmi, S. Gagné, S. Häkkinen, K. Lehtipalo, P. Aalto, M. Vana, A. Mirme, S. Mirme, U. Hõrrak, C. Plass-Dülmer, G. Stange, G. Kiss, A. Hoffer, N. TörÅ‘, M. Moerman, B. Henzing, G. de Leeuw, M. Brinkenberg, G. N. Kouvarakis, A. Bougiatioti, N. Mihalopoulos, C. O'Dowd, D. Ceburnis, A. Arneth, B. Svenningsson, E. Swietlicki, L. Tarozzi, S. Decesari, M. C. Facchini, W. Birmili, A. Sonntag, A. Wiedensohler, J. Boulon, K. Sellegri, P. Laj, M. Gysel, N. Bukowiecki, E. Weingartner, G. Wehrle, A. Laaksonen, A. Hamed, J. Joutsensaari, T. Petäjä, V.-M. Kerminen, and M. Kulmala, *Eucaari ion spectrometer measurements at 12 european sites â€“ analysis of new particle formation events,* Atmospheric Chemistry and Physics **10**, 7907 (2010).

[40] M. R. Stolzenburg, P. H. McMurry, H. Sakurai, J. N. Smith, R. L. Mauldin III, F. L. Eisele, and C. F. Clement, *Growth rates of freshly nucleated atmospheric particles in atlanta,* Journal of Geophysical Research: Atmospheres **110** (2005).

[41] N. Kivekäs, J. Carpman, P. Roldin, J. Leppä, E. O'Connor, A. Kristensson, and E. Asmi, *Coupling an aerosol box model with one-dimensional flow: a tool for understanding observations of new particle formation events,* Tellus B: Chemical and Physical Meteorology **68**, 29706 (2016).

5

CONCLUSIONS AND OUTLOOK

5.1. CONCLUSIONS

This chapter summarizes the conclusions of this thesis related to the research questions posed in Chapter 1, and gives an outlook for future research.

The main objectives of this research were to evaluate and compare innovative airborne in-situ aerosol measurements with remote sensing observations, to study the climatological characteristics of the aerosol particles at the CESAR observatory in the Netherlands and to quantify the impacts of new particle formation events on regional climate. The main research questions and findings of this thesis are listed below:

1. *Can in-situ airborne instrumentation on-board Unmanned Aerial Vehicles (UAVs) provide reliable measurements of aerosol mass concentration?*

2. *How trustworthy are the newly developed retrieval algorithms that utilize the synergy of active and passive remote sensing instrumentation to retrieve vertically resolved aerosol properties?*

Chapter 2 presents a comparison of aerosol mass concentration vertical profiles which were determined independently by in-situ and remote sensing instruments. More analytically, the in-situ measurements were realized using an Optical Particle Counter (OPC) onboard an Unmanned Aerial Vehicle (UAV), whereas for the remote sensing observations we used a multiwavelength LIDAR and a sunphotometer. The measurements were performed in the Eastern Mediterranean (Cyprus) during an intensive measurement campaign which focused on the aerosol Saharan dust particles. From the acquired dataset two cases of dust events were ideal for performing the comparison between the two measurement techniques. During those days, the UAV flew up to ca. 2 km altitude with the OPC measuring the size distributions of sampled aerosol particles having radii in the range 0.15-5 μm, from which the aerosol mass concentration was calculated. The

same information was retrieved by the concurrent LIDAR and sunphotometer measurements that were inverted using the POLIPHON method.

In one of the two days, we observed a dense dust layer extended from 2 to 4 km and a mixture of dust and almost spherical particles below 2 km. Agreement between the in-situ measurements and the LIDAR observations was very good (R = 0.9), with the in-situ measurements lying within the uncertainty limits of the remote sensing technique (38%). This yields a mean bias of -12.0 μg m^{-3} between the two observational methods that can be mainly attributed to the difference in the cut-off diameters measured by the two techniques. Corrections applied to account for this difference in the cut-off diameters further enhanced the agreement, decreasing the mean bias to -1.1 μg m^{-3}.

In the measurements carried out during the second event, a sparse dust layer was observed between 0.8-2 km altitude during the morning hours. Information from the LIDAR measurements and the backtrajectory analysis suggested that this layer was a mixture of desert dust with continental/pollution particles. Despite that, however, agreement between the airborne in-situ and remote sensing observations in this case was also very good (R = 0.9). In terms of absolute values, the corrected mass concentration measured by the airborne OPC were equal or lower than those derived from the LIDAR measurements for the entire range of altitudes and exhibited a mean bias of -1.6 μg m^{-3}. The concentrations measured by the airborne OPC were within the calculated uncertainty of the remote sensing technique.

The measurements reported here indicate that unmanned airborne OPC measurements and LIDAR observations can provide reliable ways to determine coarse mode aerosol mass concentration profiles in the atmospheric column, thereby bridging the gap between in-situ and remote sensing observations. Considering that both methods can provide dense datasets in a cost-effective manner and on a regular basis, this finding paves the way towards their systematic exploitation in climate models.

3. *What is the climatological trend of the fine particulate matter mass at Cabauw?*

Chapter 3 presents a study based on an 8-year-long dataset (2008-2015) of aerosol particle mass concentrations and size distributions, as well as on a 10-month record of aerosol hygroscopicity at the CESAR site in The Netherlands. The yearly mean mass concentration of the particles having diameters less than 2.5 μm ($PM_{2.5}$) showed a decreasing trend that can be attributed to more stringent regulations to industrial emissions and to the advanced emission treatment technologies introduced in the transportation sector over the past decade. $PM_{2.5}$ concentrations exhibit a clear seasonal variability which is primarily affected by the higher emissions and to a lesser extent by meteorological conditions such as the BLH and precipitation.

4. *What is the climatological trend of the aerosol number concentration at Cabauw and its seasonal and diurnal variation?*

In contrast to the $PM_{2.5}$, the number concentration of particles having diameters in the range 30-500 nm showed an increasing trend between 2008 and 2011 and an increasing trend from 2013 to 2015, with N_{30-500} values in 2015 being at the same level with those

in 2008, raising questions on whether air quality actually improves as the $PM_{2.5}$ measurements suggest. Seasonally, N_{30-500} was higher in spring and summer mostly due to the production of new particles by nucleation. The diurnal variation of the number concentration in winter and autumn shows pronounced peaks in the late morning and evening hours corresponding to the traffic and residential heating peaks. The measurements also show a shift towards smaller particle sizes in spring and summer, supporting that the particle number concentrations during these seasons are strongly influenced by the NPF events.

5. *What is the diurnal and seasonal variability of aerosol hygroscopicity at Cabauw?*

The hygroscopic parameter κ, for all sizes measured in this work suggests the presence of organics in the particle phase. The freshly emitted smaller particles (35 nm) are most often externally mixed compared to the chemically aged larger particles (165 nm). The diurnal patterns of the seasonally averaged κ distributions of the larger particles showed constant values throughout the day while the smaller particles exhibited diurnal variations. The 165-nm particles are mostly internally mixed in spring and summer whereas in autumn and winter the κ distributions are bimodal with the more hydrophobic peak being temporarily associated to traffic and residential heating. The smaller particles are externally mixed during all seasons and are also influenced by anthropogenic activities in the cold season as suggested be the reduced κ values during the day. In spring and summer, new particles formation events and photochemical aging are affecting the κ distribution, which is shifted to higher values during the day. Air masses of different origins (continental and marine) exhibit similar κ distributions for all sizes signifying the dominance of the local sources to particles hygroscopicity.

6. *What is the impact of new particle formation events on cloud number concentration in the Netherlands?*

7. *What is radiative forcing of the new particle formation events in the Netherlands?*

Chapter 4 examines the effect of new particle formation events on the cloud drop number concentration (N_d) and the associated indirect radiative forcing in a region that is highly affected by anthropogenic activity. To estimate N_d we combine ground-based measurements, and mean values of particle hygroscopicity, and updraft velocities reported for the region with a mechanistic cloud parameterization model. The resulting values are then used as input in a state-of-the-art radiative transfer model to determine radiative fluxes and from those the associated forcing. Our results show that N_d values during the course of the NPF events are lower compared to those during the non-event days. This observation can be explained by the lower concentration of background particles (which is a prerequisite for NPF to occur, and the fact that the N_d values associated to the NPF event days increase substantially only after the end of the event (defined here as the time when the droplet number concentration reaches the value at the start of the event), in the late evening and the night hours that solar radiation is low or absent. As a result, NPF events are associated with radiative warming; a conclusion that is counter-

intuitive to the expected/assumed impact associated to the increase of CCN during NPF events.

5.2. OUTLOOK

The work presented in this thesis provides answers to a number of scientific questions, however many others are yet to be answered. This last section of the dissertation discusses how this research could be further extended in the future.

In Chapter 2 we discussed the importance of bridging the long-lasting gap between aerosol in-situ and remote sensing observations and presented a good agreement between the two methods in the case of dust particle measurements. In the future, similar comparisons should be performed for different aerosols types as well as different instruments and retrieval methods in order to ensure the homogeneity of aerosol measurements.

Long-term measurements of the atmospheric aerosols are crucial in order to understand the atmospheric processes involving particles as well as their trends. In Chapter 3 we reported on long-term measurements of the aerosol number concentration and mass. However, the hygroscopicity dataset covered a period of less than a year, thus limiting our understanding of the temporal variation of hygroscopicity. Having long-term information on hygroscopicity, would improve the quantification of the aerosol direct effect, while, combined with an analysis similar to the one presented in Chapter 4, would shed light into the evolution of the microphysical properties of clouds and their interaction with the incoming solar radiation. Based on that, we could improve estimations of the aerosol indirect effect and further constrain the related uncertainties to climate predictions.

In addition, long-term records of aerosol hygroscopicity would answer the question of whether we need to continue measuring hygroscopicity or not. The findings of this thesis showed that, within the examined period, the fluctuation of the hygroscopicity parameter was not significant, especially for the CCN-relevant sizes, thus the impact on the cloud microphysical properties was minor. If the same holds for the inter-annual variation of hygroscopicity and, given that HTDMA hygroscopicity measurements are labor-intensive and costly, the need for continuing these measurements should be reconsidered. It is worthwhile pointing out that this conclusions hold for assessing the indirect effect of aerosol, which concerns relatively big particles. For studies where the smaller particles are more relevant (e.g., for assessing their direct effect on climate, as well as their effects upon human health), most likely such measurements are highly valuable to have on a continuous basis. This, however, would require that those measurements become more simple and less expensive to install and operate.

Another invaluable finding would be the verification of modeling studies as those presented in Chapter 4. In this work we used ground in-situ aerosol observations as input for the estimation of the cloud droplet number concentration using a cloud parameterization. Using this information, we proceeded to calculate the impact of cloud droplet number concentration changes to the incoming solar radiation. State-of-the-art remote sensing instruments and retrieval techniques allow for the calculation of the cloud drop number and the actual solar radiation that reach the Earth. Verification of the modeling results from the remote sensing measurements is needed for establishing our trust to

the models and continue using them for aerosol research. In addition, examining other locations around the globe for the universality of these conclusions would build more trust, whereas modeling work to assess the impacts on a global scale would be the final word in this direction.

ACKNOWLEDGEMENTS

"In ordinary life, we hardly realize
that we receive a great deal more than we give,
and that it is only with gratitude that life becomes rich."

Dietrich Bonhoeffer

The PhD at TU Delft was one of the most valuable experiences of my life. Not only because I gained knowledge and improved my skills, but also because it altered my personality and my way of thinking. These 4 years seems like a lonely road and at times it was, however there were many people with different roles that contributed so that I could reach my final destination. This last section of the thesis is devoted to them...

First, I would like to thank my promotor *Prof. Herman Russchenberg* for giving me the opportunity to pursue my PhD at TU Delft. I greatly value his support to almost all my ideas and requests. His curiosity, expressed through numerous questions during our meetings, used to make me feel uncomfortable at the begging, however soon enough I realized how important that was for looking at the same problem from different perspectives. Herman has always been positive, welcoming, reasonable and wise and our interaction helped me to understand better the Dutch mentality.

Many thanks to all the fellow PhD students and the GRS colleagues (*Reenu, Ricardo, Julien, Christine, Siavash, Tim, Veronica, Francesca, Olga, Lorentzo, Jiapeng, Lukas, Pedro, Igor*). It was fun working with you!

I would also like to thank *Prof. Harmen Jonker* for his support at a critical point during my PhD.

Sometimes people who are not closely related to your work can immensely influence it, the key is to listen what they have to say. *Yann* you really changed everything with your advice. I will not forget it.

I would like to thank all my colleagues from the *National Observatory of Athens, the Cyprus Institute and the TROPOS Institute* with whom I learned how it is too work hard and very long hours but at the same time having a great time! It was great pleasure working with you guys.

Dr. Fotis thank you for being a good listener and so compassionate.

Sotiria, we talked through the difficult moments and celebrated the good ones. Thanks for everything.

Also, I would like to thank my new colleague *Iris* for the translation of this thesis' summary to dutch.

Moreover, I would like to extend my sincere gratitude and thankfulness to my supervisor and mentor *Dr. George Biskos*. I deeply appreciate your positive attitude, kindness, calmness, patience and your way of looking at the world. I couldn't ask for a better colleague.

Τέλος, θα ήθελα να ευχαριστήσω τους γονείς μου Ειρήνη και Δημήτρη που μου προσέφεραν με μεγάλη αγάπη ό,τι καλύτερο μπορούσαν και που στήριξαν τις επιλογές μου έχοντας ίσως πιο μεγάλη αγωνία από εμένα για το που αυτές θα με οδηγήσουν. Επίσης ένα μεγάλο ευχαριστώ στον αδερφό μου που πάντα έστρωνε τον δρόμο για μένα και ήταν παράδειγμα προς μίμηση και στήριγμα.

CURRICULUM VITÆ

DIMITRA MAMALI

15-05-1986 Born in Athens, Greece.

EDUCATION

2004-2010 ***Diploma in Physics***
University of Athens, Greece
Thesis: Spatio-temporal analysis of rain height and soil moisture over Greece
Supervisor: Papaioannou-Kerkidou Georgia

2011-2013 ***Master in Atmospheric and Climate Science***
ETH Zürich, Switzerland
Track: Environmental Physics and Meteorology
Thesis: Lagrangian and Eulerian Analysis of Clear Air Turbulence over the United States
Supervisor: Sprenger Michael

2014 ***Internship***
Paul Scherrer Institute, Atmospheric Chemistry LAB
Villigen, Switzerland

2014-2019 ***PhD Atmospheric Physics***
Technical University of Delft
Supervisor: George Biskos
Promotor: Herman Russchenberg
Thesis: Field observations of atmospheric aerosol properties and the impacts of new particle formation in the radiative properties of clouds

2016 ***Affiliate***, Visiting doctoral researcher
Institute for Astronomy, Astrophysics, Space Applications and Remote Sensing
National Observatory of Athens, Athens, Greece

HONORS/AWARDS

2013 *International Student Scholarship* (ETH Zürich)

LIST OF PRESENTATIONS

1. **D. Mamali**, E. Marinou, M. Kottas, I. Binietoglou, P. Kokkalis, A. Tsekeri, V. Amiridis, M. Pikridas, J. Sciare, S. Bezantakos, A. Ansmann, R. Engelmann, H. Russchenberg, G. Biskos, European Aerosol Conference, Switzerland: *"Vertical profiles of the aerosol mass concentration observed by unmanned airborne in-situ and remote sensing instruments during a dust event" (Oral presentation, 2017)*

2. ***D. Mamali**, E. Marinou, M. Kottas, I. Binietoglou, P. Kokkalis, A. Tsekeri, V. Amiridis, M. Pikridas, J. Sciare, S. Bezantakos, A. Ansmann, R. Engelmann, H. Russchenberg, G. Biskos, Civil Engineering and Geoscience Seminar, TU Delft:* "Comparison of aerosol mass concentration measured by lidar and unmanned aerial vehicles." (Oral presentation, 2017)

3. Tsekeri A., Amiridis V., Lopatin A., Marinou E., Igloffstein, J., Pikridas M., Sciare J., Gerasopoulos E., Liakakou E., Birgit W., Baars H., Kottas M., **Mamali, D.**, Kokkalis P., Raptis I.P., Solomos S., Binietoglou I., Mihalopoulos N., Engelmann R., Wandinger U., Ansmann A., Dubovik O., $28^t h$ International Laser-Radar Conference, Bucharest, Romania: *"Aerosol absorption profiling from the synergy of lidar and sun-photometry in the framework of the ACTRIS-2 campaigns in Germany, Greece and Cyprus." (Oral presentation, 2017)*

4. ***D. Mamali**, , J. Mikillä, B. Henzing, M. Ehn, T. Petäjä, H. Russchenberg, and G. Biskos, Buys Ballot research school (BBOS) Autumn Symposium, Oranjewoud, the Netherlands:* "Atmospheric Aerosol Properties in the Netherlands." (Poster presentation, 2017)

5. **D. Mamali**, E. Marinou, M. Kottas, I. Binietoglou, P. Kokkalis, A. Tsekeri, V. Amiridis, M. Pikridas, J. Sciare, S. Bezantakos, A. Ansmann, R. Engelmann, H. Russchenberg, G. Biskos, European Geoscience Union Conference, Vienna: *"Vertical profiles of the aerosol mass concentration observed by unmanned airborne in-situ and remote sensing instruments during a dust event" (Poster presentation, 2017)*

6. ***D. Mamali**, , J. Mikillä, B. Henzing, M. Ehn, T. Petäjä, H. Russchenberg, and G. Biskos, European Aerosol Conference, France:* "Variability of size distribution measurements of atmospheric aerosol particles observed at Cabauw over the period 2008-2014" (Poster presentation, 2016)

7. A. Tsekeri, V. Amiridis, A. Lopatin, E. Marinou, M. Kottas, **D. Mamali**, I. Binietoglou, J. Sciare, M. Pikridas, N. Mihalopoulos, E. Liakakou, E. Gerasopoulos, P. Kokkalis, I.P. Raptis, S. Solomos, H.Baars, R. Engelmann, I. Stachlewska, U. Wandinger, A. Ansmann, O. Dubovik, P. Goloub, 2nd ACTRIS-2 WP2 Workshop, Barcelona: *"JRA1 activities in Athens, Cyprus and Crete: Aerosol vertical profiling utilizing the synergy of lidar, sunphotometry and in-situ measurements" (Poster presentation, 2016)*

8. ***D. Mamali**, E. Marinou, M. Kottas, I. Binietoglou, P. Kokkalis, A. Tsekeri, V. Amiridis, M. Pikridas, J. Sciare, S. Bezantakos, A. Ansmann, R. Engelmann, H. Russchenberg,*

G. Biskos, 2nd ACTRIS-2 WP2 Workshop, Barcelona: "Comparison of in-situ aerosol mass measurements with drones and LIDARS" (Poster presentation, 2016)

9. **D. Mamali**, , J. Mikillä, B. Henzing, M. Ehn, T. Petäjä, H. Russchenberg, and G. Biskos, CESAR Science-Day, KNMI, De Bilt, Netherlands: *"Atmospheric particle size distribution and hygroscopicity at Cabauw for the period 2008-2014" (Oral presentation, 2016)*

10. ***D. Mamali**, E. Marinou, M. Kottas, I. Binietoglou, P. Kokkalis, A. Tsekeri, V. Amiridis, M. Pikridas, J. Sciare, S. Bezantakos, A. Ansmann, R. Engelmann, H. Russchenberg, G. Biskos, APM International workshop, Cyprus:* "Saharan dust measurements during the BACCHUS campaing using LIDAR" (Oral presentation, 2016)

LIST OF PUBLICATIONS

4. **D. Mamali**, , J. Mikillä, B. Henzing, M. Ehn, T. Petäjä, H. Russchenberg, and G. Biskos, *Long term observations of the background aerosol at Cabauw, the Netherlands*, Science of the Total Environment.

3. **D. Mamali**, E. Marinou, J. Sciare, M.Pikridas, P. Kokkalis, M. Kottas, I. Binietoglou, A. Tsekeri, C. Keleshis, R. Engelmann, H. Baars, A. Ansmann, V. Amiridis, H. Russchenberg, and G. Biskos, *Vertical profiles of the aerosol mass concentration observed by unmanned airborne in-situ and remote sensing instruments during a dust event*, Atmospheric Measurement Techniques.

2. E. Marinou, M. Tesche, A. Nenes, A. Ansmann, J. Schrod, **D. Mamali**, A. Tsekeri, M. Pikridas, H. Baars, R. Engelmann, K. - A. Voudouri, S. Solomos, J. Sciare, S. Groβ, and V. Amiridis, *Retrieval of ice nucleating particle concentrations from lidar observations: Comparison with airborne in-situ measurements from UAVs*, Atmospheric Chemistry and Physics.

1. E. Proestakis, V. Amiridis, E. Marinou, I. Binietoglou, A. Ansmann, U. Wandinger, J. Hofer J. Yorks, E. Nowottnick, A. Makhmudov, A. Papayannis, A. Pietruczuk, A. Gialitaki, A. Apituley, C. Muñoz-Porcar, D. Bortoli, D. Dionisi, D. Althausen, **D. Mamali**, D. Balis, D. Nicolae, E. Tetoni,L. G. Luigi Liberti, H. Baars, Iwona S. Stachlewska, K. A. Voudouri, L. Mona, M. Mylonaki, M.R. Perrone, M. J. Costa, M. Sicard, N. Papagiannopoulos, N. Siomos, P. Burlizzi, R. Pauly, R. Engelmann, S. F. Abdullaev, G. Pappalardo , Atmospheric Chemistry and Physics.